1-1-2007

Applying of mechanical failure criteria of brittle material to the design of high temperature heat exchanger

Taha Mohamed
University of Nevada, Las Vegas

APPLYING OF MECHANICAL FAILURE CRITERIA OF BRITTLE MATERIAL TO THE DESIGN OF HIGH TEMPERATURE HEAT EXCHANGER

by

Taha Mohamed

Bachelor of Science in Mechanical Engineering
Al-Azhar University, Cairo
July 2000

A thesis submitted in partial fulfillment
of the requirements for the

Master of Science Degree in Engineering
Department of Mechanical Engineering
Howard R. Hughes College of Engineering

Graduate College
University of Nevada, Las Vegas
December 2007

UNLV
UNIVERSITY OF NEVADA LAS VEGAS

Thesis Approval

The Graduate College
University of Nevada, Las Vegas

November 1, 2007

The Thesis prepared by

Taha Mohamed

Entitled

Applying of Mechanical Failure Criteria of Brittle Material to the Design of High Temperature Heat Exchanger

is approved in partial fulfillment of the requirements for the degree of

Master of Science in Mechanical Engineering

Examination Committee Chair

Dean of the Graduate College

Examination Committee Member

Examination Committee Member

Examination Committee Member

Graduate College Faculty Representative

ABSTRACT

Application of Mechanical Failure Criteria of Brittle Material to the Design of High Temperature Heat Exchanger

by

Taha Mohamed

Dr. Mohamed Trabia, Examination Committee Chair
Professor of Mechanical Engineering
University of Nevada, Las Vegas

Previous studies have suggested using a ceramic high temperature heat exchanger as a sulfuric acid decomposer for hydrogen production within the sulfur iodine thermo-chemical cycle. The decomposer was manufactured using fused ceramic layers that allow the creation of channels with dimensions below one millimeter. The heat exchanger is expected to operate in the range of 950°C. Thermal stresses are however induced in the heat exchanger ceramic components. In this study, proper failure criteria are selected to evaluate the safety level of the ceramic components. A three-dimensional computational model is developed to investigate the fluid flow, heat transfer, stresses and chemical reactions in the decomposer. Fluid, thermal and chemical reaction analyses are performed using FLUENT software. The temperature distribution in the solid is imported to ANSYS software and used together with pressure as the load for stress analysis. Results of this research can be used as a basis for the investigation of the optimal design of the decomposer that can provide a maximum chemical decomposition performance while

maintaining stresses within design limits. The stress results are used to calculate the probability of failure based on Weibull failure criteria and the factor of safety based on Coulomb-Mohr failure criteria.

A parametric study of a straight channel sulfuric acid decomposer is made. Several different geometries of the decomposer channels which include straightforward, ribbed, hexagonal, and diamond forms are investigated. The influence of the mass flow rate and of the area of chemical reaction on the chemical decomposition performance for the decomposer are also explored. The analysis includes the steady state operating conditions and the transient operating conditions. The research considers stresses that are induced during transient scenarios, in particular, the cases of startup and shutdown.

The analysis includes also the Bayonet design of heat exchanger as silicon carbide integrated decomposer (SID) which produces sulfuric acid decomposition product - sulfur dioxide. The product can be used within the sulfur iodine thermochemical cycle portion of the hydrogen production process. A two-dimensional axisymmetric geometry of the bayonet heat exchanger is created using GAMBIT software. A computational model is developed to investigate fluid flow, heat transfer and chemical reactions in the porous medium of the decomposer. Fluid, thermal and chemical reaction analyses are performed using FLUENT software. Temperature distribution in the solid is imported to ANSYS software and used together with pressure as the load for stress analysis.

TABLE OF CONTENTS

LIST OF FIGURES

ACRONYMS AND ABBREVIATIONS

Acronyms

3-D	Three Dimensional
HTHX	High Temperature Heat Exchanger
SID	Silicon Carbide Integrated Decomposer
CAD	Computer Aided Design
DOE	Department of Energy
PZT	Lead Zirconium Titanate
NTC	Negative Temperature Coefficient
YBCO	Yttrium Barium Copper Oxide
PTC	Positive Temperature Coefficient
PLZT	Lead Lanthanum Zirconium Titanate
CTR	Critical Temperature Resistance
AZS	Alumina Zirconium Silicate
IR	Infrared
APDL	ANSYS Parametric Design Language
UDF	User Defined Function
PM	Overall Factor of Safety
FEM	Finite Element Analysis
IEEE	Institute of Electrical and Electronics Engineers

Abbreviations

°C	Celsius
Gal	Gallon
He	Helium
Hr	Hour
I	Iodine
Lb	Pound
Min	Minute
Sec	Seconds
°K	Kelvin
kg	Kilo Gram

ACKNOWLEDGMENTS

First of all I thank almighty Allah whom through his grace and blessing has supported me during these times.

I am greatly indebted to my supervisor Prof. Dr. Mohamed Trabia. This research work would not have been carried out and done without attentive supports from him. I am very thankful to Prof. Dr. Yitung Chen for his valuable guidance, and comment. I am very grateful to Prof. Dr. Ajit Roy for all of the very helpful classes and discussions. I am very grateful to Prof. Dr. Tony Hechanova for all of the very helpful comments on the presentation skills. I am grateful to Prof. Dr. Brendan O'Tool for his help and support. I am very thankful to Dr. Valery Ponyavin, for his continues support through out my research. I am very thankful to Ceramtec staffs who work with us in this research. I am very thankful to Dr. Aly Said, for his valuable advice and help. I would like to thank everyone who helped me and make it possible for me to complete this work. Finally I owe a lot to my mother Mrs. Hafiza Alazhary and my father Mr. Abd Elghafar Mohamed and my brothers, my sisters, and my nephews for accepting my absence during my study. They have been a constant source of patience and encouragement.

CHAPTER 1

INTRODUCTION AND BACKGROUND

Hydrogen has the potential to revolutionize the way energy is produced, stored, and utilized. Hydrogen would be an attractive energy carrier if it is demonstrated that it could be produced cleanly and cost-effectively on a large scale. The evolution from the fossil fuel economy to a hydrogen economy could occur in this century if technologies to bridge the gap are developed. Forsberg et al. [1] point out that hydrogen is already used extensively in industry and that the development of hydrogen-fuel vehicles already justifies the development of advanced methods to produce hydrogen. Although abundant on Earth, hydrogen is not an energy source that can be mined like coal and uranium or gathered like oil and natural gas. Hydrogen must be extracted by breaking molecules such as water or methane, which requires the input of large amounts of energy for large-scale production. Nuclear energy provides an ample and economical source of energy that can be used to produce the high temperatures required in the water splitting technologies. Using this energy that produces a high temperature depends on the usage of the High Temperature Heat Exchanger (HTHX) to transfer this heat to hydrogen production cycles like sulfur-iodine thermochemical cycle which is working in a temperature range of 120-950 °C [2]. The material that can be used in HTHX should maintain its mechanical properties at this temperature range. Most of the materials that have these characteristics are brittle materials such as, silicon carbide and quartz. Since these materials have a

different behavior than ductile materials, it is important to find a proper way to find the proper failure criteria for these materials. Using computational analysis software makes it easy to calculate, extract, and process data and represent results in quantitative and qualitative outputs.

1.1 Purpose of the Study

The main purpose of this study is to evaluate various HTHX designs under different operating conditions (steady state and transient condition) and to determine the factor of safety and the probability of failure of these designs at these operating conditions.

1.1.1 Stress Analysis of HTHX Designs Under Steady and Transient Conditions

The heat exchanger is expected to operate under a steady state in the temperature range of 120-950°C with a pressure load of 1.5 - 7.5 MPa. This operating condition will induce stress in the solid part of the HTHX as a result of the applied pressure and the temperature difference in the solid part due the thermal load. These stresses, which are caused by the temperature difference, are expected to have higher values in the transient condition, especially in the start up or emergency shutdown. Finite element analysis is helpful to simulate and calculate the expected stresses due to this applied load. The finite element molding is done using ANSYS, FLUENT and GAMBIT.

1.1.2 Safety Level Determination in Various HTHX Designs

Safety is paramount for evaluating different engineering designs. Factor of safety is defined as the ratio of the load necessary to cause structural failure to the expected service load. Factor of safety provides a degree of assurance that the component will not

fail while it is in service [3]. This application of the factor of safety concept is easily determined for ductile material because it has specified yield strength. On the other hand, brittle material calls for modification of the factor of safety concept. Because the structure of brittle materials contains a large number of randomly oriented microscopic cracks or other planer interfaces that cannot support tensile stresses [3]. There were two materials used in the proposed designs of HTHX: The first was ceramic (silicon carbide) and the second was quartz. Both of them are brittle. It is known that the results of measuring the strength for brittle material shows considerable scatter. This considerable scatter is easily explained as a result of the number and size of cracks responsible for the failure. This scatter distribution has important engineering consequences: First, the strength that can be safely used in design evidently is less than the average measured strength. Second, the large component has a greater probability of failure than a smaller one under the same stress conditions because of the larger probability of having flaws in a larger volume. From these characteristics, it is required to choose proper failure criteria that capable to justify the differences between brittle and ductile materials plus considering the probabilistic approach of the distribution of microscopic cracks and the volume of the component.

1.2 Research Questions

The focus of this research is to evaluate the HTHX designs in regard to safety requirements. The questions included in the following subsection will discuss the concepts and the techniques of applying these criteria.

1.2.1 What Are the Failure Criteria for Brittle Material?

The failure criteria for brittle material can be divided into two main categories: First, the modification of the maximum normal stress criterion gives a reasonably accurate prediction of the fracture in brittle material as long as the normal stress has the largest absolute value in tensile [3]. Divination from this criterion occurs if the normal stress has the largest absolute value in compression. This modification provides for the Coulomb-Mohr failure criteria. Second, a criterion depends on the failure statistical approach of the solid component. The statistical approaches are based upon an idealization of the fracture process and analogous to a chain, the links of which would be formed by the volume elements. The "weakest-link" concept assumes that the fracture of the bulk specimen is determined by the local strength of its weakest volume element [4]. For correct application of this concept, and for a sound statistical theory, it is important to conform to the basic assumptions. According to Freudenthal, "fracture of the specimen is identified with the unstable propagation of the most severe crack from this element throughout the bulk of the specimen, independently of the local strength of all other elements in the path of the crack" [5]. For isotropic materials, the statistical theories may be essentially grouped into three categories: Weibull, the flaw size theories, and the elemental strength approach. Weibull approach is the most widely used.

1.2.2 How to Incorporate Failure Criteria for Brittle Materials within Finite Element Analysis (FEA)?

Since the computational power of the computer have been developed to be available for different kinds of applications, the Finite Element Analysis (FEA) became an important tool in simulation, analysis, and prediction. In the FEA, the component is

divided into elements and each element consists of a number of nodes. There is an ability to apply different kinds of loads to the element itself, or to the node, and to calculate the corresponding results of these loads. From these facts, it is easy to extract the state of stresses at each node or element and use these values to calculate the factor of safety according to the Coulomb-Mohr failure criteria or to calculate the probability of failure according to the Wiebull failure criteria.

1.3 Literature Review

1.3.1 HTHX Design

The heat exchanger consists of a core or matrix containing the heat-transfer surfaces and fluid distribution elements such as headers, tanks, inlet and outlet nozzles or pipes, etc. The heat-transfer surface is in direct contact with fluids through which heat is transferred by conduction. The area of the surface that separates the fluids is referred to as the primary or direct contact surface. To increase the heat-transfer area, secondary surfaces known as fins may be attached to the primary surface. In general, industrial heat exchangers have been classified according to (1) construction, (2) transfer processes, (3) degrees of surface compactness, (4) flow arrangements, (5) pass arrangements, (6) phase of the process fluids, and (7) heat-transfer mechanisms. Furthermore, according to constructional details, heat exchangers are classified as: (1)tubular heat exchangers-double pipe, shell and tube, and coiled tube; (2) plate heat exchangers-gasketed, spiral, plate coil, and lamella; (3) extended surface heat exchangers-tube-fin, plate-fin; and (4) regenerators-fixed matrix, rotary. Shell and tube heat exchanger units can be designed for almost any combination of pressure and temperature; the plate-fin heat exchanger also can be designed for any for any temperature range but with pressure limitation [6].

The selection of the type of heat exchanger is influenced by the operating pressure and temperature. The operating conditions in the proposed design is to be used for the sulfur-iodine thermochemical cycle and, while processing highly corrosive fluids, conducted at a temperature range of 120-950°C. The IEEE describes materials, insulation systems, and transformers that are designed to operate at a maximum hottest-spot temperature above 120 °C as a high temperature application [7]. For that reason, the proposed design was classified as a high temperature heat exchanger. The descriptions of high temperature application was not found clearly in the ASME Standard, but 900 °C should be considered as high temperature. The corrosive environment, along with the high temperature range, makes it difficult for these requirements to be fulfilled using the on-shelf component; therefore, it was necessary to analyze the proposed design based on the applied operating condition.

1.3.1.1 Heat exchanger and Chemical Decomposer: Micro-channel Design

A novel heat exchanger that uses microchannels to enhance heat transfer rates was investigated for chemical reactor applications. Heat exchange fluid flows parallel through multiple channels of micron dimensions to both increase the surface area available for heat transfer and shrink the coolant boundary layer to reduce heat transfer resistance. Integrated heat removal or addition is a critical component to the design and also the scale-up of chemical reactors. Endothermic reactions require sufficient heat addition to maintain high reaction rates; whereas, exothermic reactions require adequate heat removal to prevent hot-spot formation and thermal runaway. Conventional exothermic reactors are often run with diluents, either with the mobile reactant phase or the solid catalyst phase, to limit the heat generation rate. The relative rate of heat transfer to heat

generation dictates the overall productivity for safe and economically favorable operation of a chemical reactor.

Microchannel heat exchangers are fabricated through a number of available methods and offer the potential to reduce conventional resistance for heat transfer. As such, these systems represent a radically different support construction compared to those used in conventional chemical reactor systems. Within a microchannel, the thickness of the thermal boundary layer is structurally constrained to less than or equal to half the width of the fluid channel. This reduction in the boundary layer over conventional heat exchangers is expected to provide high heat transfer capacity within a compact hardware volume. In the late 1980's, researchers at Germany's Kernforschungszentrum Karlsruhe (KFK) demonstrated a compact, 1 cm^3 cross-flow microchannel heat exchanger that provided nearly 20 kW of total heat transfer between the two working fluids. Most of the demonstrated thermal/fluid components with microscale features utilize photolithographic fabrication techniques and are an outgrowth of the semiconductor industry. Thus, many of the devices are fabricated from silicon, including micropumps, microvalves, and cryogenic coolers.

Three ceramic fabrication techniques are commonly available: first, silicon micromachining; second, deep x-ray lithography; and third, non-lithographic micromachining. The last is used to produce the microchannel heat exchanger described in this work. The tremendous investment in silicon microfabrication by the microelectronics industry has provided a wide platform specifically for the creation of microstructures in silicon. Two types of micromachining that employ photolithography are used in fabrication techniques: Surface micromachining is the process by which a thin

film (available from the microelectronics industry) is first deposited, patterned, and then chemically machined (by wet or dry chemical etching) onto the surface of the component. The other example is bulk micromachining. This is when microstructures are formed within a silicon wafer by the selective, isotropic and/or anisotropic removal of material, including wells, channels, and through-holes in substrates. Microcomponents, such as diaphragm, covered cavities for pumps, and valves can be assembled through the bonding of two, bulk micromachined structures. Additionally, other fabrication techniques are in various stages of development [8], thus stressing the importance of these applications.

The operation of the microchannel heat exchanger is illustrated in Figure 1-1. It shows a simple model for describing fluid and heat transfer characteristics of the system. Heat (q) is applied to the upper surface of the microchannel heat exchanger with the coolant flowing through the channel. The upper surface temperature can be calculated by conduction and convection equations [9].

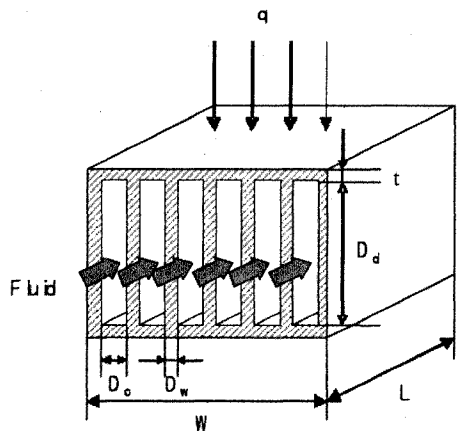

Figure 1-1 Schematic of microchannel heat exchanger[9]

1.3.1.2 Heat exchanger and Chemical Decomposer: Bayonet Design

A bayonet-tube exchanger consists of a pair of concentric tubes with a cap attached to one end of the outer tube. The advantage of this design is that the inner tubes, the outer tubes, and the shell are completely free to move independently from one another. The freely expanding elements greatly simplify the structure of the exchanger and eliminate the thermal stresses. The bayonet-tube is therefore particularly suited to extremely large temperature differentials between the two fluids. [10]

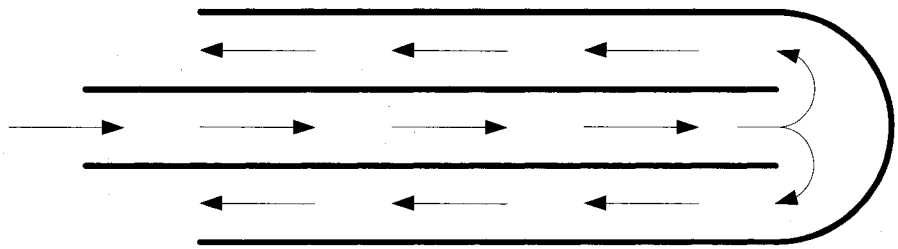

Figure 1-2 Bayonet tube with flow entering the inner tube and exiting the annulus

Schematic of bayonet heat exchanger is shown in Figure 1-2. The fluid can flow either by entering the inner tube and exiting the annulus, or by entering the annulus and exiting the inner tube. Varying the diameters of the inner and outer tubes can significantly influence the heat transfer and the tube-side pressure drop performance. Essentially, the diameters represent, for a fixed length of tube, the heat exchange surface and the cross-sectional areas of the inner and annulus regions. Hence, they determine the tube-side velocity (for a given mass flow rate), and therefore, the related pressure drop. The inner tube flow can be regarded almost entirely as a mass transfer media, with very little heat transfer taking place compared to the annulus flow. Therefore, the design should minimize the inner tube pressure drops by selecting suitable bayonet tube

diameter ratios, while simultaneously optimizing the heat transfer performance of the annulus. The selection of the optimum lengths, diameters and thicknesses, as restricted by the tube supplier's capabilities, depends on the following considerations: tubes as long as possible and practical for temperature rise/fall and economic reasons; minimizing of tube thicknesses while keeping within safety, reliability and manufacturing limits; and the variation of the outer tube outer diameter (while maintaining all other parameters constant). An example of the third consideration stated above is increasing the outer diameter which results in fewer tubes per module, a consequent reduction in total tube surface area per module, and a reduction in the module compactness. It would also result in an increase in the mass flow rate capacity of the module, and a reduction in the pressure drop penalty in the tubes [11].

1.3.2 Mechanical Properties of Ceramics

Over the past 25 years, ceramics have become key materials in the development of many new technologies because of their unique structures and properties. An understanding of the factors that influence their mechanical behavior and reliability is essential. Some of these new applications are structural and for this it is important to understand the factors that control their mechanical behavior. Non-structural applications are also being developed but in each case it is necessary to design mechanically reliable materials. This is a particular challenge for materials that are inherently brittle.[12] The approach to discuss mechanicals properties of ceramic can be divided based on different considerations like room-temperature mechanical behavior, high-temperature mechanical behavior, elastic deformation, and brittle failure. Also, based on the chemical composition and microstructure of the material, physical and mechanical properties can

vary tremendously. There are a large number of different chemical compositions that make ceramics involved in so many applications. The following applications are examples for each aspect of ceramic properties.

Table 1-1 Function and Technological Application of Ceramics [12]

Function	Primary Characteristic	Example of Application
Electrical	Electrical insulation (e.g., $A1_2O_3$, BeO)	Electronic substrates and packages, wiring, power-line insulators
	Ferroelectricity (e.g., $BaTiO_3$, $SrTiO_3$)	Capacitors
	Piezoelectricity (e.g., PZT)	Vibrators, oscillators, filters, transducers. actuators, spark generators
	Semiconductivity (e.g., $BaTiO_3$. SiC, $ZnO\text{-}Bi_2O_3$, CdS, V_2O_5)	NTC thermistor (temperature sensor) PTC thermistor (heater element, switch) CTR thermistor (heat sensor) Thick-film thermistor (IR sensor) Varistor (noise elimination surge arrestors) Solar cells, furnace elements
	Ionic conductivity (β-alumina, ZrO_2)	Solid state electrolytes (batteries, fuel cells, oxygen sensors)
	Superconductivity (YBCO)	Magnets, electronic components
Magnetic	Soft magnets (ferrites) Hard magnets (ferrites)	Magnetic recording heads Magnets electric motors
Optical	Translucency (AI_2O_3 MgO, mullite_ Y_2O_3 PLZT)	High-pressure sodium-vapor lamps, IR windows, lighting tubes and lamps laser materials, light memory, video display and storage, light modulation and shutters.
	Transparency (silicate glasses)	Magnets, Optical fibers, containers. Window components
Chemical	Chemical Sensors (ZnO, Fe_2O_3, SnO_2)	Gas sensors and alarms, hydrocarbon and fluorocarbon detectors, humidity sensor

	Catalyst carriers (cordierite, AI_2O_3)	Emission control, enzyme Carriers zeolites
	Electrodes (titanates. sulfides, borides)	Electrowinning, photochemical processes
Thermal	Thermal insulation (fiberglass aluminosilicate fibers)	IR radiators, thermal protection systems for aerospace vehicles
	Thermal conduction	Heat sinks in electronic devices
	Thermal stability (AZS, Al_2O_3)	Refractories
Structural	Hardness (SiC, TiC. TiN, Al_2O_3)	Cutting tools, wear-resistant materials, mechanical seals, abrasives armor, bearings
	Stiffness and thermal stability (SiC, Si_3N_4)	Ceramic engine parts, turbine parts, burner nozzles, radiant tubes crucibles.
Biological	Chemical stability (hydroxyapatite, Al_2O_3)	Artificial teeth, bones and joints
Nuclear	Nuclear fission (UO_2, PuO_2)	Nuclear fuels, power sources
	Neutron absorption (C, SiC, B_4C)	Cladding and shielding

1.3.3 Failure Criteria for Brittle Material

The extensive use of brittle materials in engineering application forced engineers to formulate the proper criteria needed to evaluate the strength and failure behavior of these materials. There are failure criteria already known for the ductile materials. Brittle materials have a different structure and failure behavior; therefore, it was necessary to modify these existing criteria or to use new criteria that are compatible with this structure. The Coulomb-Mohr failure criterion is a modified criterion of the maximum normal failure criterion. On the other hand, due to the scatter distribution of the brittle material behavior, the statistical approach was found as the proper approach to analyze and predict the failure behavior of the brittle materials. The Wiebull distribution is more appropriate for small strength values and simultaneously the volume dependences so that

the Wiebull distribution is used for calculation of the failure probability for small stresses and variable volume [14].

1.3.3.1 Coulomb-Mohr Failure Criteria

In the Coulomb-Mohr (C-M) criterion, fracture is hypothesized to occur on a given plane in the material when a critical combination of shear and normal stress acts on this plane. In the simplest application of this approach, the mathematical function giving the critical combination of stresses is assumed to be a linear relationship.

$$|\tau| + \mu\sigma = \tau_i \qquad 1\text{-}1$$

where τ and σ are the stresses acting on the fracture plane and μ and τ_i are constants for a given material. This equation forms a line on a plot of or σ versus $|\tau|$ as shown in Figure 1-3 .

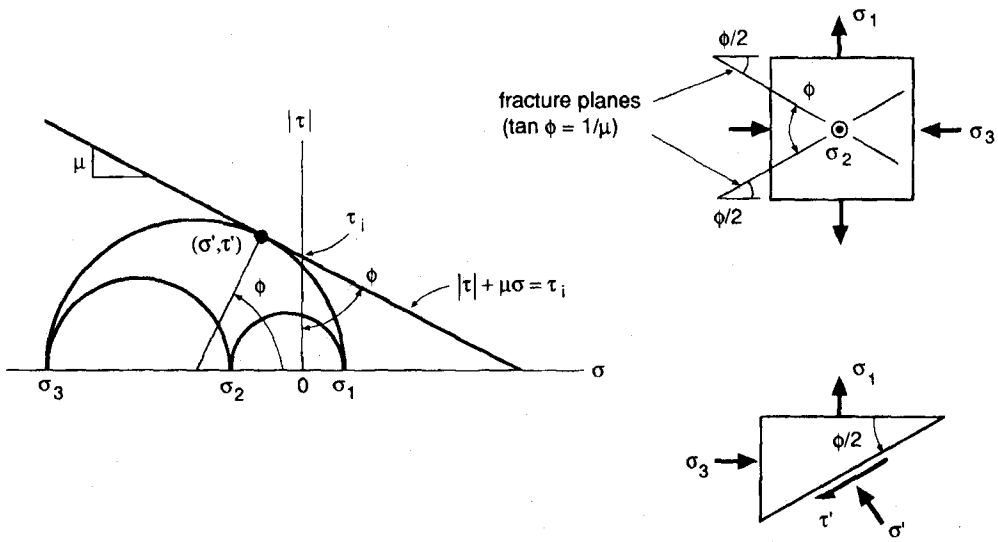

Figure 1-3 Coulomb-Mohr failure criterion as related to Mohr's circle and predicted failure plan[3].

The intercept with the τ axis is τ_i, and the slope is -□, where both τ_i and □ are defined as positive values. Now consider a set of applied stresses, which can be specified in terms of

the principal stresses, σ_1, σ_2, and σ_3, and plot the Mohr's circles for the principal planes on the same axes as Eq. 1-1. The failure condition is satisfied if the largest of the three circles is tangent to (just touches) the Eq. 1-1 line. If the largest circle does not touch the line, a safety factor greater than unity exists. Intersection of the largest circle and the line is not permissible, as this indicates that failure has already occurred. The line is therefore said to represent a failure envelope for Mohr's circle. The point of tangency of the largest circle to the line occurs at a point (σ', τ') that represents the stresses on the plane of fracture. The orientation of this predicted plane of fracture can be determined from the largest circle. In particular, fracture is expected to occur on a plane that is related to the plane where the maximum principal stress acts by a rotation $\phi/2$ in either direction. These planes are illustrated in Figure 1-3 . Also, from the geometry in Figure 1-3 , this angle ϕ can be related to the constant □.

$$\tan\phi = \frac{1}{\mu} \qquad 1\text{-}2$$

The shear stress τ' that causes failure is thus affected by the normal stress σ' acting on the same plane. In particular, τ' increases if σ' is more compressive. Such behavior is logical for materials where a brittle shear fracture is influenced by numerous small and randomly oriented planar flaws. More compressive σ' is expected to cause more friction between the opposite faces of the flaws, thus increasing the τ' necessary to cause fracture.

The Coulomb-Mohr can be expressed in terms of the principal normal stresses with the aid of Figure 1-3 .

$$\sigma' = \frac{\sigma_1 + \sigma_3}{2} + \left|\frac{\sigma_1 - \sigma_3}{2}\right| \cos\phi \qquad 1\text{-}3$$

$$|\tau'| = \left|\frac{\sigma_1 - \sigma_3}{2}\right| \sin\phi \qquad 1\text{-}4$$

where σ_1 and σ_3 are assumed to be the maximum and minimum principal normal stresses, respectively. Combining Eq. 1-1 with Eq. 1-3 and Eq. 1-4 and performing manipulation using simple trigonometric identities leads to

$$|\sigma_1 - \sigma_3| + m(\sigma_1 + \sigma_3) = 2\tau_u \qquad 1\text{-}5$$

Where the new constant m and τ_u are defined as the following

$$m = \frac{\mu}{\sqrt{1+\mu^2}} = \cos\phi \qquad 1\text{-}6$$

$$\tau_u = \frac{\tau_i}{\sqrt{1+\mu^2}} = \tau_i \sin\phi \qquad 1\text{-}7$$

Consider a test in pure torsion where at the fracture

$$\begin{aligned} &\sigma_1 = -\sigma_3 = \tau, \\ &\sigma_2 = 0 \end{aligned} \qquad 1\text{-}8$$

Substitution into Eq. 1-5 yields $\tau = \tau_u$, so that the constant τ_u the pure shear stress necessary to cause fracture. The corresponding largest Mohr's circle and predicted fracture plans are illustrated in the Figure 1-4

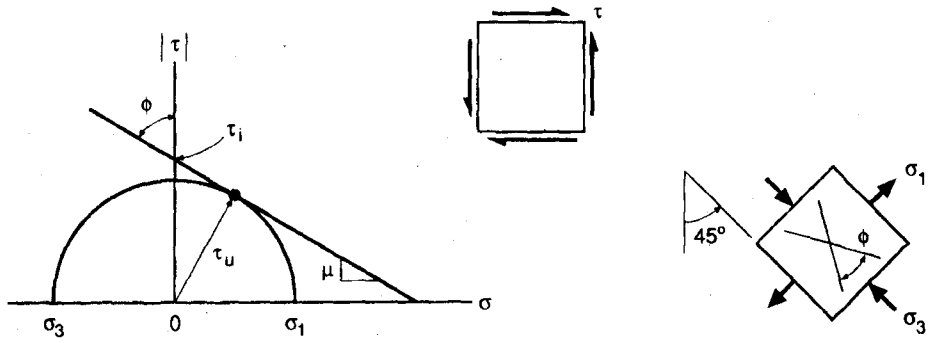

Figure 1-4 Pure torsion and the fracture planes predicted by the Coulomb-Mohr criterion [3]

Similarly applying Eq. 1-5 to uniaxial tension and compression tests gives the following equation for the ultimate strength in tension and compression σ_{ut} and σ_{uc} respectively.

$$\sigma_{ut} = \frac{2\tau_u}{1+m} \qquad 1\text{-}9$$

$$\sigma_{uc} = \frac{-2\tau_u}{1-m} \qquad 1\text{-}10$$

The Mohr's circles and predicted fracture planes for uniaxial tension and compression are shown in Figure 1-5 Eliminating τ_u form Eq. 1-9 and Eq. 1-10 gives the predicted relationship between σ_{ut} and σ_{uc}.

$$\sigma_{ut} = -\sigma_{uc}\left(\frac{1-m}{1+m}\right) \qquad 1\text{-}11$$

Also solving for *m* can give

$$m = \left(\frac{\sigma_{uc}+\sigma_{ut}}{\sigma_{uc}-\sigma_{ut}}\right) \qquad 1\text{-}12$$

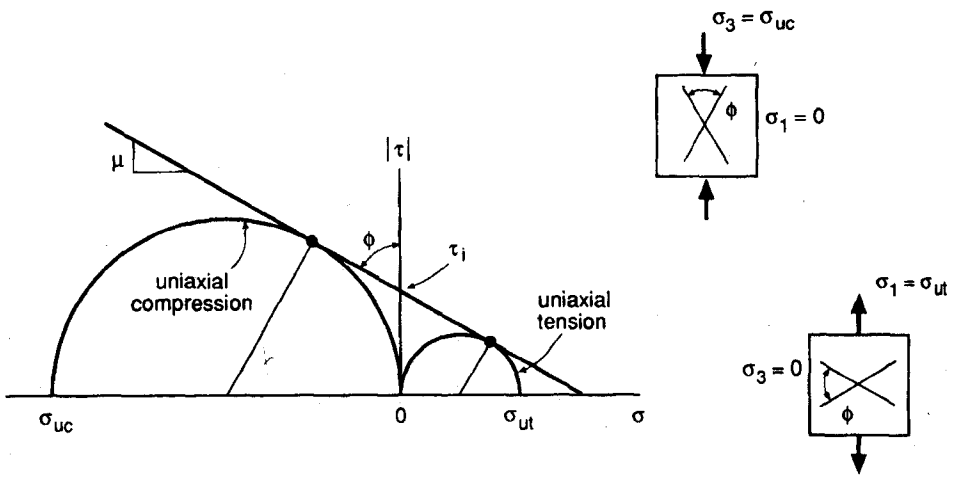

Figure 1-5 Fracture planes predicted by the Coulomb-Mohr criterion for uniaxial tests in tension and compression [3].

Thus, the Coulomb-Mohr criterion predicts that a single constant *m* can be used to relate the strengths in tension, compression, and shear. For positive values of *m*, the strength in tension is predicted to be less than that in compression, which is in agreement with the trend observed for brittle materials.

Coulomb-Mohr Criterion can be graphically represented if the subscripts for the principal stresses are assumed to be arbitrarily assigned, and then Eq.1-5 must be generalized to

$$|\sigma_1 - \sigma_3| + m(\sigma_1 + \sigma_3) = 2\tau_u \qquad 1\text{-}13$$

$$|\sigma_2 - \sigma_3| + m(\sigma_2 + \sigma_3) = 2\tau_u \qquad 1\text{-}14$$

$$|\sigma_3 - \sigma_1| + m(\sigma_3 + \sigma_1) = 2\tau_u \qquad 1\text{-}15$$

Note that these actually represent six equations due to the absolute values, fracture being predicted if any one of them is satisfied. For plane stress with $\sigma_3 = 0$, these reduce to

$$|\sigma_1 - \sigma_3| + m(\sigma_1 + \sigma_3) = 2\tau_u \qquad 1\text{-}16$$

$$|\sigma_3| + m(\sigma_3) = 2\tau_u \qquad 1\text{-}17$$

$$|\sigma_1| + m(\sigma_1) = 2\tau_u \qquad 1\text{-}18$$

The six lines represented by the latter equations form the boundaries of a region of no failure as shown in Figure 1-6.

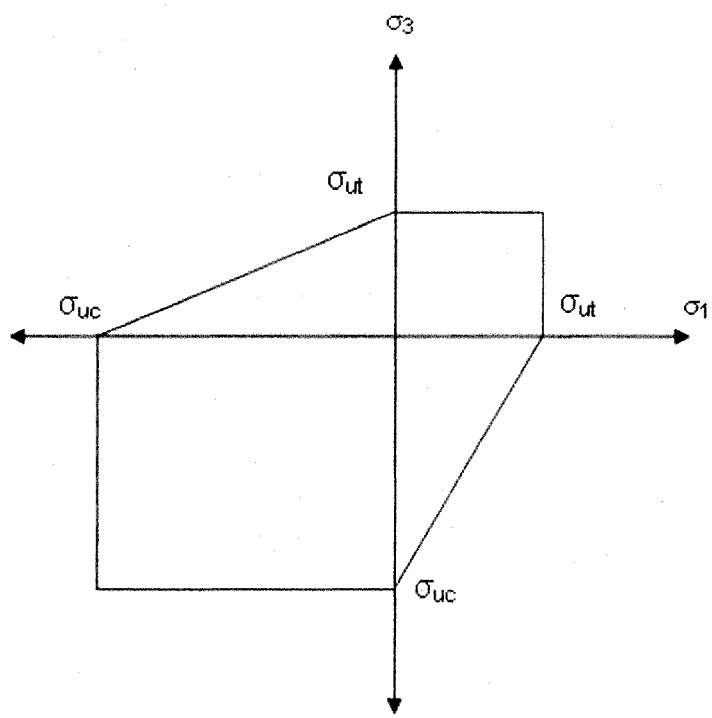

Figure 1-6 No failure locus for the Coulomb-Mohr failure criteria

The unequal fracture strengths in tension and compression are related to τ_u by Eq.1-9 and Eq.1-10 for the general case of a three-dimensional state of stress, Eq.1-13, Eq.1-14 and Eq.1-15 represent six planes that give a failure surface as shown in Figure 1-7. The

surface forms a vertex along the line $\sigma_1 = \sigma_2 = \sigma_3$ at the point

$$\sigma_1 = \sigma_2 = \sigma_2 = \frac{\tau_u}{m} \qquad 1\text{-}19$$

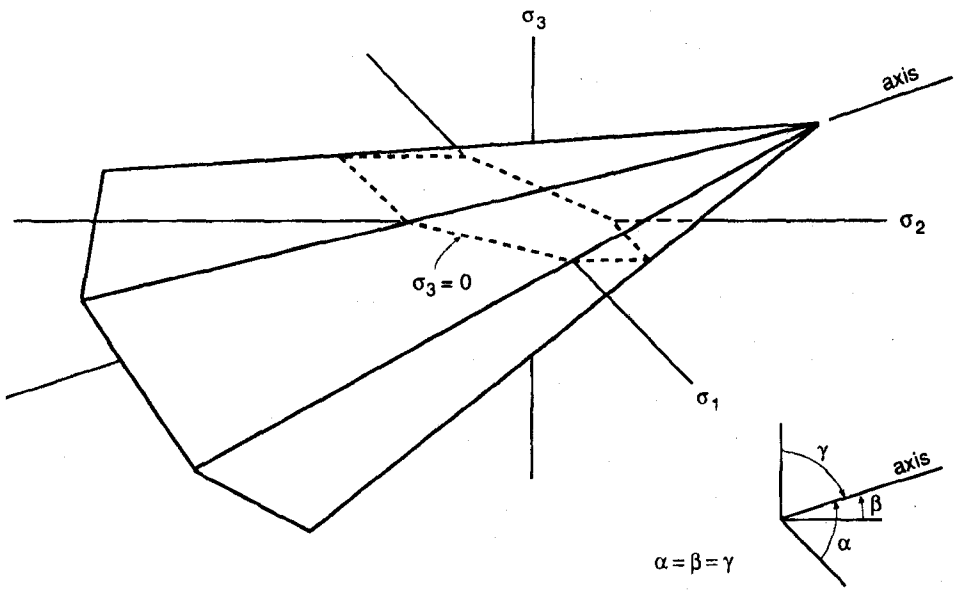

Figure 1-7 Three-dimensional failure surface for the Coulomb-Mohr fracture criterion [3].

Hence, the value of *m*, or of the closely related constant □, determines where the vertex is formed. Higher values of *m* or □ indicate that the six planes are tilted more abruptly relative to one another and form a vertex closer to the origin. If any one of σ_1, $\sigma_{2,\text{ or }}$ σ_3 is zero, the intersection of this surface with the plane of the remaining two principal stresses forms the shape of Figure 1-7. A cross section of the failure surface along a plane normal to the line $\sigma_1 = \sigma_2 = \sigma_{3\text{ forms}}$ a six-sided figure. However, due to the tilting of the planes relative to one another, such a cross section is not a regular hexagon, and it changes its size depending on the distance from the origin[3].

1.3.3.2 Wiebull Failure Criteria

Wiebull failure criteria comes form using Wiebull distribution for statistical analysis to describe the strength distribution of a brittle material. Wiebull distribution was proposed by Waloddi Weibull 1939. His theory can be summarized as: If a variable X is attributed to the individuals of a population, the distribution function (df) of X, denoted F(x), may be defined as the number of all individuals having an $X \leq x$, divided by the total number of individuals. This function also gives the probability P of choosing at random an individual having a value of X equal to or less than x, and thus we have

$$P(X \leq x) = F(x) \qquad 1\text{-}20$$

Any distribution function may be written in the form

$$F(x) = 1 - e^{-\varphi(x)} \qquad 1\text{-}21$$

This seems to be a complication, but the advantage of this formal transformation depends on the relationship

$$(1-P)^n = e^{-n\ \varphi(x)} \qquad 1\text{-}22$$

The merits of this formula will be demonstrated on a simple problem. If testing shows that the probability of failure is P for a given load x, which is applied to a single link. The probability of failure P_n for a chain consisting of n links, formulation have to be base upon the proposition that the chain as a whole has failed, if any one of its parts has failed. Accordingly, the probability of nonfailure of the chain, $(1-P_n)$, is equal to the probability of the simultaneous nonfailure of all the links. Form this $(1-P_n) = (1-P)^n$. If the df of a single link takes the form Equation 1-21, it will be available to obtain;

$$P_n = 1 - e^{-n\ \varphi(x)} \qquad 1\text{-}23$$

Equation 1-23 gives the appropriate mathematical expression for the principle of the

weakest link in the chain, or, more generally, for the size effect on failures in solids.

The same method of reasoning may be applied to the large group of problems, where the occurrence of an event in any part of an object may be said to have occurred in the object as a whole, e.g., the phenomena of yield limits, statistical or dynamical strengths, electrical insulation breakdowns, life of electric bulbs, or even death of man, as the probability of surviving depends on the probability of not having died from many different causes. The function $\varphi(x)$ is key element of the distribution. The only necessary general condition this function has to satisfy is to be a positive, nondecreasing function, vanishing at a value of $x = x_u$. The value of x_u is not of necessity equal to zero. The simplest function satisfying this condition is;

$$\left(\frac{x - x_u}{x_0}\right)^m \qquad 1\text{-}24$$

and thus

$$F(x) = 1 - e^{-\left(\frac{x - x_u}{x_0}\right)^m} \qquad 1\text{-}25$$

The only merit of this df is to be found in the fact that it is the simplest mathematical expression of the appropriate form, Equation 1-21, which satisfies the necessary general conditions. Experience has shown that, in many cases, it fits the observations better than other known distribution functions.

The objection has been stated that this distribution function has no theoretical basis. But in so far as the author understands, there are-with very few exceptions-the same objections against all other df, applied to real populations from natural or biological fields, at least in so far as the theoretical basis has anything to do with the population in question. Furthermore, it is utterly hopeless to expect a theoretical basis for distribution

functions of random variables such as strength properties of materials or of machine parts or particle sizes, the particles being fly ash, or even adult males.[13]

Measurement of the strength of a series of nominally identical ceramic specimens typically produces considerable scatter in the results. This phenomenon is easy to explain qualitatively as resulting from a scatter in the size of the cracks responsible for failure. The existence of this scatter has important engineering consequences. First, the strength that can safely be used in design is evidently less than the average measured strength. Second, the probability of failure of a large specimen is greater than a small specimen under the same stress, because of the larger probability of having a serious flaw in a larger volume. It is desirable to have some means of describing these effects quantitatively and incorporating this description into a method of design for safe use. Weibull statistics facilitate such a means. Weibull statistics is a form of extreme value statistics dealing with a weakest link situation in which the failure of a single element of a specimen causes failure of the whole specimen[14]. Using Weibull statistics to determine the probability of failure will be explained in the next section.

If any quantity, say, the strength σ, is measured repeatedly, say, N times, a series of values will be obtained: $\sigma_1, \sigma_2, \ldots \sigma_N$. The mean value is;

$$\sigma_m = \frac{1}{N}\sum_{i=1}^{N}\sigma_i \qquad 1\text{-}26$$

If the strength can assume only certain fixed values, the distribution function $p(\sigma)$ can be defined by

$$p(\sigma)=\frac{\text{Number occurrence of the value } \sigma}{\text{N}} \qquad 1\text{-}27$$

The distribution function for strength can be defined equivalently in terms of the number of strength value falling in successive equal intervals. When these values are not limited to certain fixed values. In either case the distribution so defined is normalized; that is,

$$\sum_{i=1}^{N} p(\sigma_i) = 1 \qquad 1\text{-}28$$

Or

$$\int_0^{\infty} p(\sigma)d\sigma = 1 \qquad 1\text{-}29$$

For continues distribution the mean can be written in terms of the distribution function as

$$\sigma_m = \sum_{i=1}^{N} \sigma_i p(\sigma_i) \qquad 1\text{-}30$$

Or

$$\sigma_m = \int_0^{\infty} \sigma\, p(\sigma)\, d\sigma \qquad 1\text{-}31$$

Other important quantities associated with the distribution are the deviation, the variance, and the standard deviation; the deviation, ε, is the amount that value differs from the mean.

$$\varepsilon_i = \sigma_i - \sigma_m \qquad 1\text{-}32$$

The variance s^2 is defined as

$$s^2 = \frac{1}{N-1} \sum_{1}^{N} \varepsilon_i^{\,2} \qquad 1\text{-}33$$

N-1 rather than *N* is used in this definition because one degree of freedom is used in calculating the mean. The standard deviation is defined as the square root of the variance.

The distribution $p(\sigma)$ defined above gives the probability of failure in an intervals σ to $\sigma + d\sigma$. The same behavior can be described by $P(\sigma)$, the cumulative probability of failure under all stresses up to the value σ. The two distribution function are related by

$$P(\sigma) = \int_0^{\sigma} p(x)\,dx \qquad 1\text{-}34$$

Or equivalently by

$$p(\sigma) = \frac{dP(\sigma)}{d\sigma} \qquad 1\text{-}35$$

Gaussian distribution is the most commonly used distribution for general treatment of experimental data. This distribution is usually described in terms of $p(\sigma)$, written in terms of the mean σ_m and the variance s^2 and normalized to give unit probability of failure when integrated over all stresses, the form of Gaussian distribution is

$$p(\sigma) = \frac{1}{s(2\pi)^{1/2}} e^{\left(-\frac{(\sigma-\sigma_m)^2}{2s^2}\right)} \qquad 1\text{-}36$$

Gaussian distribution can be used to represent the distribution of strength data for values not too far from the mean, but for small strength value it suffers from the fact that it gives a finite probability of occurrence of negative strength values. That is, it can not be corrected for strength values far below the mean. The Weibull distribution has a more appropriate form for small strength values and also brings in the volume dependence so that the Weibull distribution is used for calculation of failure probability for small stresses and variable volumes.

Weibull distribution, which is generally used for treatment of the statistics of brittle failure, is usually described in terms of $P(\sigma)$. The Weibull treatment of failure is in two parts (1) a weakest link argument leading to volume dependence for the average

strength and (2) the assumption of the distribution function. The weakest link argument is based on the idea that failure at any flaw leads to total failure and the material is homogeneous in the sense of the distribution of flaws throughout the volume (Weibull 1939). Consider a material divided into n equal volume elements δV_i under stress σ. Take $P_f(\sigma, \delta V_i)$ as the probability of failure from the stress for the ith volume element. The probability of survival of this element is $(1-P_f(\sigma,\delta V_i))$. Since the stress is taken to be the same for all volume elements and since the specimen is assumed to be homogeneous, all $P_f(\sigma, \delta V_i)$ can be taken the same, say $P_{f1}(\sigma)$. For the specimen to survive under the stress, all the volume elements must survive so that the total probability of survival, $1- P_f(\sigma, V)$, of a specimen of volume $V= n\,\delta V_i$ under uniform stress is given by

$$1-\mathrm{P}_f(\sigma, V) = \left(1-\mathrm{P}_{f1}(\sigma)\right)^n = \left(1-\frac{V\,\mathrm{P}_{f1}(\sigma)}{V}\right)^n$$
$$= [1-\frac{V}{n}\frac{\mathrm{P}_{f1}(\sigma)}{\delta V}]^n = [1-\frac{V\varphi(\sigma)}{n}]^n \qquad 1\text{-}37$$

where it is assumed that as δV decreases, $\frac{p_{f1}(s)}{dV}$ approaches a limit $\varphi(\sigma)$. For large values of n it is known that:

$$\lim_{n\longrightarrow\infty}\left(1-\frac{x}{n}\right)^n = e^{(-x)} \qquad 1\text{-}38$$

$$\lim_{n\longrightarrow\infty}\left(1-\frac{V\,\varphi(\sigma)}{n}\right)^n = e^{(-V\varphi(\sigma))} \qquad 1\text{-}39$$

So that

$$1-\mathrm{P}_f(\sigma, V) = e^{(-V\varphi(\sigma))} \qquad 1\text{-}40$$

The above equations show that the probability of failure of the specimen depends exponentially on the specimen volume times a function $\varphi(\sigma)$ that characterizes the stress dependence of cumulative failure probability per unit volume at a limit of small volume. This weakest link argument dose not give a specific form for $\varphi(\sigma)$. According to Weibull $\varphi(\sigma)$ was assumed to be as the following:

$$\varphi(\sigma) = \left(\frac{\sigma - \sigma_u}{\sigma_0} \right) \quad \text{for} \quad \sigma > \sigma_u \qquad 1\text{-}41$$

$$\varphi(\sigma) = 0 \quad \text{for} \quad \sigma \leq \sigma_u \qquad 1\text{-}42$$

This gives the Weibull distribution for the probability of survival of the whole specimen P_s and the probability of failure of the whole specimen P_f as

$$\mathrm{P}_s = 1 - \mathrm{P}_f = e^{\left(-V \left(\frac{\sigma - \sigma_u}{\sigma_0} \right)^m \right)} \quad \text{for} \quad \sigma > \sigma_u \qquad 1\text{-}43$$

$$\mathrm{P}_s = 1 - \mathrm{P}_f = 1 \quad \text{for} \quad \sigma \leq \sigma_u \qquad 1\text{-}44$$

Taking into consideration that, V must be nondimensional if σ_0 has dimension of stress, so that V should be expressed as V/V_0, where V_0 is some chosen unit volume. If V is instead absorbed into σ_0 then σ_0 must have dimension of stress times (volume)$^{1/m}$ this point is sometimes ignored in calculating the Weibull parameter from a set of data taken on specimen of constant volume. This procedure is equivalent to taking the specimen volume as the unit volume. When Weibull analysis applied to specimen of various volumes, the definition of V and σ_0 must be recalled and properly taken into account. Weibull's assumption of a form for the stress dependence of survival probability allows the treatment to be extended to the situation where the stress varies with the position in specimen. The result is

$$P_s = e^{\left(-\int_V \left(\frac{\sigma-\sigma_u}{\sigma_0}\right)^m dV\right)} \qquad 1\text{-}45$$

Weibull distribution function, $P_S(\sigma)$, contains three parameters: m, σ_u, and σ_0. These are generally treated as empirical parameters and determined experimentally. The parameter σ_u, is a stress level below which there is zero probability of failure. For a ceramic specimen, there is a remote possibility that a very large flaw exists. Therefore, it is customary to take $\sigma_u = 0$, which gives the most conservative estimate for survival probability. The resulting Weibull distribution is usually termed a two-parameter Weibull distribution. The process of determining the Weibull parameters m and σ_0 is easiest to describe using strength values of n specimens determined in a tensile test. The form of the Weibull function for constant stress can then be used. Two procedures are possible: (1) least-squares fitting of a linearized form of the distribution or (2) the method of maximum likelihood. The latter procedure is preferred by some authors but is more complicated, so that, discussion will focus on the first one. The least-squares method is in widespread use and is now discussed. Taking natural logarithms twice of the two-parameter Weibull distribution for tensile testing gives

$$\ln\ln\frac{1}{P_s} = \ln V + m\ln\sigma - m\ln\sigma_0 \qquad 1\text{-}46$$

The Weibull parameters can then be determined by fitting a straight line to ($\ln \ln(1/P_S)$) as a function of ($\ln \sigma$) [14]. The parameter m is simply the slope and σ_0 is related to the intercept on the ($\ln \ln(1/P_S)$) axis at $\ln \sigma = 0$ by as shown in Figure 1-8.

$$\ln V - m\ln\sigma_0 = \text{intercept} \qquad 1\text{-}47$$

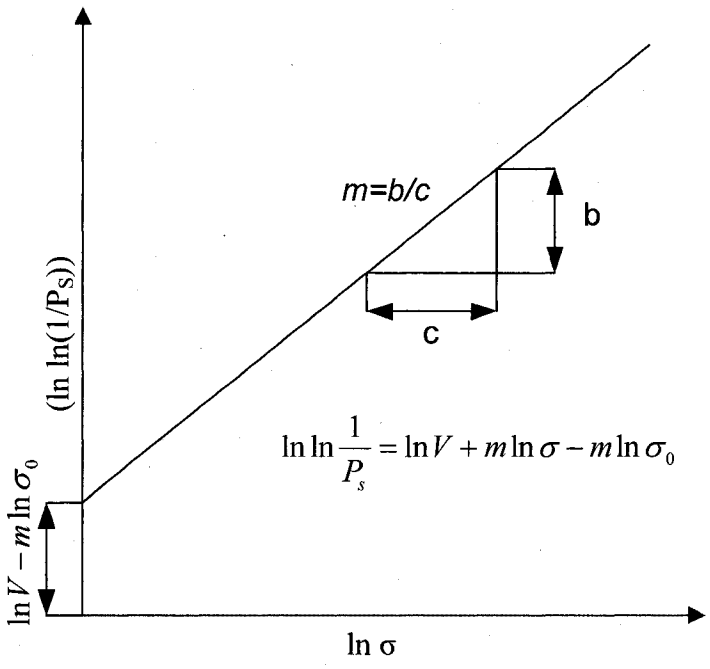

Figure 1-8 Weibull distribution for tensile testing fitted as a straight line

Here the point made earlier about the choice of how to treat V is evident again. Sometimes the volume term is simply ignored for a set of measurements taken on specimens having all the same volume and σ_0 is calculated from;

$$\sigma_0 = \left(e^{-(\ln V - m\ln\sigma_0)}\right)^{\frac{1}{m}} \qquad 1\text{-}48$$

CHAPTER 2

SIGNIFICANCE OF THE STUDY

Introduction

In this study a finite element model was created to simulate analyze and calculate the induced stresses due to the applied load. In this model the component will be divided into smaller units which called elements and each element has a number of nodes. These induced stresses could be extracted in two form of output: first, nodal solution which gives the stresses value at each node; second, elemental solution which gives the stresses value for the element surfaces. Since Coulomb-Mohr Failure criterion dealing with the state of stress at each point the nodal solution will be used for Coulomb-Mohr failure criterion calculation, on the other hand, Weibull failure criterion is dealing with; stresses applied to component that has a certain volume, the distribution of the cracks in that volume, and the chain theory that consider each element as single link of the chain, therefore, elemental solution will be used for Weibull failure criterion calculation. The significance of this study is explained in the following subsection.

2.1 Incorporation of Coulomb-Mohr Failure criterion within the finite element analysis

From the finite element model it will be applicable to extract the nodal solution of the first, second and third principal stresses σ_1, σ_2 and σ_3 that determine the state of

stress for each node. Figure 1-6 shows the envelop of Coulomb-Mohr failure criteria. The component will be safe if the state of the stresses lies inside this envelope which formed by six equations, Table 2 represents the expected cases and criterion requirement:

Table 2-1 Expected Cases for the Different Combination of States of Stresses

Case	Principal Stresses	Criterion requirements
Both in tension	$\sigma_1 > 0$, $\sigma_3 > 0$	$\sigma_1 > \sigma_{ut}$, $\sigma_3 > \sigma_{ut}$
Both in compression	$\sigma_1 < 0$, $\sigma_3 < 0$	$\sigma_1 > \sigma_{uc}$, $\sigma_3 > \sigma_{uc}$
σ_1 in tension, σ_3 in compression	$\sigma_1 > 0$, $\sigma_3 < 0$	$\frac{\sigma_1}{\sigma_{ut}} + \frac{\sigma_3}{-\sigma_{uc}} < 1$
σ_3 in tension, σ_1 in compression	$\sigma_1 < 0$, $\sigma_3 > 0$	$\frac{\sigma_1}{-\sigma_{uc}} + \frac{\sigma_3}{\sigma_{ut}} < 1$

The output of using Coulomb-Mohr failure criterion is factor of safety (SF). The value of the factor of safety should be more than one to prove the component is safe under this state of stresses. Mechanical properties of ceramics like ultimate tensile strength and ultimate compressive strength change with temperature, this change affect the envelope represented in Figure 1-6. Based on Coulomb-Mohr failure criterion calculation of factor of safety depends on: the calculated principal stresses σ_1, σ_2, and σ_3, the ultimate tensile strength and the ultimate compressive strength. The latter two parameters change with temperature. Form the finite element model the temperature distribution of the solid part is imported to ANSYS [15] by using the FLUENT's volume mapping function[16]. The strength of the heat exchanger material varies with temperature according the following equation for ceramic(SiC) [17],

$$\sigma_{ut} = (0.0142857)T + 200 \qquad MPa \qquad 2\text{-}1$$

Ultimate compressive strength for brittle martial is considered to be three multiplies tensile strength [3].

$$\sigma_{uc} = -3\,\sigma_{ut} \qquad 2\text{-}2$$

Figure 2-1 shows the graphical representation of how the calculation is conducted for example if there is a state of stress (A) at which (σ_1, σ_3) has value of (X,Y). The factor of safety (SF) is the ratio between the state of stress (A) and the point where a line starting at origin (O) and passing through (A) intersects the Mohr-Coulomb envelope.

$$SF = \frac{OB}{OA} \qquad 2\text{-}3$$

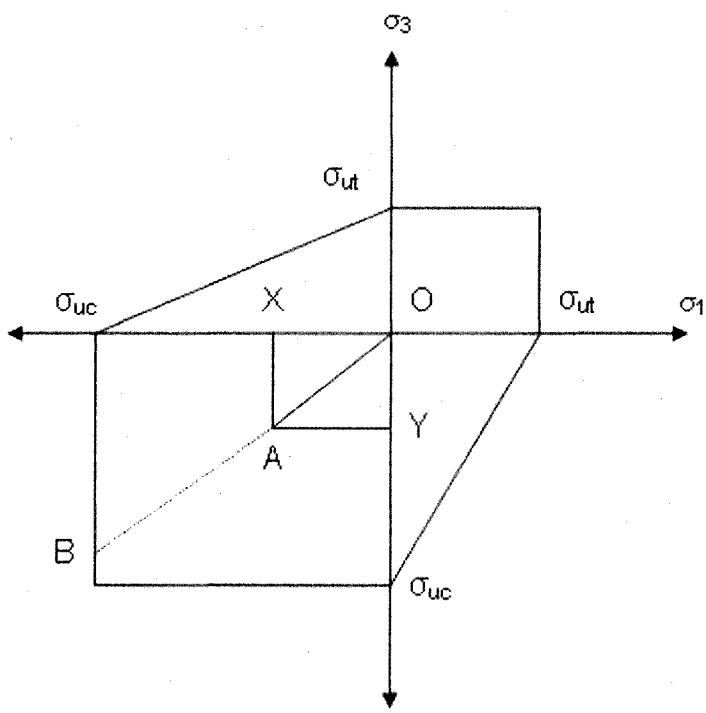

Figure 2-1 Graphical representation of safety factor calculation

To put this methodology in an effective form, a MATLAB code is created to calculate the value of factor of safety for each node using Coulomb-Mohr failure criteria. The program imports nodal principal stresses and temperatures as well as element nodal connectivity data and volumes. It follows these steps to calculate the factor of safety:

A. Substitute nodal temperature into Eq.2-1 and Eq.2-2 to calculate the material strength at each node.

B. Substitute principal stresses into the appropriate Coulomb-Mohr equation at each node.

C. Export factor of safety values for each node back to ANSYS for plotting.

D. Calculate an average factor of safety for each element using the following formula:

$$fse_i = \frac{\sum_{j=1}^{8} fsn_j}{8} \qquad 2\text{-}4$$

E. Calculate an overall factor of safety performance measure for the heat exchanger in the form of:

$$PM = \frac{\sum_{i=1}^{n_e} fse_i \, v_i}{\sum_{i=1}^{n_e} v_i} \qquad 2\text{-}5$$

2.2 Incorporation of Weibull Failure Criterion within the Finite Element Analysis

In recent years, the strength of ceramics has been routinely analyzed using Weibull statistics. This approach is very popular because of its ease of application. According to Weibull, the cumulative probability of failure of a brittle structure, which is subjected to an applied stress field σ, is generally written as:

$$P_f = 1 - e^{-\int_x \left(\frac{\sigma-\sigma_u}{\sigma_0}\right)^m dx} \qquad 2\text{-}6$$

The parameters m, σ_0, and σu are designated the Weibull modulus (shape parameter), the characteristic strength (scale parameter), and the minimum strength, respectively. The integral is defined as the risk of rupture R. The integration may be carried out over the entire specimen volume or surface area depending upon the location of failure-causing flaws. Accordingly, the variable x is replaced by area A or volume V [18] as the following:

$$P_f = 1 - e^{-\int_v \left(\frac{\sigma-\sigma_u}{\sigma_0}\right)^m dV} \qquad 2\text{-}7$$

If the above integration is computed over a unit volume and the value of σ_u taken to be zero, the probability of failure becomes,

$$P_f = 1 - e^{-\left(\frac{\sigma}{\sigma_0}\right)^m} \qquad 2\text{-}8$$

The above equation can be further rearranged,

$$ln\left(ln\left(\frac{1}{1-P_f}\right)\right) = m\, ln(\sigma) - m\, ln(\sigma_0) \qquad 2\text{-}9$$

The above equation represents a straight line equation between $\ln\left(\ln\left(\frac{1}{1-P_f}\right)\right)$ and $ln(\sigma)$.

The parameters of the equation, m and σ_0, are usually based on the results of testing specimens. The above approach can be adapted in finite element analysis by performing numerical integration of $((\sigma_i-\sigma_u)/\sigma_0)^m$ over the volume as shown in the following equation:

$$P_f = 1 - e^{-\sum_{i=1}^{N}\left(\left(\frac{\sigma_i-\sigma_u}{\sigma_0}\right)^m v_i\right)} \qquad 2\text{-}10$$

where, N is the total number of elements

v_i is a nondimensional volume of element *i,* which is expressed in form of (V_i/V)

V_i is the actual volume of element *i,*

V is the total volume of the solid part

The following steps can be used to incorporate Weibull distribution within finite element analysis to calculate the probability of failure:

1. For each element, extract element volume (V_i), element nodal connectivity information, and the three principal stresses σ_{i1}, σ_{i2}, and σ_{i3}.
2. Extract nodal temperatures.
3. Calculate average temperature for each element.
4. Calculate the mechanical strength of the material at the temperature obtained in the previous step according to Eq.1-30
5. If stress is compressive equates it to zero as ceramics mainly fail due to tensile stresses. Calculate the probability of failure of the solid part for each of the three principal stresses.

Temperature distribution of the solid part of the decomposer is imported to ANSYS [15] by using the volume mapping function of FLUENT [16]. Thermal loads are used to calculate stresses in the solid part of the model. As mentioned earlier, a uniform pressure of 1.5 MPa is applied to all surfaces that are adjacent to fluid flow.

2.3 Determination of Factor of Safety and Probability of Failure of Ceramic Components in HTHX under Steady State Conditions

The temperature distribution in solid part under steady state condition is imported in a proper format to ANSYS software. This temperature distribution is used as a thermal

load that induce stresses in solid part. ANSYS software is used to calculate these stresses. Factor of safety and probability of failure are calculated based on the output of ANSYS. Results of this research can be used as a basis for investigation optimal design of the decomposer that can provide maximum chemical decomposition performance while maintaining stresses within design limits.

2.4 Determination of Factor of Safety and Probability of Failure of Ceramic Components in HTHX under Transient Conditions

The induced stresses depend on the temperature difference. It is expected that, startup and shutdown of the decomposer will induce higher stresses, therefore it was important to calculate the probability of failure of the decomposer under transient regimes, which is the focus of this work. Literature survey failed to find directly relevant work due to the novel nature of the proposed heat exchanger and decomposer with micro-channels.

CHAPTER 3

MODELING OF THE HEAT EXCHANGER AND CHEMICAL DECOMPOSER MICRO-CHANNEL DESIGN

3.1 Preliminary Data

The real designs of the shell, plate heat exchanger and decomposer were developed by Ceramatec's Inc. (Salt Lake City, USA) and shown in the Figure 3-1 the geometry of the heat exchanger was designed according to the process design of sulfur-iodine cycle. The process design of the sulfur- iodine cycle is shown in Figure 3-2 this cycle consists of three chemical reactions that result in the dissociation of water. The sulfur–iodine cycle was proposed by General Atomics in the mid-1970s. It consists of the following three chemical reactions that yield the dissociation of water [2]:

$$I_2+SO_2+2H_2O \rightarrow 2HI+H_2SO_4 \quad (120°C \text{ min.}) \qquad (1)$$

$$H_2SO_4 \rightarrow H_2O+SO_2+\tfrac{1}{2}O_2 \quad (850°C \text{ min.}) \qquad (2)$$

$$2HI \rightarrow H_2+I_2 \quad (450°C \text{ min.}) \qquad (3)$$

The whole process takes in water and high-temperature heat, and releases hydrogen and oxygen as shown in Figure 3-3 . All reactions are in fluid interactions. All reagents are to be recycled; there are no effluents. Each of the chemical reactions in this process was demonstrated in the laboratory. Japan Atomic Energy Research Institute has also worked on the research, development and demonstration of the sulfur–iodine cycle. Decomposition of sulfuric acid and hydrogen iodide involve aggressive chemical

environments. Hence, the material candidates for the sulfur–iodine cycle hydrogen plant should be chosen carefully to accommodate corrosion problems as well [19].

One of the important and critical parts of the plant is the high temperature heat exchanger for SI (Sulfuric Acid) Processes - Preheater & Decomposer. The processes in the part of the plant are shown schematically in Figure 3-2 . The SI decomposer is used as part of the plant for hydrogen production. To obtain the design optimization of a SI decomposer, a three-dimensional conjugate heat transfer and fluid flow numerical model was developed for this reason[19].

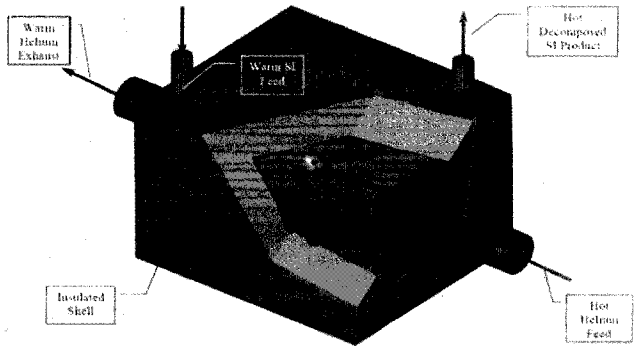

Figure 3-1 Shell and plate heat exchanger.

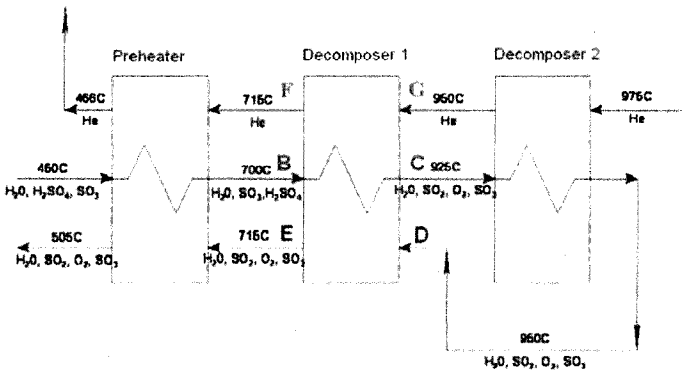

Figure 3-2 Process Design.

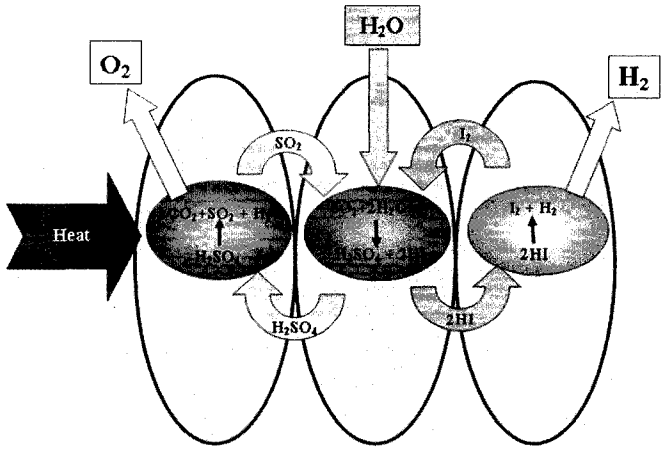

Figure 3-3 Sulfur-Iodine Thermo Chemical Water Splitting Cycle

The hot helium from nuclear reactor (T=975°C) is used to heat the SI feed components (H_2O, H_2SO_4, SO_3) to get appropriate condition for the SI decomposition reaction (T>850°C).

For this study the process analysis and optimization of the Decomposer 1 Figure 3-2 was performed. The main reason why the Decomposer 1 was chosen for the study is because the Decomposer 1 is much more complex comparing with Preheater and Decomposer 2 due to the presence of chemical reactions. [19]

3.1.1 Material Properties

Decomposition of sulfuric acid and hydrogen iodide involve aggressive chemical environments. Hence, the material candidates for the sulfur–iodine cycle hydrogen plant should be chosen carefully to accommodate corrosion problems as well. At least three major classes of high-temperature materials provide promising candidates for these applications:

1) High-temperature nickel-based alloys (e.g. Hastelloy): Good materials compatibility potential for helium and molten salts up to temperatures in the range of 750°C. Also a

candidate material for sulfuric acid thermal decomposition. Limited capability under fusion neutron irradiation.

2) High-temperature ferritic steels (particularly oxide-dispersion ferritic steels): Good performance under fusion and fission neutron irradiation, to temperatures around 750°C. Good potential for compatibility with lead/bismuth under appropriate chemistry control. Demonstrating compatibility with molten salts would have substantial value for the fusion application. Silica bearing steels provide a candidate material for sulfuric acid thermal decomposition.

3)Advanced carbon and silicon carbide composites: With excellent mechanical strength to temperatures exceeding 1000°C, these are now used for high temperature rocket nozzles to eliminate the need for nozzle cooling and for thermal protection of the space shuttle nose and wing leading edges. Many options are available that trade fabrication flexibility and cost. Neutron irradiation performance, and coolant compatibility can potentially be used with helium and molten salt coolants. Silicon carbide is also compatible with sulfur-iodine thermochemical hydrogen production. Major opportunities and research challenges exist to apply these materials to high-temperature heat transport applications. Form the above three options advanced carbon and silicon carbide was selected as an excellent material that can maintain it's mechanical properties at high temperature and can resist corrosion at the same time.

The primary concern in the use of advanced ceramics in structural applications has continued to be the issue of reliability. In the past, it has not been unusual that different batches of a given material prescription would yield measurably distinct characteristics. More recently, however, the production characteristics of several advanced ceramic

materials have matured sufficiently that their material properties are routinely reproducible as judged by the consistency of numerous studies in independent laboratories. Furthermore, progress in concurrent engineering and electronic product design tools such as the evolving Standard for the Exchange of Product Data (STEP) has increased the need for well defined data sets. Consequently, it has become meaningful and desirable to construct and assess comprehensive set of properties that characterize these materials.

Sintered α-SiC has evolved as a major structural ceramic with applications that include heat exchangers for high temperature and aggressive environments, seals, bearings, and wear resistant components. Several reviews of the properties of silicon carbide have contributed to this evolution by delineating the ranges of performance characteristics that can be expected for this general class of materials.

Sintered α-SiC ceramics typically are produced using submicrometer powders that have been extracted from an Acheson furnace and ground to a fine particle size. Boron and carbon are used as sintering aids to achieve improved densification during sintering which is typically conducted at a temperature on the order of 2500 °C. The resulting microstructure consists predominantly of fine, equiaxed grains of the hexagonal SiC polytype 6H. A small amount of free carbon and isolated B_4C grains may be present also as remnant artifacts of the sintering aids.

Since the properties of ceramics can vary significantly with composition and microstructure, it is important to restrict attention to a consistently defined material specification. In this study, the material specification is patterned after a commercial material, Hexoloy SA™, abbreviated here as SA, for which a considerable amount of data

can be gleaned from numerous independent studies. For this material, the density is approximately (98 ± 1)% of the density of single crystal SiC(6H) with a mean grain size of (6±1) μm. The mass fractions of boron and free carbon in the sintered composition are (0.4± 0.1) % and (0.5±0.1) % respectively. The combined standard uncertainties for these values are estimated using the standard deviation of the respective reported values[17].

Using of sintered α-SiC in HTHX raise the point of how the properties of this material will change with temperature. The following section will show some of these properties and their changes with temperature. According to Munro[17], thermal conductivity of the α-SiC is temperature-dependent as shown in Figure 3-4.

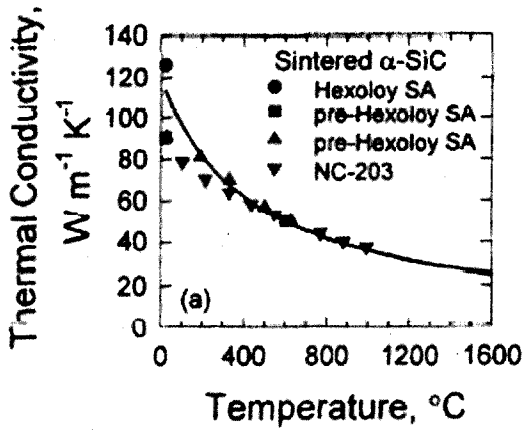

Figure 3-4 Thermal conductivity of sintered α-SiC with temperature [17].

Out of this data a polynomial represents the relation between the thermal conductivity of the sintered α-SiC with temperature were developed as in Eq. 3-1 [19]

$$k_{SiC} = 1.94777 \cdot 10^{2} - 3.60612 \cdot 10^{-1} \cdot T + 3.30843 \cdot 10^{-4} \cdot T^{2} - 1.46006 \cdot 10^{-7} \cdot T^{3} + 2.47588 \cdot 10^{-11} \cdot T^{4} \quad 3\text{-}1$$

Density and specific heat of the α-SiC do not depend on the temperature significantly are shown in Figure 3-5 and Figure 3-6. Therefore, the properties are assumed as constant for the design temperature range properties, for the temperature range (973~1223°K): ρ_{SiC}=3130 kg/m3; Cp_{SiC}=1200 J/(kg·K).

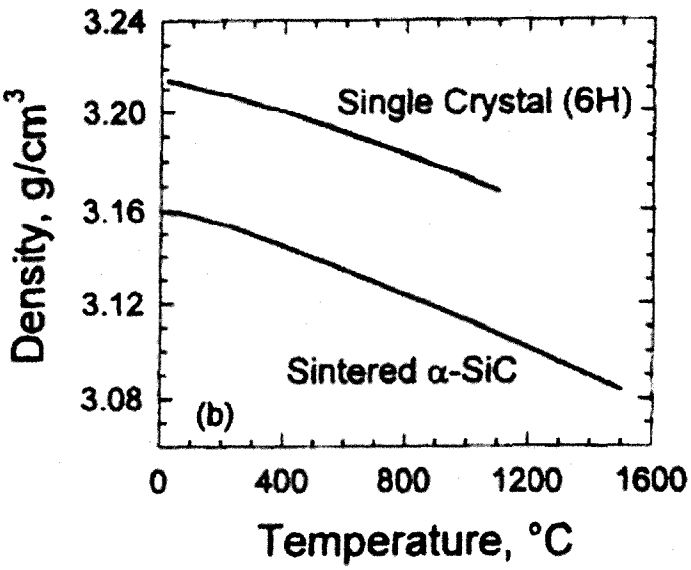

Figure 3-5 Density of sintered α-SiC with temperature [17].

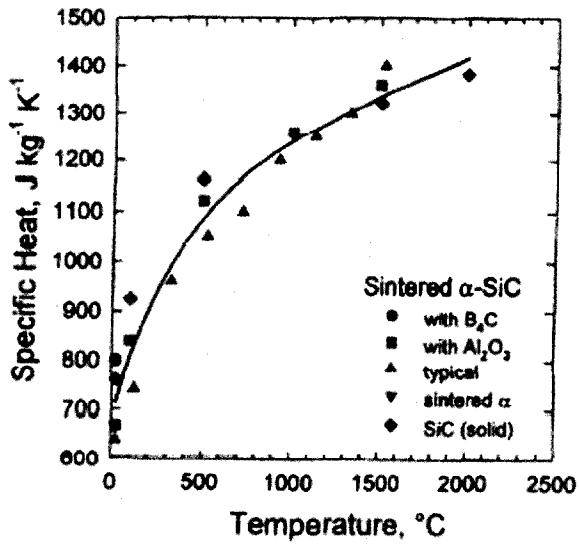

Figure 3-6 Specific heat of the variety of sintered α-SiC material [17].

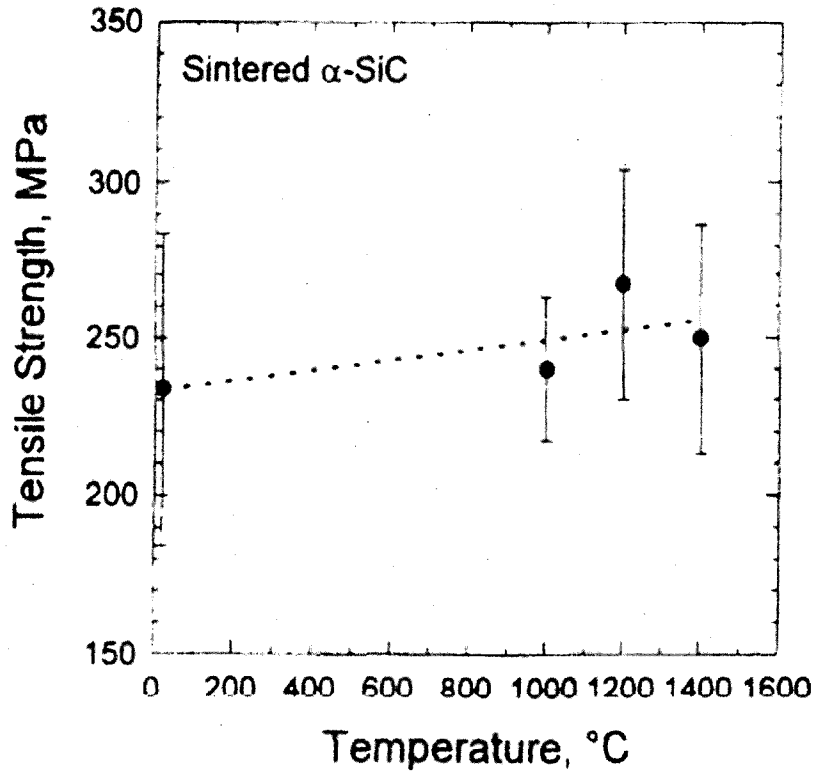

Figure 3-7 Tensile strength of sintered α-SiC with temperature [17].

Tensile strength of sintered α-SiC varies with temperature is shown in Figure 3-7 Out of the data represented in Figure 3-7 a polynomial represents the relation between tensile strength of the sintered α-SiC and temperature were developed as in Eq. 3-2. In this polynomial the constant (0.0142857) represents the slope of the straight line. The 200 represent the intercept of the line with the tensile strength axis. It is noticed on the figure that there is a range for each point. The lower limit for the points was considered to form Eq 3-2. This relation is used in the calculation of safety factor or probability of failure. The compression strength will be calculated also by using Eq. 3-3 [19]

$$s_{ut} = (0.0142857)T + 200\,MPa \qquad 3\text{-}2$$

The ultimate compression strength was determined according to the assumption that it is three time of the tensile strength for brittle material [3].

$$s_{uc} = -3\, s_{ut} \qquad 3\text{-}3$$

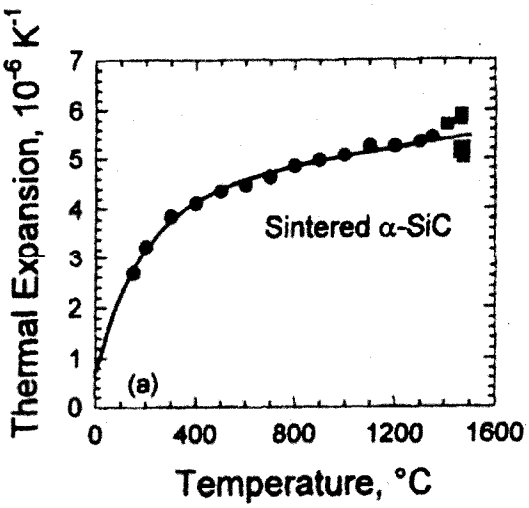

Figure 3-8 Change of thermal expansion with temperature [17].

Thermal expansion to several temperatures have been reported and it is shown in Figure 3-8. Elastic properties of sintered α-SiC structural ceramics are relatively stiff materials whose elastic properties like elastic modulus, shear modulus, and passion ratio exhibit relatively weak temperature dependencies, and the polycrystalline sintered specimens tend to have isotropic elastic moduli as shown in Figure 3-9. Also the change of passion ratio with temperature is shown in Figure 3-10.

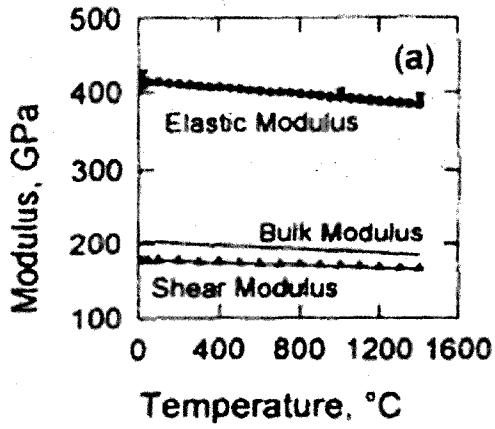

Figure 3-9 Change of Elastic Modulus, Bulk Modulus and Bulk Modulus with temperature [17].

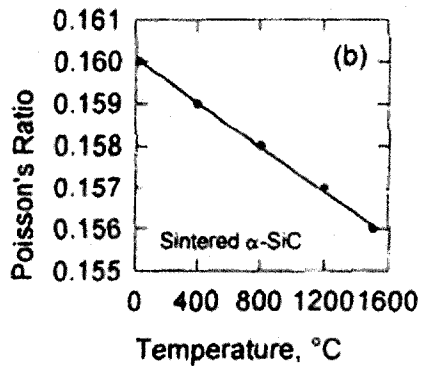

Figure 3-10 Change of passion ratio with temperature [17].

3.1.2 Geometry and dimensions

The geometry of the baseline SI decomposer is shown in Figure 3-11, which represents a cross section through the design of Figure 3-1. A computational model for a single channel is developed to reduce computation load. It has only one half of an internal channel due to the existence of a symmetry plane. It is also assumed that a uniform flow rate distribution for all of the plate channels occurs.

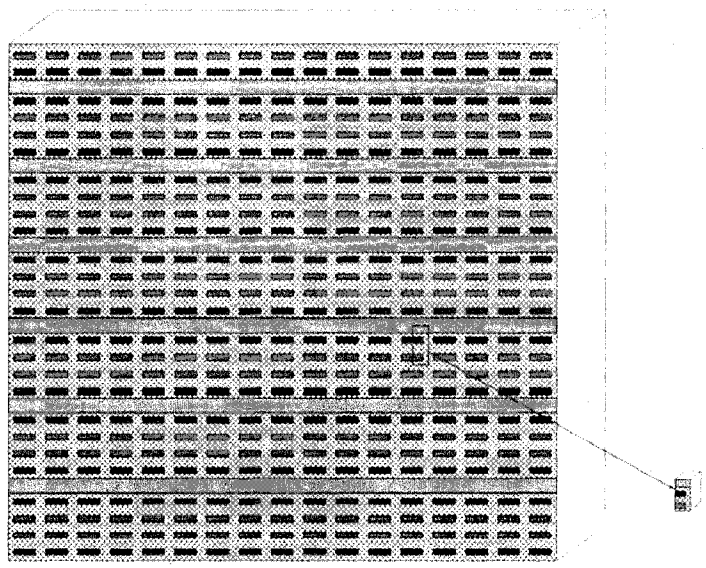

Figure 3-11 Extraction of the single channel geometry from the large scale design [20].

As it shown in Figure 3-11 the assembly of that design is made out of staked layers of silicon carbide. These layers have different geometries that form channels to allow different fluid to flow in their passages. Figure 3-12 shows the different layers and Figure 3-13 shows the assembly of these layers. The original dimensions for the geometry (baseline design) along with the different fluid legend are shown in Figure 3-14.

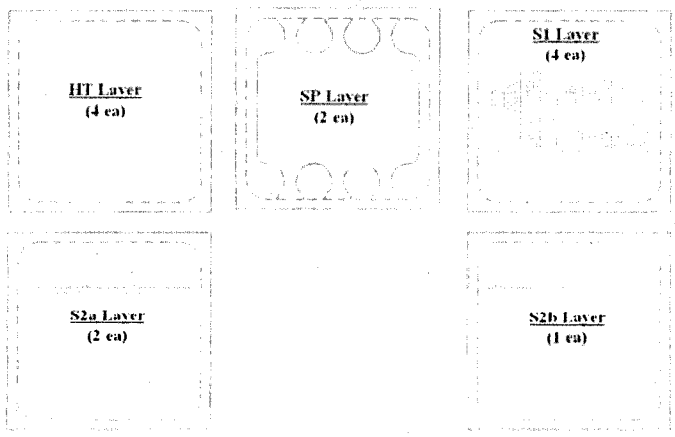

Figure 3-12 Layers of Decomposer [20]

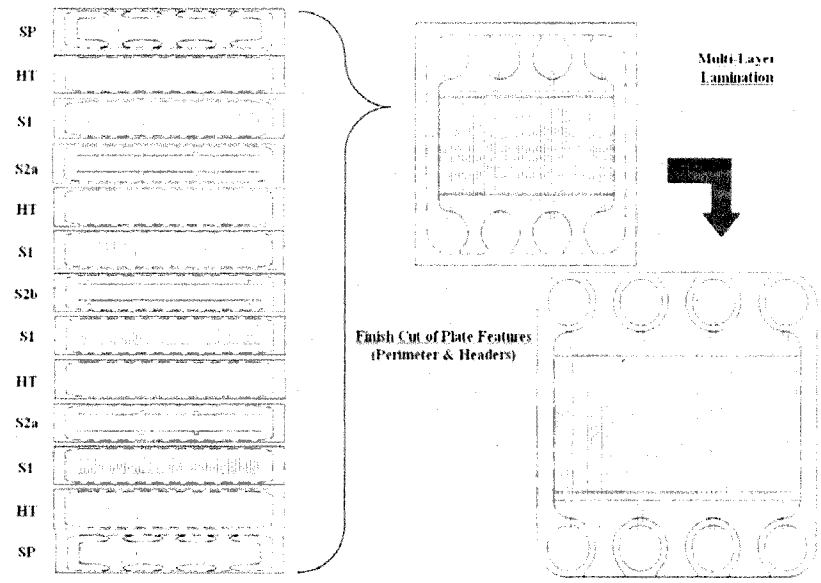

Figure 3-13 Schematic of Decomposer assembly [20]

$h_{SP} = 0.85\,mm;$ $h_{HT} = 0.3\,mm;$ $h_{S1} = 0.424\,mm;$
$h_{HT+S2a} = 0.75\,mm;$ $h_{1/2S2b} = 0.225\,mm;$
$W_1 = 0.635\,mm;$ $W_2 = 0.381\,mm;$ $L = 52.324\,mm.$

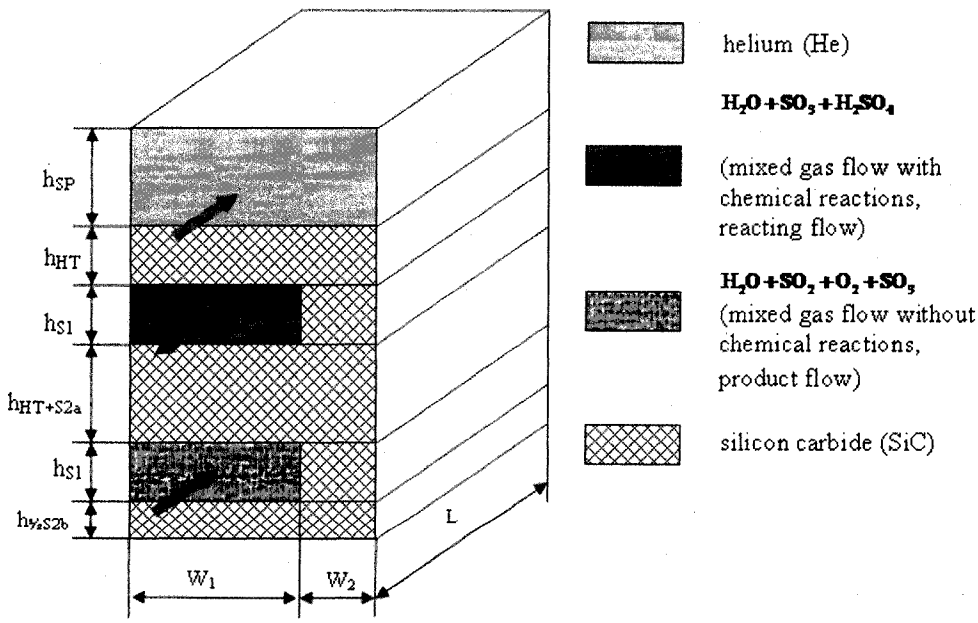

Figure 3-14 Sketch of the single channel geometry [20]

3.1.3 Boundary and Operating Condition

The boundary conditions on the top, bottom, left and right sides are planes of symmetry. The thermal boundary conditions for the front and back sides are adiabatic conditions. Inlet velocity profiles are uniform and they were calculated by using area, density and mass flow rate. For outflow conditions, the pressure-outlet boundary conditions are used (pressure outlet boundary conditions require the specification of a static (gauge) pressure at the outlet boundary; all other flow quantities are extrapolated from the interior). The operation pressure is 1.5 MPa. Figure 3-15 shows the boundary conditions used in stress analysis[20]. The boundaries of the calculation domain are shown in Figure 3-16.

Inlet conditions for He part: $\dot{m}=2.8175\cdot10^{-6}$ kg/sec; T=1223.15°K (950°C).

SI inlet for reacting flow: $\dot{m}=6.296\cdot10^{-6}$ kg/sec; T=974.9°K (701.75°C);

$x_{SO_3}=0.8163$; $x_{SO_2}=0$; $x_{O_2}=0$; $x_{SO_3}=0.1837$

SI inlet for non-reacting flow: $\dot{m}=6.296\cdot10^{-6}$ kg/sec; T=974.9°K (701.75°C);

$x_{SO_3}=0$; $x_{SO_2}=0.6532$; $x_{O_2}=0.1631$; $x_{SO_3}=0.1837$

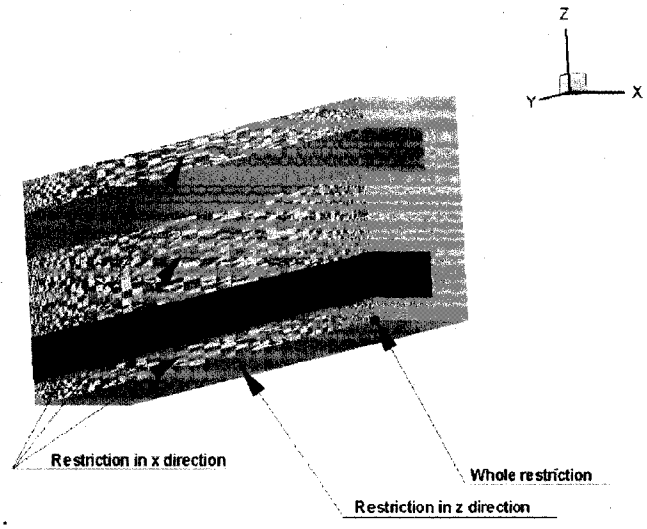

Figure 3-15 Displacement restrictions for the stress analysis [20]

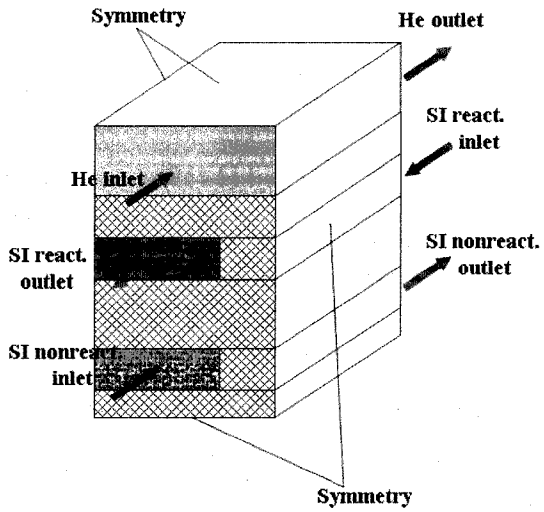

Figure 3-16 Schematic of boundaries [20]

3.2 Finite Element Model

The finite element model was developed to investigate different aspects of the proposed design. Since the SI thermochmical cycle includes chemical compositions enter the ceramic microchannel of the decomposer at certain flow rates and temperatures, it

was necessary to analyze and optimize the design from chemical decomposition, heat transfer, fluid flow, and stress analysis point of views.

Two different methods for optimization studies of Ceramatec sulfuric acid decomposer have been investigated:

(a) The first method is to use APDL (ANSYS parametric design language) code for optimization studies. The geometry, mesh, and boundary and initial conditions can be adjusted by using this code. The code uses commands of the ANSYS Multi-field solver for the simulation fluid, thermal and structure parts of the decomposer. With the APDL code, all of the modules, which include the fluid flow, heat transfer and stress analysis, are solved separately. During the calculation, the solver iterates between each physics field until loads transferred across the physics interfaces converge. The method includes the calculations of geometry deformations as result of thermal and mechanical stresses. Because of the geometry deformations, the mesh regeneration procedure occurs during the each iteration. But according to the investigations, for the Ceramatec sulfuric acid decomposer, the influence of the geometry deformations on the resulting parameters distributions is negligible. Therefore, it is not necessary to regenerate mesh as result of the material deformations for the current optimization study.

(b) The second method is to use FLUENT software for the fluid/thermal analysis of whole decomposer and use ANSYS software for the stress analysis of the solid structure of the decomposer. In this model, the temperature distribution of the solid part was imported to ANSYS by using the FLUENT's volume mapping user defined function (UDF). For this method, the mesh independence study on the data transferring procedure

from FLUENT to ANSYS has been accomplished. According to the study, the error for the data transferring is less than 1% even for coarse mesh.

A comparison between the two methods showed that the second method works much faster than the first one and the second method is more reliable for the flow/thermal analysis. Therefore, the second method of analysis has been chosen for the all of the optimization studies [21].

Preliminary CFD analysis showed that mass flow rate in all channels can be made almost uniform with the proper design of channel manifolds. Therefore, a single-channel model is developed to reduce computation load without sacrificing the accuracy of the calculations. Due to the existence of a symmetry plane, the developed model includes only one half of an internal channel [20].

3.2.1 Geometry and Mesh Creation

The geometry and mesh files have been created using mesh generator Gambit version 2.0.4. For optimizing the geometry, a Gambit journal file was used. With the help of the journal file, it is possible to change any geometrical parameter of the investigated section. The example of the mesh for the base case is shown in Figure 3-17.

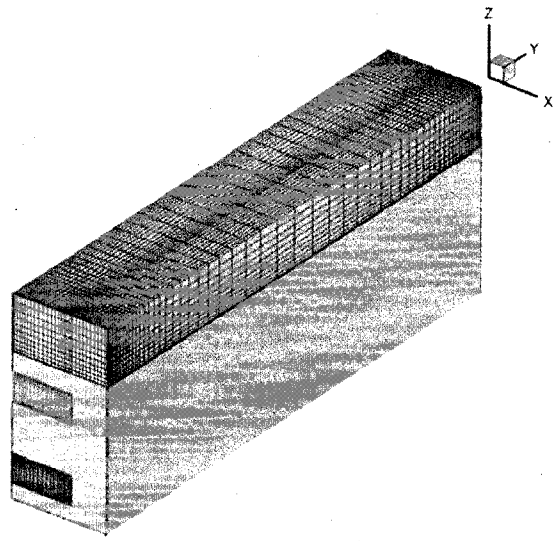

Figure 3-17 Computational mesh (163,735 nodes, 145,800 cells)[20]

Mesh refinement is an important parameter in finite element analysis that affects the required computational power if the mesh is refined more than enough, or it affects the result accuracy if the mesh is coarse. In the current study, the mesh is refined wherever solid and fluid meet. Mesh stability studies are performed.

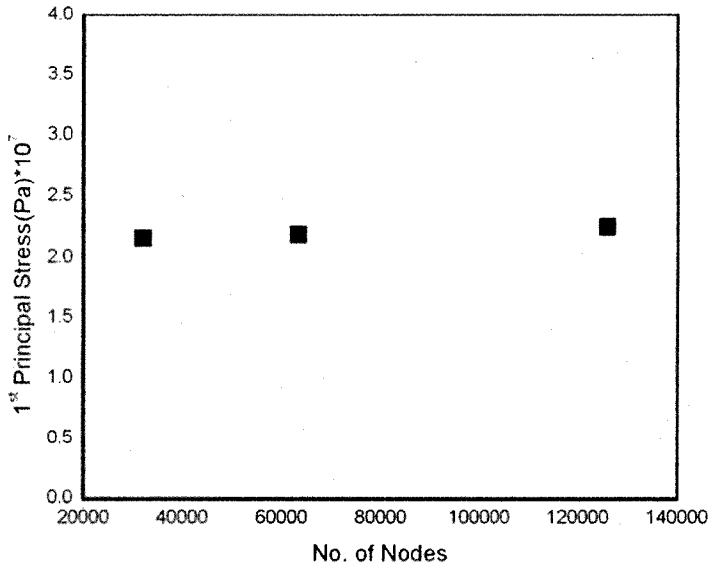

Figure 3-18 Mesh independence study for the baseline design

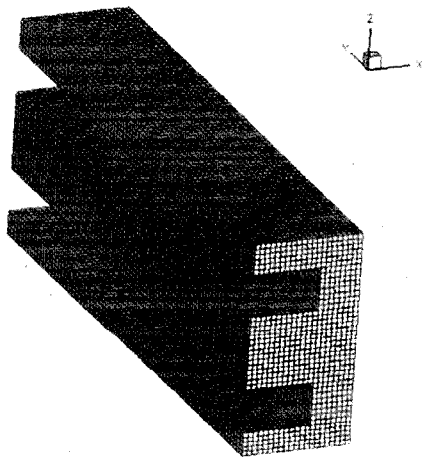

Figure 3-19 Computation mesh for the stress analysis (63,342 nodes 55,200 cells) [20]

3.2.2 Extraction and Data Processing

The finite element model has already imported to ANSYS to calculate the nodal and elemental solutions for the applied load. The process generally includes three consecutive phases: First, extract the nodal and elemental solutions of the stress analysis calculation in a proper format. APDL code was created to extract these solutions. This code is listed in Appendix A under the name of "dataextraction" [A.1]. Second, processing these extracted solutions to calculate the factor of safety and probability of failure. Matlab codes were created to conduct these calculations. These codes are listed in Appendix B under names of "mohr.m" [B.1] for factor of safety calculation and "probability.m" [B.2] for probability of failure calculation. Third, the factor of safety results for each node is plotted by using ANSYS APDL code. The code is listed in appendix A under name of "resultplotting.txt"[A.2]. Figure 3-20 through Figure 3-22 show the nodal solution for the three principal stresses associated with the applied thermal and pressure loads. Factor of safety and probability of failure were calculated for the baseline design. Figure 3-23 shows that the resulting nodal factor of safety is extremely high, as the decomposer does not experience significant thermal gradient effects. Calculated overall factor of safety PM equals 183. The probability of failure for the three principal stresses σ_1, σ_2, σ_3 was (0, 0, 0) respectively.

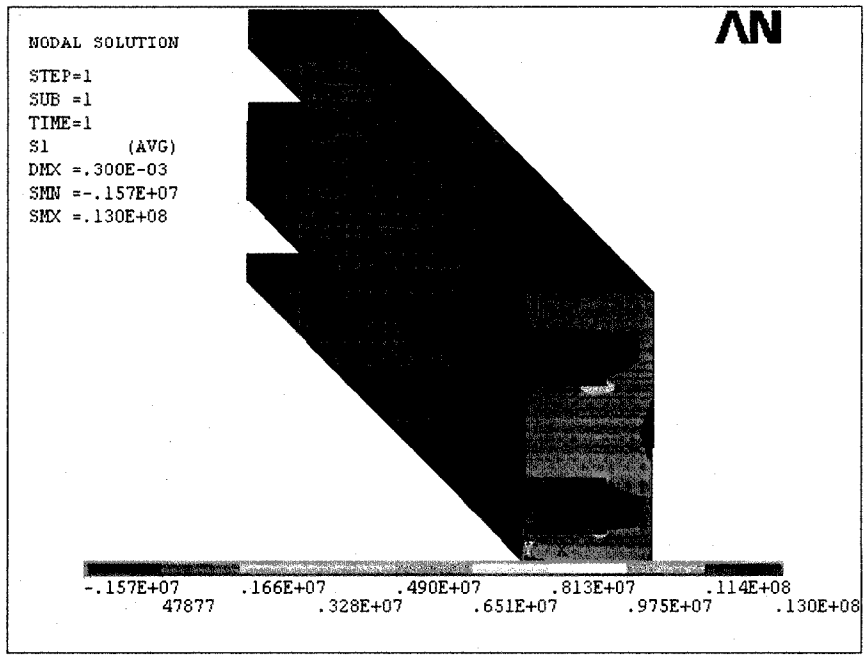

Figure 3-20 First principal stress distribution, Pa

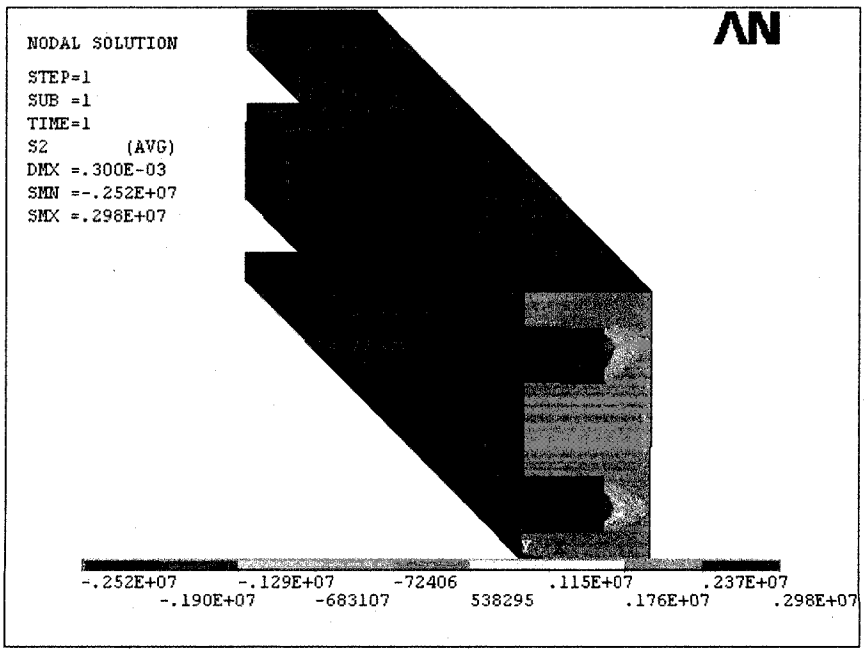

Figure 3-21 Second principal stress distribution, Pa

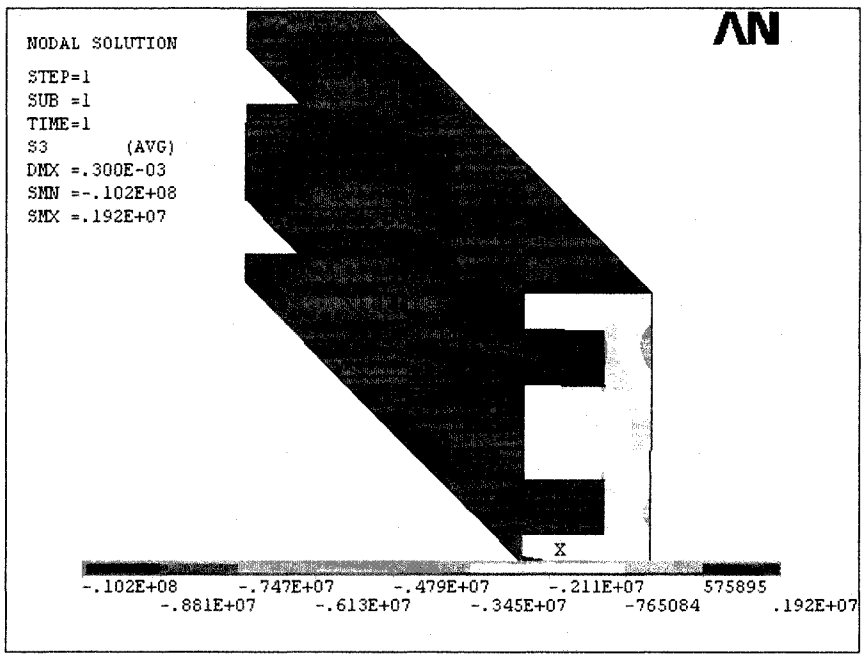

Figure 3-22 Third principal stress distribution, Pa

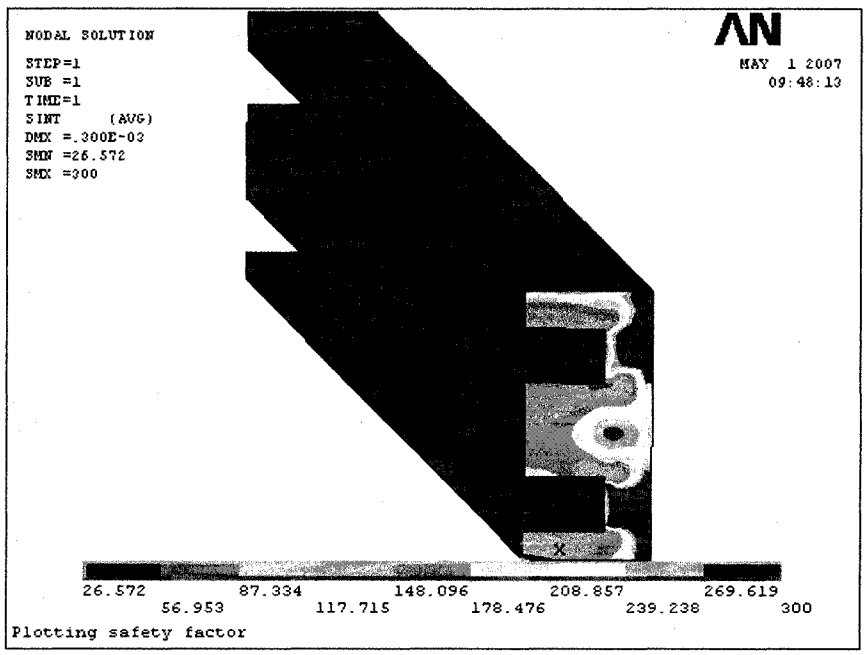

Figure 3-23 Factor of safety based on Coulomb-Mohr failure criteria

CHAPTER 4

PARAMETRIC STUDIES OF HTHX DESIGN PARAMETERS

Introduction

Many current and future nuclear engineering applications require heat exchangers that operate at high temperatures. The operating conditions and performance requirements of these heat exchangers present special design challenges. The performance of these heat exchangers is controlled by certain parameters such as, channel geometry, temperature difference, pressure, and mass flow rate. Previously, several parametric studies were performed to evaluate the effect of these parameters. It was noticed that the majority of these studies focused on the heat transfer and effectiveness, which is defined as the ratio between the actual heat transfer rate and theoretical maximum heat transfer rate based on the difference between the hot and cold inlet temperatures of the heat exchanger. James C. Govern [28] have conducted one of these studies focusing on the effect of channel length, channel spacing, and flow rate on the heat transfer and effectiveness.

The safety of the heat exchanger is extremely important especially in the nuclear application; however, previous parametric studies did not discuss the effect of the different parameters on the induced thermal or mechanical stresses. This study focused on the stress analysis and the calculation of the factor of safety and probability of failure for different channel designs. These designs differ from the baseline (straight channel) design only in

the geometry of the channels with chemical reaction. These alternative designs provide greater surface area of chemical reaction, which can enhance the decomposition. At the same time, these designs produce bigger pressure drop and thermal stresses. The effect of the channel length and fluid pressure was also investigated. Since the focus here is on stress analysis, the following sections show the evaluation for each case based on the Mohr's and Wiebull's failure criteria. The baseline case was mentioned before in Section (3.2.2) but it will be mentioned here again for consistency.

4.1 Straight Channel Baseline Design

The evaluation of the straight channel baseline design based on Mohr's and Wiebull's failure criteria was mentioned before in Section (3.2.2) that; 26.572 as a minimum factor of safety which is quite high factor of safety. The distribution of factor of safety is shown in Figure 4-1. The probability of failure is consistent with the factor of safety calculation, where probability of failure for the three principal stresses σ_1, σ_2, σ_3 are (0, 0, 0) respectively.

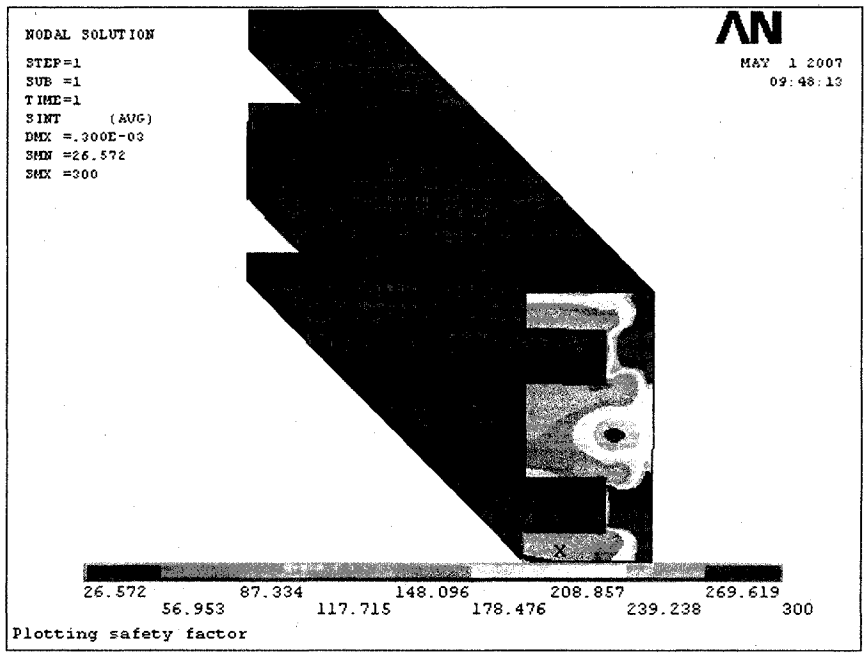

Figure 4-1 Nodal factor of safety for straight channel baseline design

4.2 Straight Channel with Ribbed Ground Surface, with rib height of 0.1 mm.

Since the amount of heat transfer depends on the surface area of the heat exchanging surface, increasing of this area will increase the heat transfer. Adding ribs was one of the proposed designs to increase the surface area. Figure 4-2 shows the variables of a straight channel with ribbed ground where (s) represents the spacing between two consecutive ribs, (h) represents the rib height, and (w) represents the rib width.

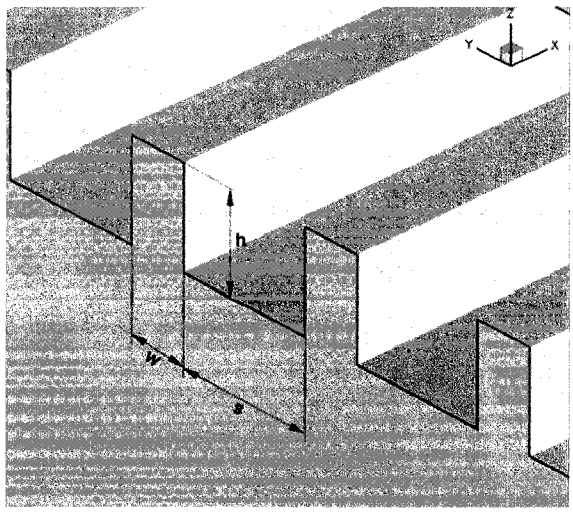

Figure 4-2 Ribs geometry and dimension.[22]

The evaluation of the straight channel with ribbed ground surface, h=0.1 mm based on Mohr's and Wiebull's failure criteria give that; 50.814 as a minimum factor of safety and the distribution of factor of safety is shown in Figure 4-3. The probability of failure for the three principal stresses σ_1, σ_2, σ_3 are (0, 0, 0) respectively.

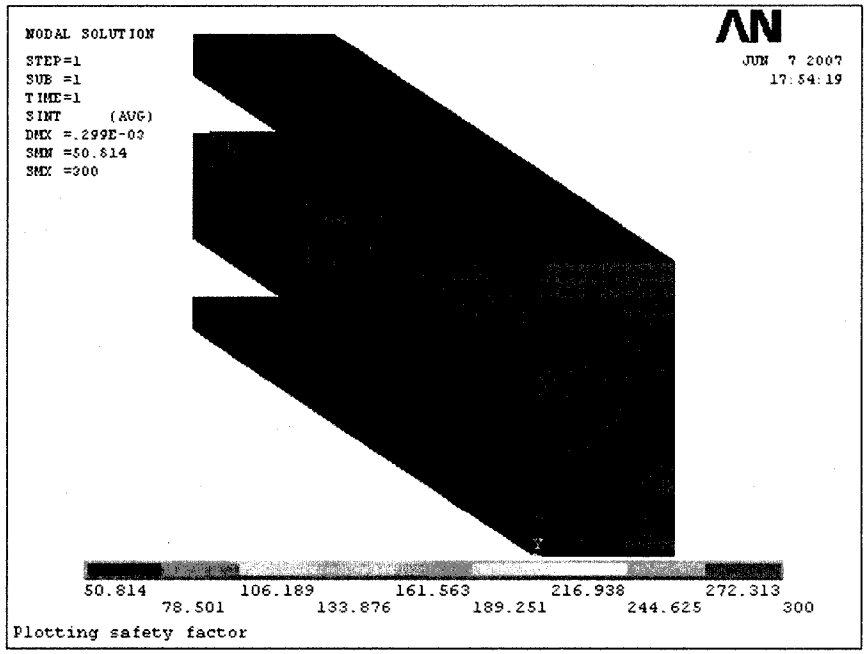

Figure 4-3 Nodal factor of safety for straight channel with ribbed ground surface, h=0.1 mm

4.3 Straight Channel with Ribbed Ground Surface, h=0.2 mm

The results of the case of the ribbed channel with height 0.1 mm showed that the minimum safety factor is twice of the minimum safety factor of the baseline design without ribs. Therefore, the height h was selected to study its effect on the design safety. Therefore, the case with h=0.2 mm was investigated. The minimum safety factor for this case is 10.866as shown in Figure 4-4. The results for the Wiebull's failure criteria for the three principal stresses σ_1, σ_2, σ_3 are (0, 0, 0) respectively. The decrease of the safety factor in the case of h=0.2 mm from the case of h=0.1 mm is the increase of the temperature difference and induced stresses especially in the area of contact between the ribs and the vertical wall.

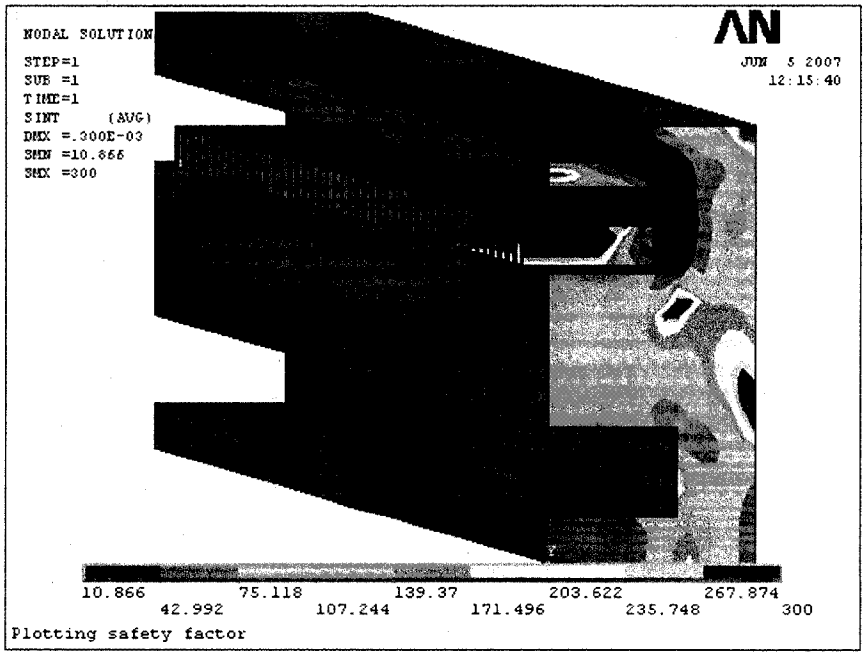

Figure 4-4 Nodal factor of safety for straight channel with ribbed ground surface, h=0.2mm

4.4 Channel with Two Hexagonal Layers Under 50% of Layers Overlapping

Another way of increasing the surface area is to use two hexagonal layers. Figure 4-5 shows the geometry and dimension of the hexagonal layers. There are too many parameters that can affect this design thickness, and the degree of overlapping. Two different degrees of overlapping was selected. The other parameter could be investigated in the future work. Result for the Mohr's criteria for the case of the channel with two hexagonal layers under 50% of layers overlapping is: 14.692 as a minimum factor of safety and the distribution of factor of safety are shown in Figure 4-6. The probability of failure for the three principal stresses σ_1, σ_2, σ_3 are (0, 0, 0) respectively.

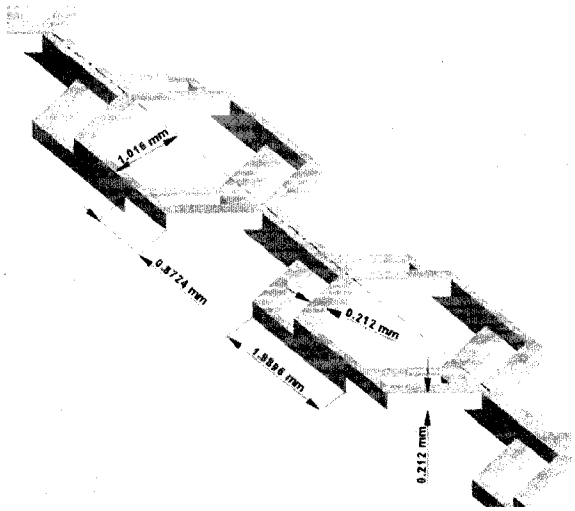

Figure 4-5 Hexagonal layers geometry and dimension with 50% overlapping [22]

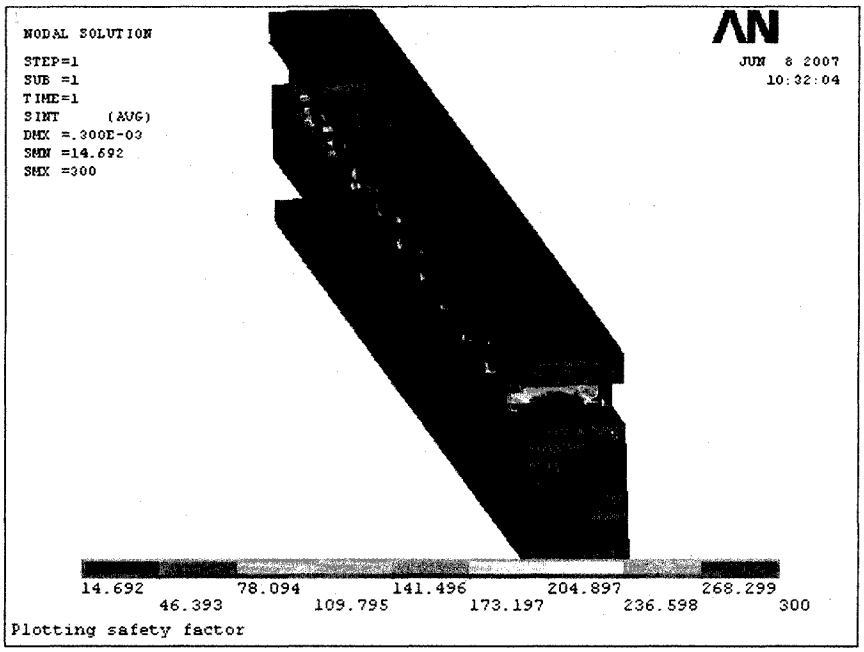

Figure 4-6 Nodal factor of safety for channel with two hexagonal layers under 50% of layers overlapping

4.5 Channel with Two Hexagonal Layers Under 100% of Layers Overlapping

The degree of overlap was selected to find its effect on the induced stresses and on the safety of the proposed design. In addition to the case of the previous section, the

evaluation of a channel with two hexagonal layers under 100% of overlapping based on Mohr's and Wiebull's failure criteria is; 24.768 as a minimum factor of safety. The distribution of factor of safety is shown in Figure 4-7. The expected reason for increasing of the minimum safety factor in the case of 100% overlapping is the reduction in the contact area between the two hexagonal layers. The reduction in the contact area reduces the temperature difference and the induced stresses in these volumes. The probability of failure for the three principal stresses σ_1, σ_2, σ_3 are (1.11e-016, 0, 0) respectively.

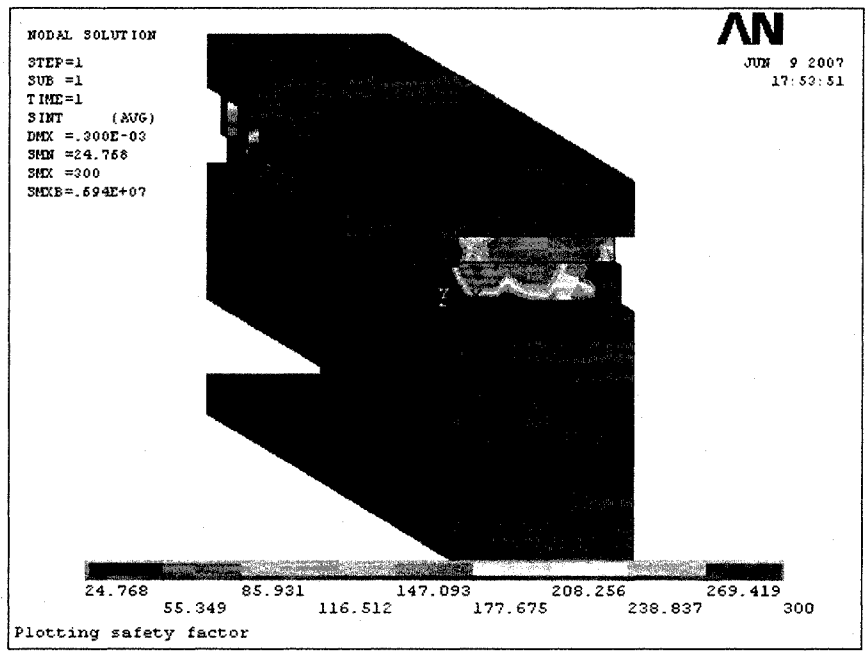

Figure 4-7 Nodal factor of safety for channel with two hexagonal layers under 100% of layers overlapping

4.6 Channel with Two Diamond-Shaped Layers

As the hexagonal design is used to increase the surface area of heat transfer, diamond geometry proposed to attain the same purpose. Figure 4-8 shows the geometry

and dimension of the two diamond-shaped layers. The evaluation of the channel with two diamond-shaped layers based on Mohr's and Wiebull's failure criteria is; 44.499 as a minimum factor of safety. The increase of the minimum safety factor in this case because of the reduction of the contact area between the two layers. The reduction of the contact area reduces the temperature difference and the induced stresses in these volumes. The distribution of factor of safety is shown in Figure 4-9. The probability of failure for the three principal stresses σ_1, σ_2, σ_3 are (0, 0, 0) respectively. The reason of using two diamond-shaped layers is to increase the surface area of heat transfer.

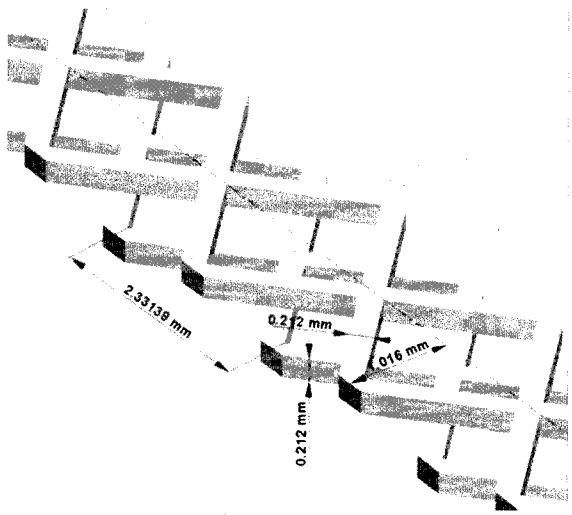

Figure 4-8 Diamond Layers Geometry and Dimension [22]

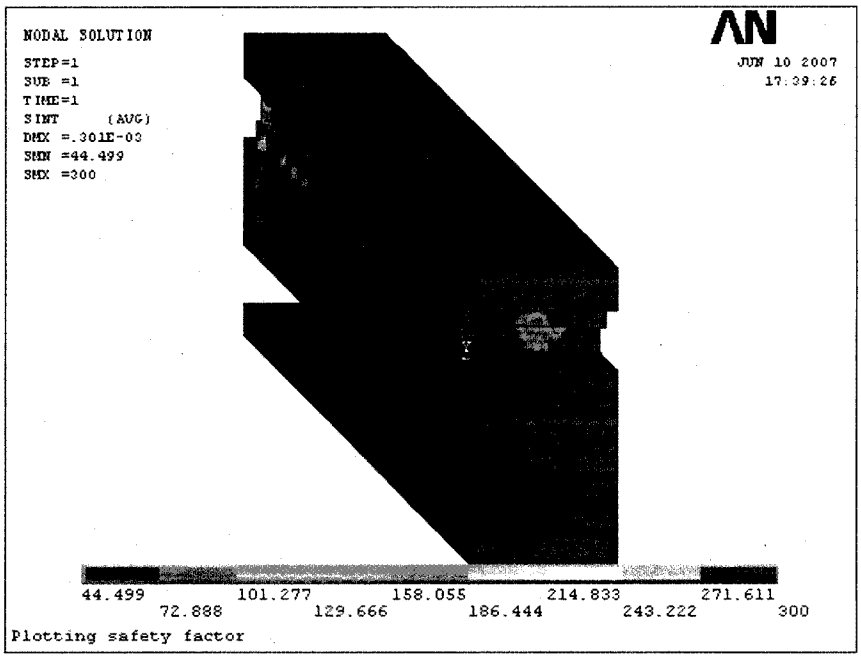

Figure 4-9 Nodal factor of safety for channel with two diamond-shaped layers

4.7 Longer Straight forwarded Channel

Increasing the channel length and using the simple design (baseline design) is also a valid option to increase the surface area of the heat transfer. The original length of the baseline design is 52.324 mm. A four times length channel 209.296 mm was also evaluated. The evaluation of the straight forwarded channel 4- times longer based on Mohr's and Wiebull's failure criteria is; 18.976 as a minimum factor of safety and the distribution of factor of safety is shown in Figure 4-10. The probability of failure for the three principal stresses σ_1, σ_2, σ_3 are (0, 0, 0) respectively.

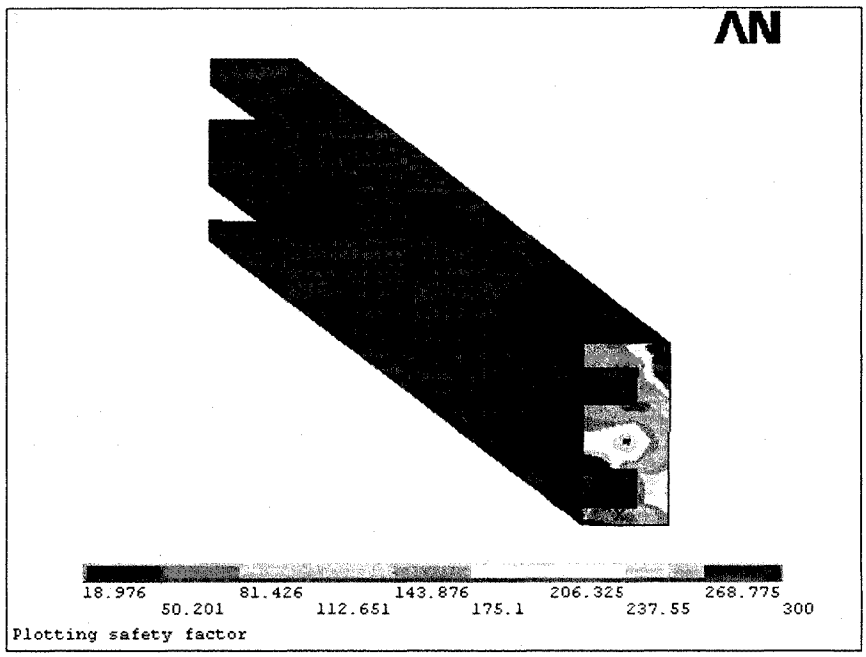

Figure 4-10 Nodal factor of safety for straight forwarded channel 4- times longer

4.8 Straight forward channel with 7.5 Mpa

Increasing pressure is a way of increasing the heat transfer was also investigated using the baseline design. The evaluation of the straight forward channel with 7.5 Mpa based on Mohr's and Wiebull's failure criteria is; 8.717 as a minimum factor of safety and the distribution of factor of safety is shown in Figure 5-11. The expected reason of having the lower value for the minimum factor of safety is the applied pressure load produce stresses. The probability of failure for the three principal stresses σ_1, σ_2, σ_3 are (0, 0, 0) respectively.

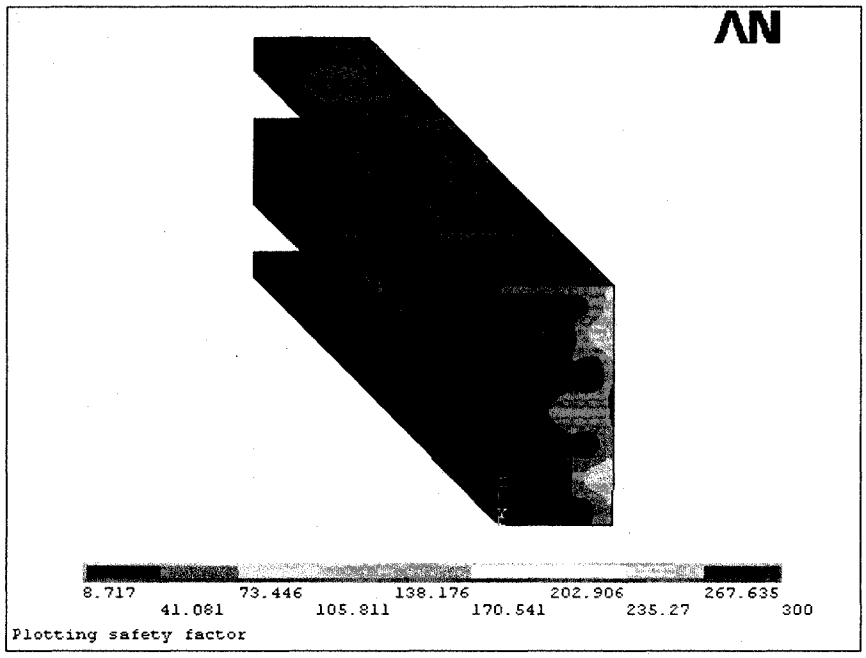

Figure 4-11 Nodal factor of safety for straight forward channel with 7.5Mpa

Based on the stress analysis calculation, and by reviewing the above results it is noticed that the design of straight channel with ribbed ground surface, with rib height of 0.1 mm have the highest value of the minimum factor of safety 50.814 and the probability of failure for the three principal stresses σ_1, σ_2, σ_3 are (0, 0, 0) respectively. On the other hand, for straight channel with ribbed ground surface, h=0.2 mm the value of the minimum factor of safety dropped to 10.866 while the probability of failure for the three principal stresses σ_1, σ_2, σ_3 are still (0, 0, 0) respectively. From this it is clear how the ribs parameter can affect the safety of the design. More studies for the rib parameters are required to find out the value that gives highest value of the minimum factor of safety. The two designs are safe, so there is a need to use other parameters to prefer on design over another. Pressure drop and Percentage of SO3 decomposition could be used

in the comparison. Table 4-1 shows the pressure drop and Percentage of SO3 decomposition for each design.

Table 4-1 pressure drop and percentage of SO3 decomposition for each design.[30]

Name of case	**Percentage of SO_3 decomposition, %**	**Pressure drop, Pa**
Straightforward channels (case 1)	63.81	128.7
Ribs - 0.1 mm (case 2)	64.25	240.8
Ribs 0.2 mm (case 3)	65.57	573.2
Hexagons - 50% overlap (case 4)	76.31	802.4
Hexagons - 100% overlap (case 5)	77.73	3815.8
Diamonds (case 6)	79.95	1570.3

From Table 4-1 it is noticed that as the percentage of SO3 decomposition increases as the pressure drop increase. Since all these design are safe based on Mohr's and Wiebull's failure criteria, design of channel with two diamond-shaped layers provides the highest percentage of SO3 decomposition which should be considered as the best design. On the other hand, the cost of this pressure drop will be another factor that needs to be investigated to find out the best economical proposed design.

CHAPTER 5

TRANSIENT ANALYSIS OF THE CERAMIC COMPONENT OF HTHX (STRAIGHT CHANNEL BASELINE DESIGN)

Introduction

A transient analysis is developed to evaluate the thermal performance of industrial-scale heat exchangers. Testing a heat exchanger in the transient state may be the only viable alternative where conventional steady-state testing procedures are impossible or infeasible [29]. Most of the transient analysis studies were conducted to evaluate the heat exchanger thermal performance. However, stress analysis evaluation of the high temperature heat exchanger is very important criterion especially in the transient state, literature survey failed to find directly relevant work due to the novel nature of the proposed heat exchanger and decomposer with micro-channels [23]. In the case of the startup and shutdown of the decomposer, the stresses can be much higher than those at steady state conditions. Therefore, it is very important to estimate the factor of safety and probability of failure of the decomposer under the transient regimes. The stress results are used to calculate the factor of safety based on the Mohr failure criterion and probability of failure based on the Weibull failure criterion. Earlier analysis showed that the proposed design is safe at steady state operating conditions. The focus of this chapter is to consider stresses that are induced during transient scenarios. In particular, the cases of the startup and shutdown of the heat exchanger.

5.1 Start up Process

The transient regime started from no-flow conditions at room temperature (293.15 K). Suddenly, hot helium with temperature of 1223.15 K is allowed to flow in the helium channel. This study focuses on tensile values of the first principal stress as they will be the most relevant for failure studies. Factor of safety and probability of failure have been calculated at six different time instances: 0, 1, 10, 30, 60, and 120 seconds after the beginning of the helium flow respectively. The following sections will include an analysis and the first principal stress, factor of safety, and probability of failure for different periods of load applications.

5.1.1 Calculation for 0 sec. case

There is no fluid flow or applied pressure in all channels in this case. Figure 5-1 shows the first principal stress associated with this case. The factor of safety and probability of failure indicate that this case is safe because there is no applied pressure or high temperature gradient. Figure 5-2 shows the calculated factor of safety. The calculated probabilities of failure for the three principal stresses σ_1, σ_2, and σ_3 are $1.554e^{-015}$,0.0, and 0.0 respectively.

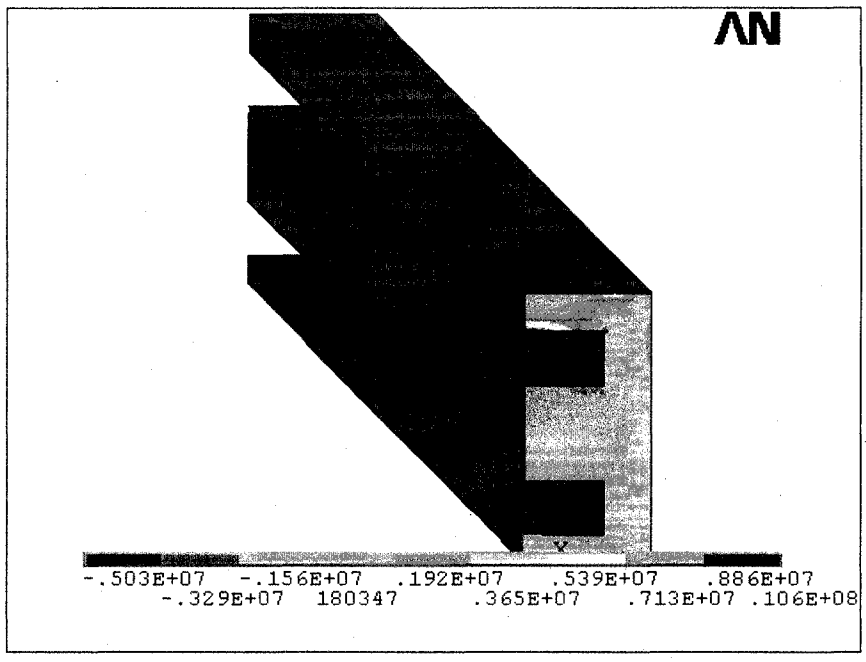

Figure 5-1 First principal stress (Pa) distribution after 0 sec.

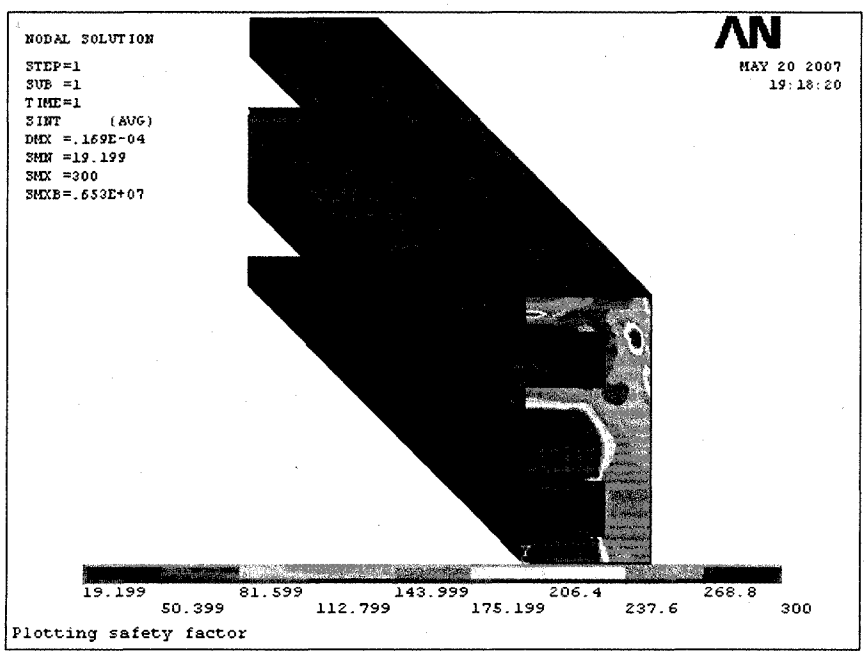

Figure 5-2 Factor of safety after 0 sec.

5.1.2 Calculation for 1 sec. case

Helium and chemicals was allowed to flow with the applied pressure load. The induced stresses from these operating conditions were extracted to conduct the factor of safety and probability of failure calculation. Figure 5-3 shows the first principal stress associated with the applied thermal and pressure loads at this case. Figure 5-4 shows the calculated factor of safety. The calculated probabilities of failure for the three principal stresses σ_1, σ_2, and σ_3 were $8.325e^{-012}$, $2.220e^{-016}$, and 0.0 respectively. It was noticed from the result how the stresses and the probability of failure are higher than that in the 0 second case which lead also to decrease of the factor of safety.

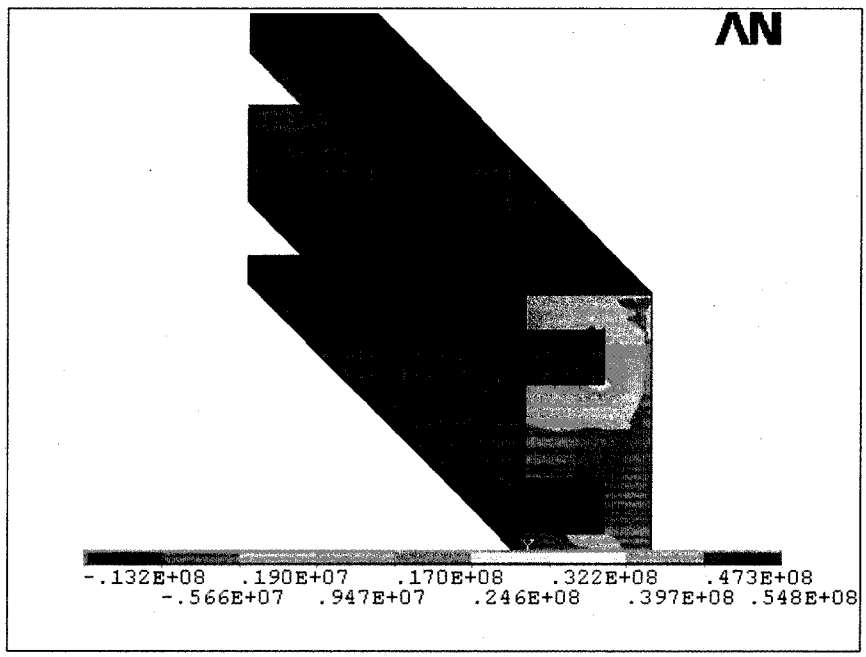

Figure 5-3 First principal stress (Pa) distribution after 1 sec.

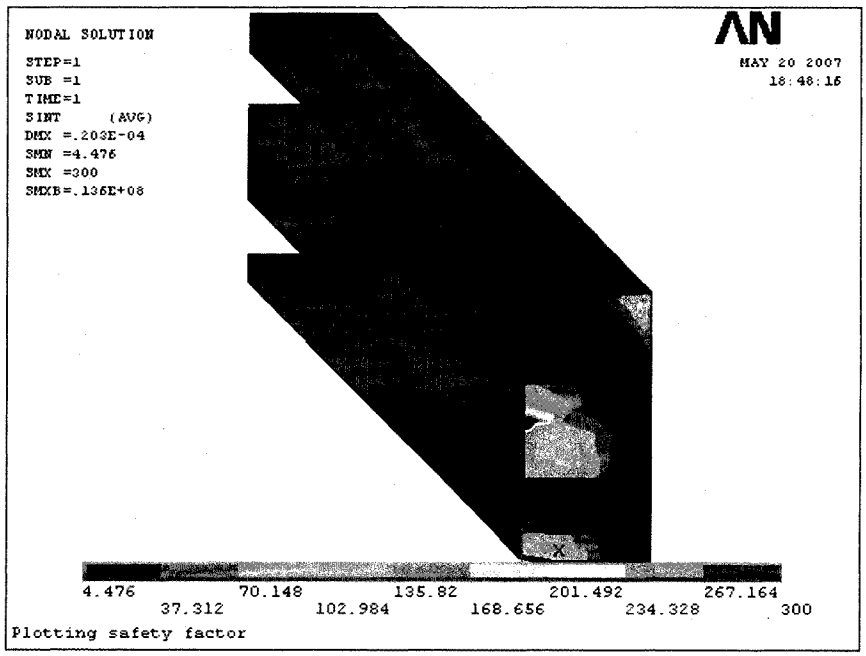

Figure 5-4 Factor of safety after 1 sec.

5.1.3 Calculation for 10 sec. case

Figure 5-5 shows the first principal stress associated with the applied thermal and pressure loads after 10 seconds of the beginning of helium flow. Figure 5-6 shows the plotting of the calculated factor of safety. The calculated probability of failure for the three principal stresses σ_1, σ_2, and σ_3 was $3.008e^{-011}$, $9.992e^{-016}$, and 0.0 respectively.

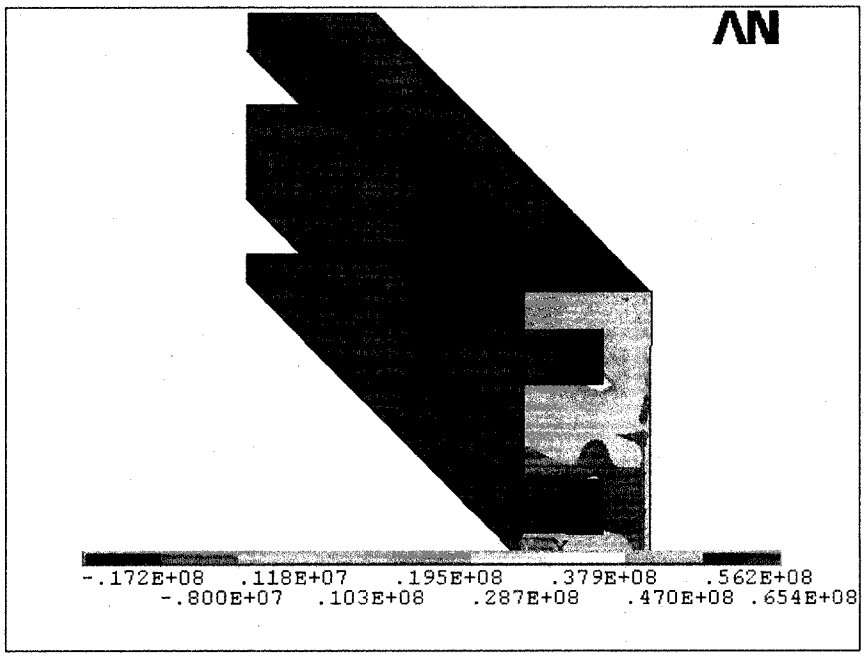

Figure 5-5 First principal stress (Pa) distribution after 10 sec.

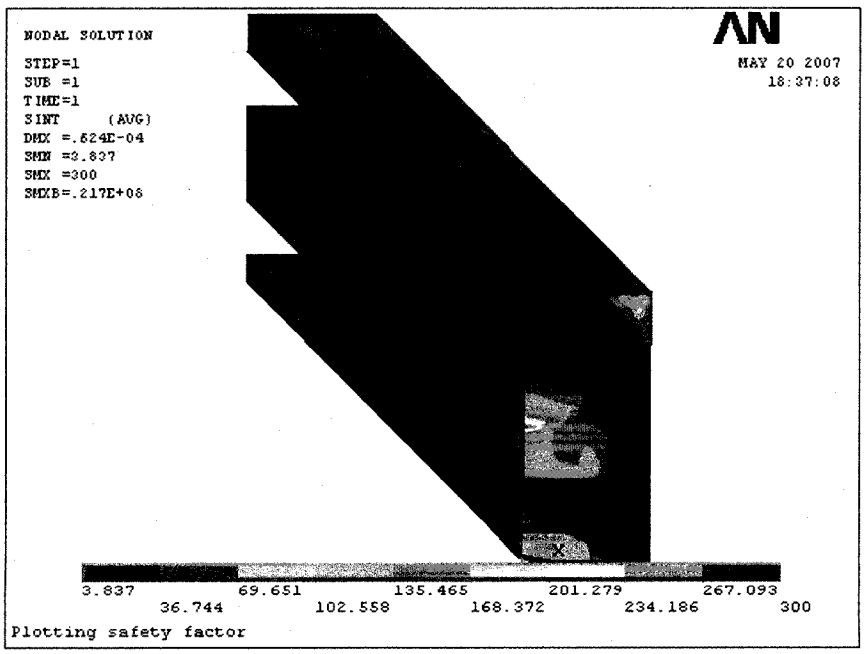

Figure 5-6 Factor of safety after 10 sec.

5.1.4 Calculation for 30 sec. case

Figure 5-7 shows the first principal stress associated with the applied thermal and pressure loads after 30 seconds of the beginning of helium flow. Figure 5-8 shows the calculated factor of safety. The calculated probability of failure for the three principal stresses σ_1, σ_2, and σ_3 was $3.881e^{-012}$, $1.465e^{-014}$, and 0.0 respectively. The first principal stress after 30 seconds increased when compared to its value at 10 seconds due to increase of thermal gradient within the walls of the channel. In the meantime, factor of safety also increased. This discrepancy can be explained by the fact that ceramic tensile strength increases with temperature as mentioned in Section (3.1.1).

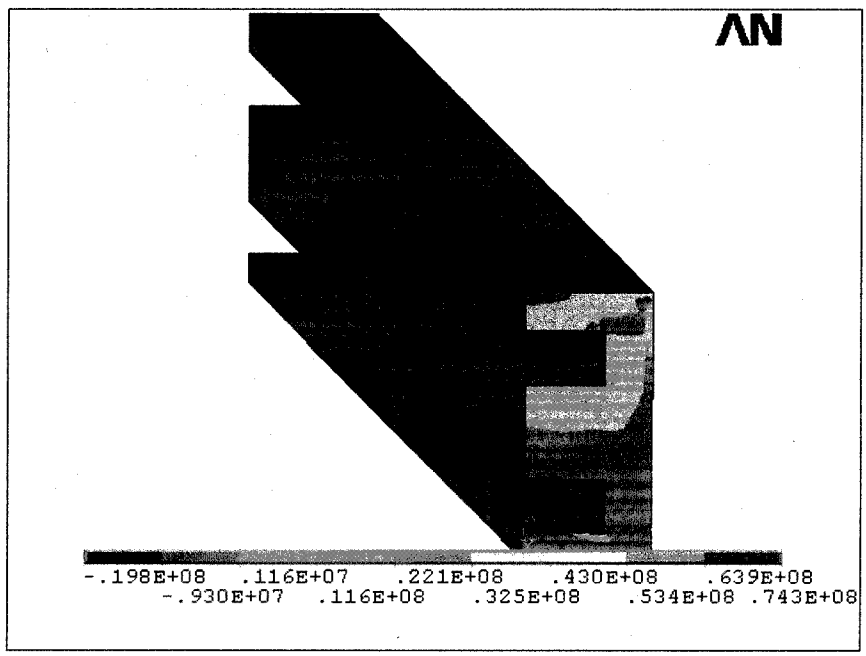

Figure 5-7 First principal stress (Pa) distribution after 30 sec.

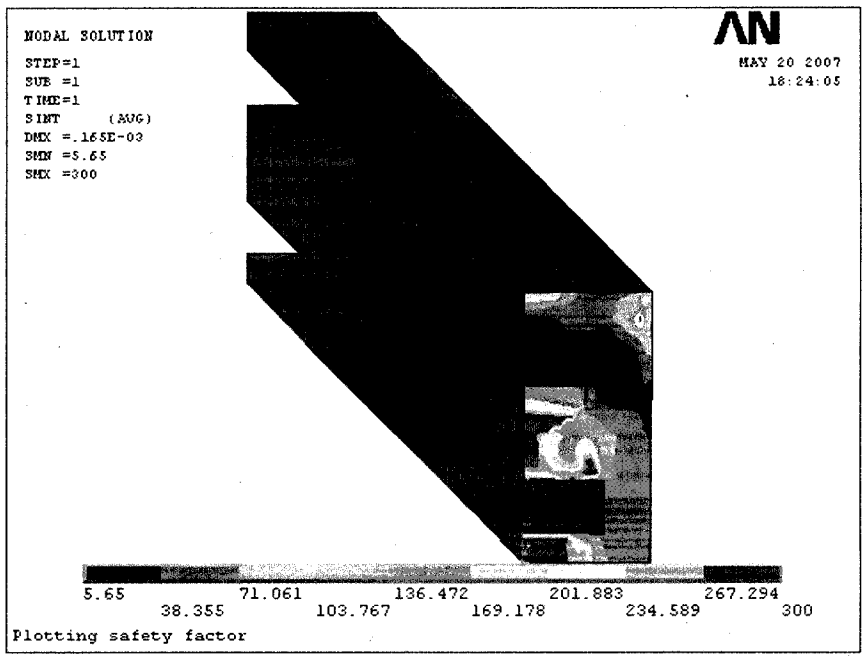

Figure 5-8 Factor of safety after 30 sec.

5.1.5 Calculation for 60 sec. case

Since the thermal load is main factor of the induced stresses, it is expected that as the time increase the temperature difference and the induced stresses will decrease. After 60 seconds. Figure 5-9 shows the first principal stress associated with the applied thermal and pressure loads after 60 seconds of the beginning of helium flow. Comparing results with the previous case shows that the first principal stress decreased. Figure 5-10 shows an increase of the calculated factor of safety. The calculated probability of failure for the three principal stresses σ_1, σ_2, and σ_3 was $1.332e^{-015}$, 0.0, and 0.0 respectively, which also indicates a lower probability of failure.

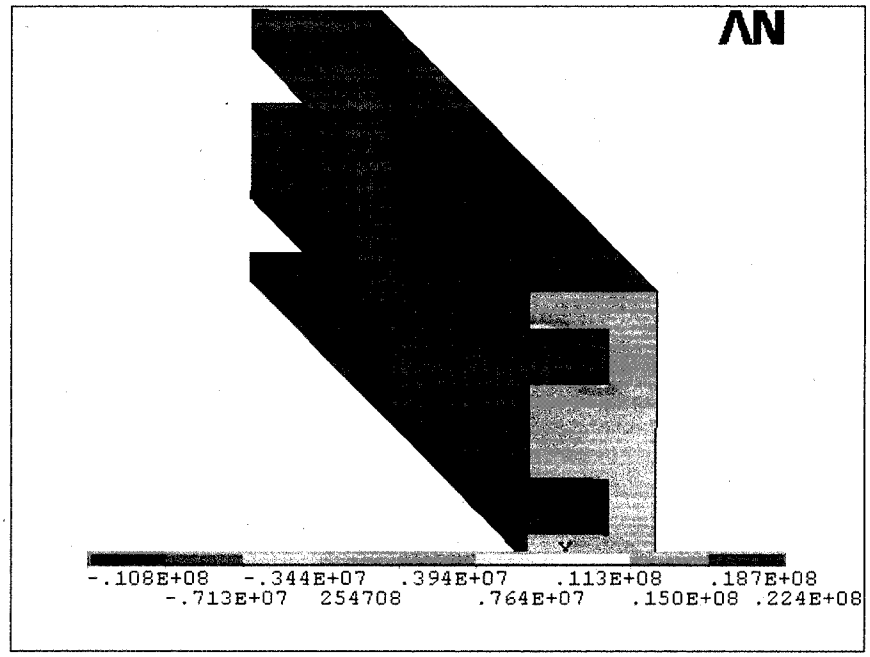

Figure 5-9 First principal stress (Pa) distribution after 60 sec.

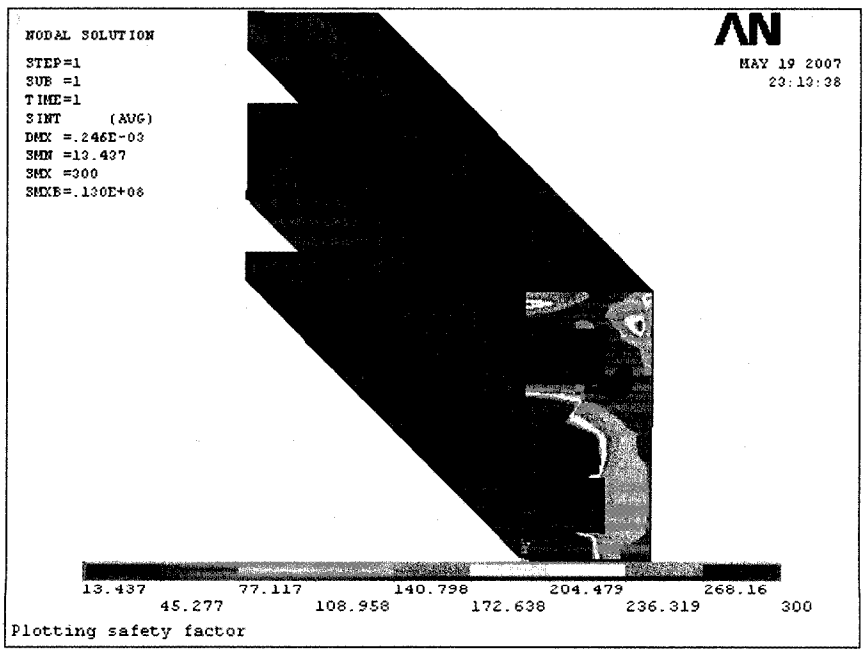

Figure 5-10 Factor of safety after 60 sec.

5.1.6 Calculation for 120 sec. case

As it was expected, the induced stresses will decrease as the time increase. After 120 sec. the induced stress decreases than that for the 60 sec. case. Figure 5-11 shows the first principal stress associated with the applied thermal and pressure loads after 120 sec. of the beginning of helium flow. Figure 5-12 shows the increase of the calculated factor of safety than that in the 60 sec. case. The calculated probability of failure for the three principal stresses σ_1, σ_2, and σ_3 was $7.771e^{-016}$, 0.0, and 0.0 respectively.

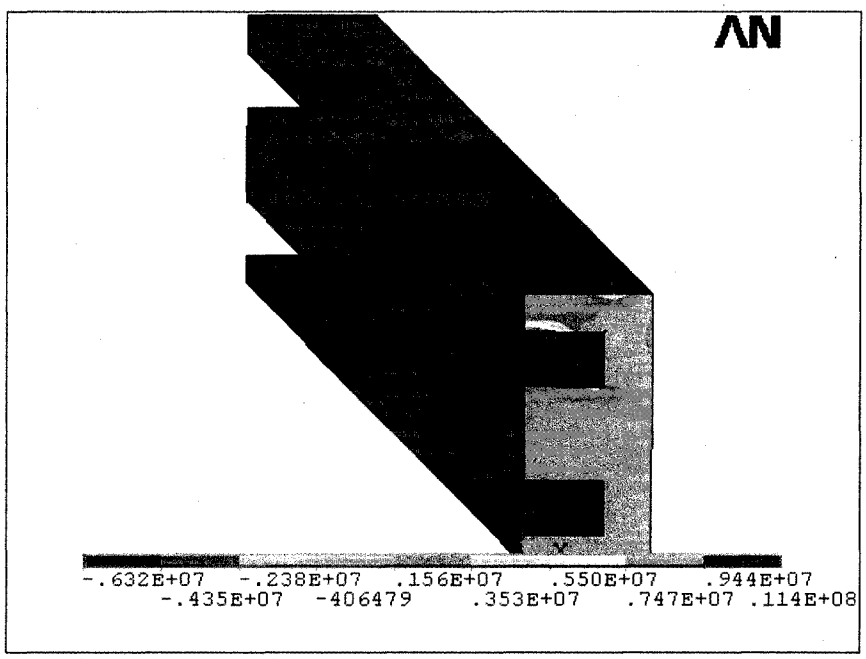

Figure 5-11 First principal stress (Pa) distribution after 120 sec.

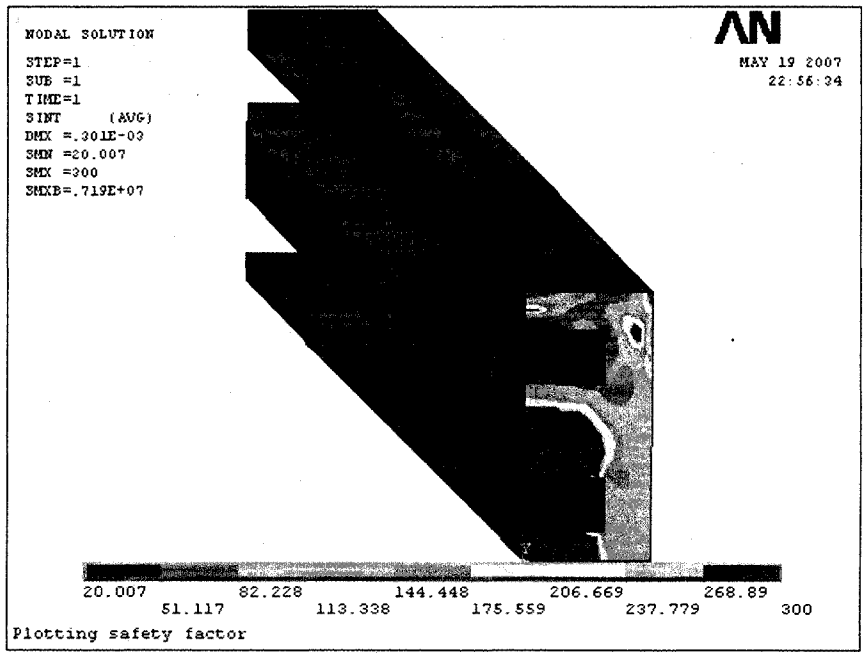

Figure 5-12 Factor of safety after 120 sec.

5.2 Shutdown process

The transient regime in the shutdown process started from working condition and suddenly all of the inlets and outlets closed simultaneously. In this case there are no sources of adding or absorbing heat, as a result of this the temperature difference will decrease. After that, the temperature distribution in the ceramic part of the decomposer started to change and reached practically uniform distribution. Maximal temperature non-uniformity in the ceramic part was less than 5 K [23]. The summary and comparison of the transient analysis will be presented in section (0)

CHAPTER 6

MODELING OF THE HEAT EXCHANGER AND CHEMICAL DECOMPOSER BAYONET DESIGN

6.1 General Idea and Mechanism of Bayonet Design

The SID, also called the bayonet heat exchanger, was designed by the Sandia National Lab (SNL) [31]. The integrated acid decomposer combines the function of boiler, superheater, decomposer and recuperater in a single silicon carbide unit is shown in Figure 6-1. This design uses Teflon for components in the low temperature regions and silicon carbide and quartz for components in the high temperature regions. The integrated silicon carbide decomposer has several advantages over others decomposers because of the presence of the recuperater which heats the incoming acid gases. This would minimize the total input energy required to the system. This design uses concentrated sulfuric acid (35 to 40 mol %), which comes from a sulfuric acid concentrator and then pumped into the inlet of the bayonet heat exchanger [24].

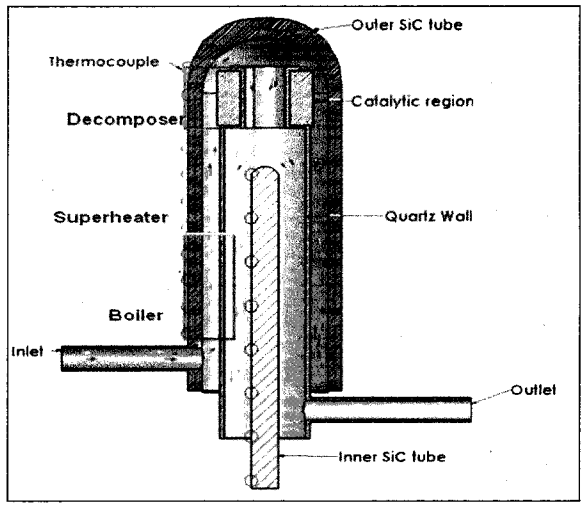

Figure 6-1 Schematic of the silicon carbide integrated decomposer (SID) [24].

6.1.1 Working conditions and dimensions

The bayonet heat exchanger can handle both high temperature and low temperature regions in a single unit. The inlet is made of Teflon and maintained at temperatures below 200°C. The water vapor and the sulfuric acid enter the boiler which would heat the sulfuric acid to 450°C to produce a sulfuric acid vapor. The superheater would heat the sulfuric acid vapor from 450°C to 700°C and the decomposer would heat the vapors to the maximum operating temperature plus provide the heat necessary to dissociate the sulfur trioxide to sulfur dioxide and oxygen. The working conditions are obtained from [25] and [26]. The decomposed vapors which are coming from the decomposer are recuperated either in the superheater or in the boiler to minimize the total required input energy to the system. The flow path is designed such that concentrated acid enters the Teflon manifold inlet and flows up along the outer annulus. At the bottom of this annular region, heat is recuperated from the flow downward along the inner annulus, and the combined heat from the recuperator and the electrical heater vaporizes the incoming acid. Further heating superheats the acid in the outer annulus, and the

vaporized acid decomposes almost completely to SO_3 and H_2O prior to reaching the catalyst. The catalyst is held at the top of the annular region outside the central tube and inside the outermost tube. Further heating in the catalyst region decomposes the SO_3 to SO_2 and O_2. The vapors from the catalyst bed flow down and out through the annular region between the central and innermost tubes. As the heat is recuperated the down-flowing stream temperature drops, and the remaining SO_3 combines with steam to form H_2SO_4. Further reduction in the temperature allows for the condensation of H_2SO_4. The inner tube is open at the bottom and is used to house a thermocouple tree. No fluid flows through the innermost tube. The exit temperature is maintained low enough to allow for using Teflon for the manifold and the tubing but it should be in the range that maintains water as a vapor. The Teflon manifold maintains the spacing of the inner tubes and allows for the connection of the inlet and the outlet ports. By maintaining flow gaps within inner annular quartz and SiC tubes, heat transfer conditions can be optimized for effective heat transfer. Figure 6-2 shows the lab scale model of the bayonet heat exchanger with dimensions[24].

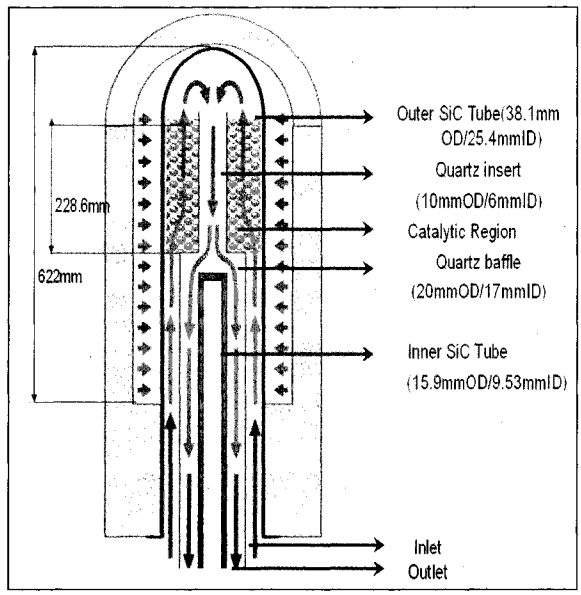

Figure 6-2 Dimensions of bayonet heat exchanger [24]

6.1.2 Design of the catalytic region

The decomposer region is located at the top of the bayonet heat exchanger as shown in Figure 6-1 and Figure 6-2. It houses the pellets. The pellets are made of silicon carbide which contain approximately one percent of weight of platinum. The pellets are spherical shaped with simple cubical packing. The diameter of a pellet is 5 mm[24].

6.1.3 Material properties

Because of the highly corrosive nature at elevated temperatures, choice of materials for the construction of the decomposition section is limited. Corrosion tests indicated that all common metals typically used for construction of high-temperature pressurized systems exhibited very high corrosion rates and were unacceptable for use in this process. Therefore, the solid parts of the decomposer are made from glass, silicon carbide (SiC), or Teflon lined steel. The density and specific weight of the SiC do not significantly depend on the temperature. Therefore, for the calculations the material

properties are assumed as constants for the design temperature range (873-1173 K). Silicon carbide mechanical properties were considered as the properties of sintered α-SiC, which have been mentioned in Chapter (3) Section (3.1.1). Quartz mechanical properties it was assumed to be constant with the temperature for the stress analysis calculation. Table 6-1 shows the required properties

Table 6-1 Quartz mechanical properties [27]

Properties	Units	Temperature	Value
Coefficient of thermal expansion	m/m°C	0° - 900° C	$4.8\ e^{-7}$
Tensile Strength	Pa	20° C	$4.9\ e^{7}$
Compressive Strength	Pa	20° C	$1.1\ e^{9}$
Young's Modulus	Pa	20° C	$7.3\ e^{11}$
Poisson's Ratio		20° C	0.17

6.2 Finite Element Model

A finite volume model was created to simulate the decomposition and fluid flow. The same model exported to ANSYS to be used for stress analysis. The bayonet design of the high temperature heat exchanger has a cylindrical component of ceramic and quartz that makes it more adequate to use the axisymmetric element in the creation of the finite element model. Figure 6-3 shows the schematic representation of the model.

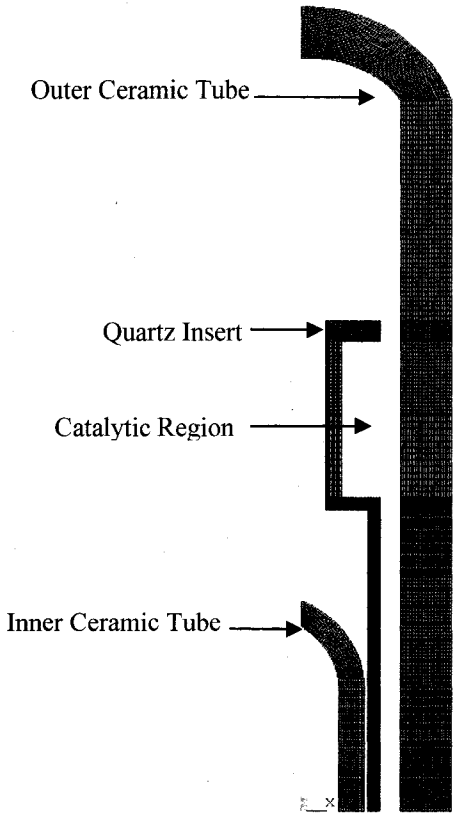

Figure 6-3 Mesh of the axisymmetric finite element model

6.2.1 Mesh independence study

A mesh independence study was conducted to get the proper mesh refinement. Figure 6-4 shows the results of mesh independent study. According to the study, the proper number of cells and nodes (33036 cells, 35374 nodes) are selected for the future meshing. The calculated geometry is meshed using the mesh generator GAMBIT 2.2.30, and the grid independent study is done for the model. The mesh is quadrilateral.

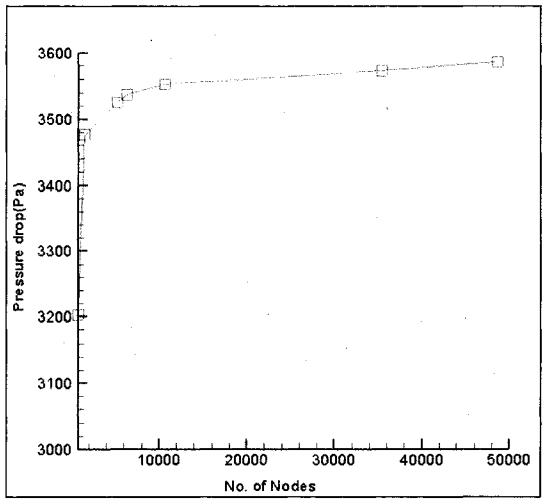

Figure 6-4 Mesh independence study [24]

6.2.2 Boundary and operating conditions

The boundary condition of the decomposer region is as follows:

Inlet condition for the decomposer region:

Inlet velocity v = 5.5 $m \cdot s^{-1}$;

Inlet temperature T = 873K (600°C);

Inlet mass flow rate $\dot{m}$ = 0.43.10-3 $kg \cdot s^{-1}$;

Percentage of acid feed = 40 mol %;

Mass fraction of SO3 = 53 %;

Volumetric flow rate, Q = 15 ml·min-1.

The temperature of the outer wall is 1123K. The upper wall is maintained under adiabatic conditions. The value for density of sulfur trioxide mix with water is obtained from commercial software Fluent 6.2.16. The operation is carried out under atmospheric pressure. Pressure outlet is selected as outflow boundary condition [24].

6.3 Stress Analysis of Bayonet Design Components

The temperature distribution was calculated throughout the model using FLUNT using the boundary conditions described in the previous section. After that, the stresses induced due to the temperature difference were calculated by using ANSYS. These stresses were exported to complete the probability of failure and factor of safety calculations. Figure 6-5 shows the 1st principal stress distribution for the ceramic and quartz component.

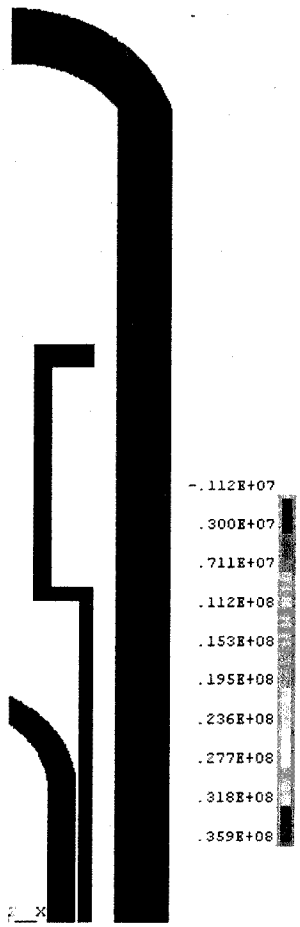

Figure 6-5 1st principal stress in Pa

6.3.1 Probability of failure calculation

Probability of failure calculation depends on volume and stresses, in the case of analyzing separated volumes the calculation should be done for each volume individually. Therefore, the probability of failure calculation was established for outer ceramic tube, quartz insert and inner ceramic tube. The procedures of this calculation was explained in section 2.12.2

6.3.2 Factor of safety calculation

Factor of safety calculation was made based on the nodal stresses values and there was no need to do it for each volume individually. MATLAB code was created to calculate the factor of safety for each node using Coulomb-Mohr failure criteria. The program imports nodal principal stresses, temperatures as well as element nodal connectivity data and element volumes. The details of these steps were mentioned in section 2.1.

6.4 Results

Stresses calculation shows that the stresses are concentrated only in the fluid entrance at which there is a higher temperature difference. The maximum calculated stress is 3.59E+07 Pa at the outer ceramic tube. According to the factor of safety calculation the minimum value of the factor of safety is 17.128 which is still pretty high safety factor. Figure 6-6 shows the factor of safety values for each node.

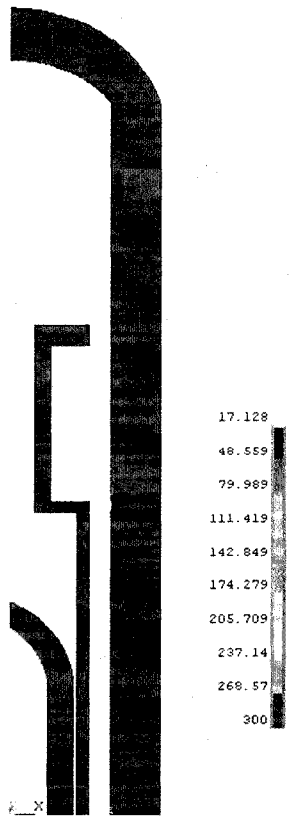

Figure 6-6 Factor of safety

The probability of failure was calculated for the outer ceramic tube, quartz insert, and for inner ceramic tube. For the three parts the probability of failure for the three principal stresses σ_1, σ_2, and σ_3 is 0.0, 0.0, and 0.0 respectively. The first principal stress is significantly higher than the two other principal stresses. However, all stresses are significantly below the maximum tensile stress for the quartz or the ceramic, for this reason probabilities of failure is zero for the three principal stresses. The probability of failure calculation showed consistency with the result of the factor of safety calculation.

CHAPTER 7

COMPARISON, CONCLUSION, AND RECOMMENDATIONS

7.1 Comparison of the Safety Factor and Probability of Failure for All Geometries

To enhance the performance of the decomposer, alternative designs are explored. These designs differ from the baseline design only in the geometry of the reacting flow channel. All of other dimensions as in baseline design (case 1). Five alternative designs are investigated:

(1) Channel with ribbed ground surface, h=0.1 mm,

(2) Channel with ribbed ground surface, h=0.2 mm,

(3) Channel with two hexagonal layers under 50% of layers overlapping

(4) Channel with two hexagonal layers under 100% of layers overlapping

(5) Channel with two diamond-shaped layers.

The inlet and outlet reacting flow channel parts of the alternative designs have rectangular shape without the microcomponents (ribs, hexagons or diamonds) to avoid backflow in the outlets and to provide an entrance zone for each channel. The length of the inlet and parts is about 10% of the total channel length.

These alternative designs can provide the breakdown of the thermal and hydrodynamic boundary layers to boost the heat transfer. On the other hand, these designs may produce large pressure drop and thermal/mechanical stresses.

Table 7-1 Results of calculations for baseline and alternative designs [30]

Name of case	Area of chemical reaction, m^2	Volume of reacting flow, m^3	Area/ Volume, m^2/m^3	Percentage of SO_3 decomposition, %	Pressure drop, Pa
Straightforward channels (case 1)	8.864·10-5	1.409·10-8	6291	63.81	128.7
Ribs - 0.1 mm (case 2)	9.320·10-5	1.319·10-8	7065	64.25	240.8
Ribs 0.2 mm (case 3)	9.756·10-5	1.234·10-8	7906	65.57	573.2
Hexagons - 50% overlap (case 4)	1.330·10-4	1.903·10-8	6989	76.31	802.4
Hexagons - 100% overlap (case 5)	1.359·10-4	1.903·10-8	7141	77.73	3815.8
Diamonds (case 6)	1.480·10-4	1.736·10-8	8525	79.95	1570.3

According to the data from Table 7-2, SO3 decomposition with ribbed ground does not increase significantly as compared with baseline design, as this design creates stagnation zones between the ribs, which prevent moving products of the chemical reaction into the main direction of flow.

On the other hand, percentage of SO3 decomposition for the channels with hexagonal and diamond layers is significantly higher (20-25%) than that in the baseline design. The highest decomposition rate is obtained for the geometry with diamond shaped channels. These results may show that the ratio of surface of chemical reaction to the volume of reacting flow can be used to predict the percentage of SO3 decomposition when channels have no ribs. This observation can be used as a basis for future channel designs.

Pressure drop for the five alternative designs increase significantly when compare with baseline design (see Table 7-1). However, the even the case with highest pressure

(hexagons - 100% overlap) is still within the 10 kPa design limits of the decomposer pressure drop.

While stresses somehow increased for all alternative designs, probability of failure for channel with ribbed ground is equal to zero for the three principal stress directions. Similarly, the probabilities of failure are also equal to zero for the three principal stress directions of the hexagonal and diamond-channel cases. Therefore, all channel designs presented in this work are safe under the proposed operating condition.

7.2 Comparison of Transient Analysis Results

Figure 7-1 through Figure 7-3 show the consistency of the results. Initially, there is no applied pressure or heat addition or removal so the heat exchanger has the lower temperature difference, maximum first principal stress, and probability of failure. As the time increases the temperature difference increases and the maximum first principal stress, and probability of failure increases too until it reach the maximum. After that the whole component temperature goes up but the temperature difference decreases and the maximum first principal stress, and probability of failure decreases too. However, the highest principal stress and probability of failure appear after 5 to 40 sec. range for startup; the factor of safety and probability of failure calculation for startup and shutdown determined that the design is safe in both cases: startup and shutdown.

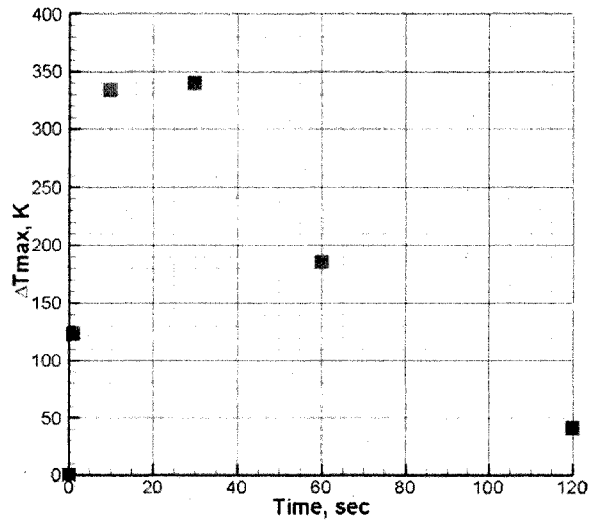

Figure 7-1 Variation of maximum temperature difference within SiC during the startup process [23]

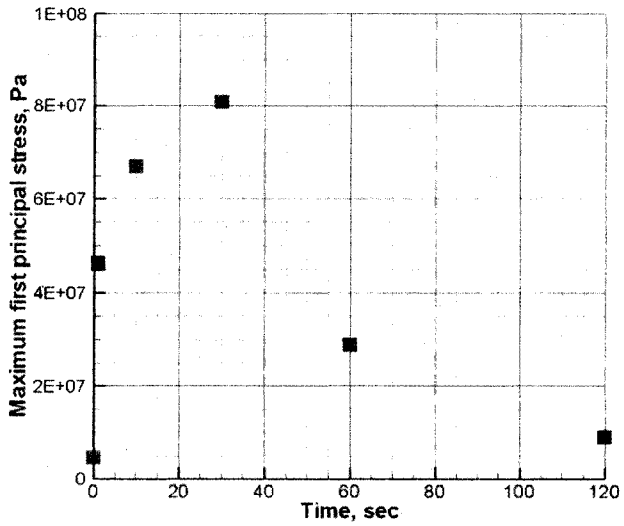

Figure 7-2 Variation of maximum first principal stress within SiC during the startup process [23]

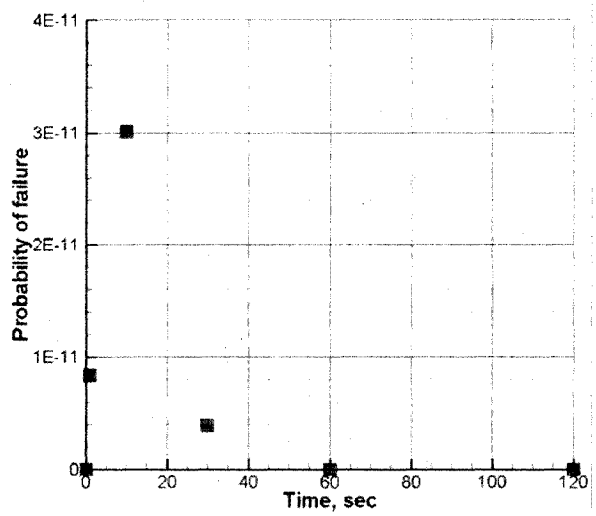

Figure 7-3 Probability of failure within SiC during the startup process[23]

Combining of the probability of failure and minimum factor of safety gives a proof of the consistency of both approaches. Figure 7-4 shows the compatibility of result for the same time region.

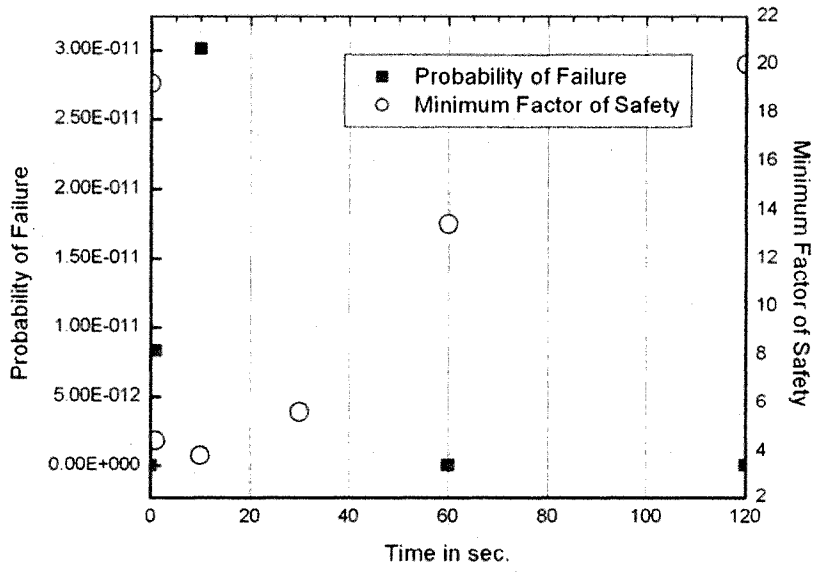

Figure 7-4 Probability of failure with the minimum factor of safety SiC during the startup process.

7.3 Conclusion

The applied pressure and thermal loads induce stresses on the HTHX components. The results of this study show that stresses are mainly caused by the thermal loads. Thermal stresses are a function of the coefficient of thermal expansion and temperature difference. Coefficient of thermal expansion is a physical property for the material, so temperature difference is the variable that determines the stress magnitude. Temperature difference is function of many parameters. These parameters can be classified into two groups:

First, parameters that related to the component geometry and design as it have been seen in the parametric study in Chapter 4 for example the design of straight channel with ribbed ground surface, with rib height of 0.1 mm have the highest value of the minimum factor of safety 50.814 while the design of straight channel with ribbed ground surface, h=0.2 mm have the lowest value of the minimum factor of safety dropped to 10.866. Table 7-2 represents summary of the factor of safety and probability of failure calculation.

Bayonet design is one of the simplest proposed designs for HTHX. The bayonet design was analyzed form the stress point of view. Using finite element model, the calculated induced stresses was higher than that of the base line design. Even though the bayonet design has higher stress than that of the base line design, it has minimum factor of safety of 17.128. This fact determines that bayonet design is a safe design too.

Table 7-3 Summary of the factor of safety and probability of failure calculation

Design	Minimum factor of Safety	Overall Safety Factor	Probability of Failure
Straight channel base line design	26.572	183	0.0, 0.0, 0.0
Channel with ribbed ground surface with rib height h=0.1 mm	50.814	5240	0.0, 0.0, 0.0
Channel with ribbed ground surface with rib h=0.2 mm	10.866	174	0.0, 0.0, 0.0
Channel with two hexagonal layers under 50% of layers overlapping	14.692	2606	0.0, 0.0, 0.0
Channel with two hexagonal layers under 100% of layers overlapping	24.768	1080	1.11e-016, 0.0, 0.0
Channel with two diamond-shaped layers	44.499	2145	0.0, 0.0, 0.0

Second, parameters that related to operating condition and the elapsed time of load application as it have been seen in the transient analysis in Chapter 5. Testing a heat exchanger in the transient state may be the only viable alternative where conventional steady-state testing procedures are impossible or infeasible. Factor of safety and probability of failure have been calculated at six different time instances: 0, 1, 10, 30, 60, and 120 seconds after the beginning of the helium flow. It was noticed that as time increases the temperature difference increases and the maximum first principal stress, and probability of failure increase too until it reaches the maximum. After that the whole component temperature goes up and the temperature difference, the maximum first principal stress, and probability of failure decrease too. The conclusion of the factor of

safety and probability of failure calculation for startup and shutdown determined that the design is safe in both cases: startup and shutdown. Table 7-3 shows the result summary of the transient analysis calculation.

Table 7-4 Result summary of the transient analysis.

Time (s)	Minimum Safety Factor	Overall Safety Factor	Probability of Failure
0	19.199	193.569	1.54e-015 ,0.0, 0.0
1	4.476	117.105	8.32e-012, 2.22e-016, 0.0
10	3.837	75.57	3.0e-011, 9.99e-016, 0.0
30	5.65	68.944	3.88e-012, 1.46e-014, 0.0
60	13.437	123.05	1.332e-015, 0.0, and 0.0
120	20.007	200.83	7.771e-016, 0.0, 0.0

7.4 Recommendations

Several recommendations are presented based on the results of this study. These recommendations can be separated as follows:

7.4.1 Recommendation for using of micro channel heat exchanger and decomposer

- Using of Mohr Coulomb and Weibull failure criteria should be considered as a consistent measure for the safety level determination of the brittle material.

- Comparing the stress in the michrochannel design with the bayonet design it is found that the stress is higher in bayonet design at the entrance region 3.59E+07Pa while it is 1.3E+07Pa.
- Compared with the microchannel base line design bayonet design has lower value of minimum factor of safety which gives a preference of microchannel base line design over bayonet design.
- However the bayonet design has a higher stress, it is existed only in the outer ceramic tube at the entrance region. It was expected for the bayonet design to have lower stress than that of the microchannel design. The reason for this high stress may be the sharp edge and there is a strong possibility if the model for the bayonet design is recreated without this sharp edge it may have much lower stress.
- In all design the high stress region exists at the stagnation points of fluids. At theses points the heat transfer rate is lower and the temperature difference in the solid part increases and induce higher stress. Eliminating these points of stagnation will give a safer design.
- Adding ribs with h=0.1mm increases the minimum factor safety from 26.572(base line design) to 50.814. On the other hand increases the height of the ribs to be h=0.2mm decreases the minimum factor of safety to 10.866. Studying more cases with different heights will give more complete picture to the effect of the ribs height on the induced stresses
- Using ribs is not an effective method to improve the chemical performance of the decomposer.

- Channel design with two hexagonal layers under 50% and 100% of layers overlapping gives minimum factor of safety of 14.692 and 24.678 respectively. Both values are lower than that of the base line design (26.572) but it points out the effect of the degree of overlapping on the induced stresses.
- Channels with hexagonal and diamond layers provide significant improvement where it have higher percentage of SO3 decomposition (20-25%) than that in the baseline design.
- Pressure drops for the five alternative designs increase significantly when compared with baseline design. However, the case with highest pressure drop (hexagons - 100% overlap) is still within the 10 kPa design limits of the decomposer pressure drop.
- Initial cost (closely related to the micro-channel design) and running cost (closely related to the pressure drop within the channel) of the heat exchanger should be compared with the need to maximize the productivity of SO3 decomposition.
- Since the temperature difference and the induced stresses are higher in transient case than under the steady state conditions, transient analysis provides a reasonable venue to assess the heat exchanger safety. While the selected time increments give reasonable results, studying additional cases will be helpful in getting more complete picture, especially between 5 and 40 seconds.

7.4.2 Recommendation for the bayonet heat exchanger and decomposer

- Design simplicity is the main advantage for bayonet design. Its components are easy to manufacture and assemble.

- According to the stress result and safety factor calculation the minimum safety factor of safety for bayonet design (17.128) is lower than that of the michrochannel design 26.5. Even though bayonet design is still a safe design.
- Bayonet design gives lower percentage of decomposition of sulfur trioxide (SO3) than the micro channel design.
- Bayonet design has different regions with different phases of reaction. There are many parameters that affect these reactions for example pressure drop and Reynolds number. Studying the effect of these parameters will be a good way to improve the bayonet design performance.
- The modeling assumption stated that there are no cracks caused by the corrosive environment. Studying the effect of microcrack on the safety will be an important point of research.
- Emergency study of having cases of sudden increase or decrease of the temperature, pressure, or mass flow rate will be important to find the safety level in these cases.

APPENDIX A– ANSYS CODE

A.1 dataextraction.txt

```
%-------------------------------------------------------------------------%
% Taha Mohamed
%
% Thesis - APPLYING OF MECHANICAL FAILURE CRITERIA OF BRITTLE MATERIAL TO THE DESIGN %
OF HIGH TEMPERATURE HEAT EXCHANGER
%
% Department of Mechanical Engineering
% University of Nevada, Las Vegas
%
% Revision 0 - August 15, 2007
%
%-------------------------------------------------------------------------%
%
% !--------------- this file is to extract the elemental and nodal solution
data---------


*GET, NN01, node, , num, max, ,   ! determine the total node number

*GET, EN01, elem, , num, max, ,   ! determine the total element number

!----------------------------------------
! applying safety factor criteria          to form arrays to be filled with data
!----------------------------------------
*dim, NODAL_MASK01, array, NN01
*dim, NODAL_STRSS_101, array, NN01
*dim, NODAL_STRSS_201, array, NN01
*dim, NODAL_STRSS_301, array, NN01
*dim, nodal_temp01, array, NN01
*dim, sf01, array, NN01
*dim, evol01, array, eN01
*dim, elecon01, array, eN01
*dim, ELEM_STRSS101, array, EN01
*dim, ELEM_STRSS201, array, EN01
*dim, ELEM_STRSS301, array, EN01
*dim, ELE_CON0101, array, EN01
*dim, ELE_CON0102, array, EN01
*dim, ELE_CON0103, array, EN01
*dim, ELE_CON0104, array, EN01
*dim, ELE_CON0105, array, EN01
*dim, ELE_CON0106, array, EN01
*dim, ELE_CON0107, array, EN01
*dim, ELE_CON0108, array, EN01

/POST1
AVPRIN, 0, s1,           ! adding the element tables
ETABLE, , S, 1
!*
AVPRIN, 0, s2,
ETABLE, , S, 2
```

```
!*
AVPRIN,0,s3,
ETABLE,  ,S,3
!*

!*
AVPRIN,0,volu,
ETABLE,  ,VOLU,
!----------------------------------------
! Get masking vectors
!----------------------------------------
nsle,s,all

*vget,NODAL_MASK01(1),node,,nsel

!----------------------------------------
! Get stresses                              filling of the arrays with the
required data
!----------------------------------------
*vmask,NODAL_MASK01(1)
*vget,NODAL_STRSS_101(1),node,,s,1
*vget,NODAL_STRSS_201(1),node,,s,2
*vget,NODAL_STRSS_301(1),node,,s,3
*vget,nodal_temp01(1),node,,BFE,TEMP
*VGET,evol01,ELEM,evol,ETAB,VOLU,  ,2
*VGET,ELEM_STRSS101,ELEM  ,ETAB,S1,  ,2
*VGET,ELEM_STRSS201,ELEM  ,ETAB,S2,  ,2
*VGET,ELEM_STRSS301,ELEM  ,ETAB,S3,  ,2

*VGET,ELE_CON0101(1),elem  ,node,1
*VGET,ELE_CON0102(1),elem  ,node,2
*VGET,ELE_CON0103(1),elem  ,node,3
*VGET,ELE_CON0104(1),elem  ,node,4
*VGET,ELE_CON0105(1),elem  ,node,5
*VGET,ELE_CON0106(1),elem  ,node,6
*VGET,ELE_CON0107(1),elem  ,node,7
*VGET,ELE_CON0108(1),elem  ,node,8



*CFOPEN,nodalstress01,dat
*VWRITE,NODAL_STRSS_101(1),NODAL_STRSS_201(1),NODAL_STRSS_301(1),nodal_temp01(1
)        ! Write array in given format to file "disp.dat"
(6x,e12.6,6x,e12.6,6x,e12.6,6x,e12.6,6x,e12.6)
*CFCLOSE


*CFOPEN,temp01,dat
*VWRITE,nodal_temp01(1)          ! Write array in given format to file "disp.dat"
(6x,e12.6)
*CFCLOSE

*CFOPEN,evol01,dat
*VWRITE,evol01(1)          ! Write array in given format to file "disp.dat"
(6x,e12.6)
*CFCLOSE

*CFOPEN,elemstress01,dat
*VWRITE,ELEM_STRSS101(1),ELEM_STRSS201(1),ELEM_STRSS301(1)       ! Write array
in given format to file "disp.dat"
(6x,e12.6,6x,e12.6,6x,e12.6,6x,e12.6)
*CFCLOSE
```

```
*CFOPEN, ELECON01, dat
*VWRITE, ELE_CON0101(1), ELE_CON0102(1) , ELE_CON0103(1), ELE_CON0104(1)
, ELE_CON0105(1), ELE_CON0106(1) , ELE_CON0107(1), ELE_CON0108(1)    ! Write array
in given format to file "disp.dat"
(6x, e12.6, 6x, e12.6, 6x, e12.6, 6x, e12.6, 6x, e12.6, 6x, e12.6, 6x, e12.6, 6x, e12.6)
*CFCLOSE
```

A.2 resultplotting.txt

```
%-------------------------------------------------------------------------%
% Taha Mohamed
%
% Thesis - APPLYING OF MECHANICAL FAILURE CRITERIA OF BRITTLE MATERIAL TO THE DESIGN %
OF HIGH TEMPERATURE HEAT EXCHANGER
%
% Department of Mechanical Engineering
% University of Nevada, Las Vegas
%
% Revision 0 - August 15, 2007
%
%-------------------------------------------------------------------------%
%
%!--------------- this file is to extract the elemental and nodal solution
data---------


*GET, NN01, node, , num, max, ,   ! determine the total node number

*GET, EN01, elem, , num, max, ,   ! determine the total element number

!----------------------------------------
! applying safety factor criteria          to form arrays to be filled with data
!----------------------------------------
*dim, NODAL_MASK01, array, NN01
*dim, NODAL_STRSS_101, array, NN01
*dim, NODAL_STRSS_201, array, NN01
*dim, NODAL_STRSS_301, array, NN01
*dim, nodal_temp01, array, NN01
*dim, sf01, array, NN01
*dim, evol01, array, eN01
*dim, elecon01, array, eN01
*dim, ELEM_STRSS101, array, EN01
*dim, ELEM_STRSS201, array, EN01
*dim, ELEM_STRSS301, array, EN01
*dim, ELE_CON0101, array, EN01
*dim, ELE_CON0102, array, EN01
*dim, ELE_CON0103, array, EN01
*dim, ELE_CON0104, array, EN01
*dim, ELE_CON0105, array, EN01
*dim, ELE_CON0106, array, EN01
*dim, ELE_CON0107, array, EN01
*dim, ELE_CON0108, array, EN01

/POST1
AVPRIN, 0, s1,           ! adding the element tables
ETABLE, , S, 1
!*
AVPRIN, 0, s2,
ETABLE, , S, 2
!*
```

```
AVPRIN,0,s3,
ETABLE,  ,S,3
!*

!*
AVPRIN,0,volu,
ETABLE,  ,VOLU,
!---------------------------------------
! Get masking vectors
!---------------------------------------
nsle,s,all

*vget,NODAL_MASK01(1),node,,nsel

!---------------------------------------
! Get stresses                              filling of the arrays with the
required data
!---------------------------------------
*vmask,NODAL_MASK01(1)
*vget,NODAL_STRSS_101(1),node,,s,1
*vget,NODAL_STRSS_201(1),node,,s,2
*vget,NODAL_STRSS_301(1),node,,s,3
*vget,nodal_temp01(1),node,,BFE,TEMP
*VGET,evol01,ELEM,evol,ETAB,VOLU,  ,2
*VGET,ELEM_STRSS101,ELEM,  ,ETAB,S1,  ,2
*VGET,ELEM_STRSS201,ELEM,  ,ETAB,S2,  ,2
*VGET,ELEM_STRSS301,ELEM,  ,ETAB,S3,  ,2

*VGET,ELE_CON0101(1),elem,  ,node,1
*VGET,ELE_CON0102(1),elem,  ,node,2
*VGET,ELE_CON0103(1),elem,  ,node,3
*VGET,ELE_CON0104(1),elem,  ,node,4
*VGET,ELE_CON0105(1),elem,  ,node,5
*VGET,ELE_CON0106(1),elem,  ,node,6
*VGET,ELE_CON0107(1),elem,  ,node,7
*VGET,ELE_CON0108(1),elem,  ,node,8




*VREAD,sf01(1),sf01,dat,,,ijk,1,0
(2x,e14.4)
*vput,sf01(1),node,,s,int

/GRAPHICS,  full
/title,Plotting safety factor
/DSCALE,ALL,1.0
/EFACET,1
plnsol,s,int
```

APPENDIX B – MATLAB® CODE

B.1 mohr.m

```
%-------------------------------------------------------------------------%
% Taha Mohamed
%
% Thesis - APPLYING OF MECHANICAL FAILURE CRITERIA OF BRITTLE MATERIAL TO THE DESIGN %
OF HIGH TEMPERATURE HEAT EXCHANGER
%
% Department of Mechanical Engineering
% University of Nevada, Las Vegas
%
% Revision 0 - August 15, 2007
%
%-------------------------------------------------------------------------%
%
% This program attempts to calculate factor of safety
% based on Mohr's criteria for failure of brittle materials
% the input files are
% 1- ('npsbt01') nodal solution for the principal stresses and temperature
% 2- ('ev01')    element volume
% 3- ('elecon01') node in each element

clear all;

%define material characteristics

%read input data

Stress=load('npsbt01');
bb=size(Stress.npsbt01);
n_node=bb(1,1);
sp=Stress.npsbt01;
temp=sp(:,4);
k=0.0142857*10^6;              %slope of the liner relation between "sut" or
"suc" with temperature


%calculate factor of safety at each node
for t = 1:n_node;
    % avoid cases for the mid-line nodes where ANSYS does not calculate
    % stress

    sut(t)=(k*temp(t))+200e6;       %ultimate tensile strength as a function in
temperature
    suc(t)=(k*temp(t))+600e6;       %ultimate compressive strength as a function
in temperature
    if(sp(t,1)==0 & sp(t,2)==0 & sp(t,3)==0);
        sp(t,5)=1e1;
        sp(t,6)=1e1;
    else
        %define ratio between s1 and s3
        sp(t,5)=abs(sp(t,3)/sp(t,1));
```

```
        %1st quadrant
        if any (sp(t,1)>0)&(sp(t,3)>0)&(sp(t,5)>1);
            sp(t,6)=abs(sut(t)/sp(t,3));
        else
            sp(t,6)=abs(sut(t)/sp(t,1));
        end

        %2nd quadrant
        if any (sp(t,1)<0)&(sp(t,3)<0)&(sp(t,5)>1);
            sp(t,6)=abs(suc(t)/sp(t,3));
        else
            sp(t,6)=abs(suc(t)/sp(t,1));
        end
        %4th quadrant
        if any (sp(t,1)>0)&(sp(t,3)<0);
            slintersection=(suc(t)*sut)/(suc(t)+(sp(t,5)*sut));
            sp(t,6)=slintersection/sp(t,1);
        end

        %2nd quadrant
        if any (sp(t,1)<0)&(sp(t,3)>0);
            slintersection=(suc(t)*sut(t))/(sut(t)+(sp(t,5)*suc));
            sp(t,6)=slintersection/sp(t,1);
        end
    end
%     if sp(t,6)>1
%         sp(t,6)=1;
%     end;
end
%calculate min. value of factor of safety and its location
[fs, Critical_node]=min(sp(:,6));
sf01(:,1)=1:n_node;
sf01(:,2)=sp(:,6);
sf001(:,1)=sp(:,6);
save sf01.dat sf001 -ascii

% Calculating the over all safety factor

load('ev01');                                   % volume for each node
ev = size (ev01);
v =(1:ev)';
ev001=[v ev01];
%%%%%%%%%%%%%%%%%%%%
load ('elecon01');                                  % node in each element
ec= size (elecon01);
elem_no=ec(1,1);
nod_perelem=8;
ss=(1:elem_no)';
elecon001=[ss elecon01];
%%%%%%%%%%%%%%

for w = 1:elem_no;
    sumsf(w)=0;
    for q = 1:nod_perelem;
        sumsf(w)= sumsf(w)+ sf01(elecon001(w,q+1),2);
    end
    averagsf01(w)=sumsf(w)/8;
end
averagsf01= (averagsf01');
save averagsf01.mat

totvol=sum(ev001(:,2));                 % calculate the total volume
```

```
volsf=averagsf01(:,1).*ev001(:,2);      %multiply the element volume with the
average safety actor of element
sumvolsf=sum(volsf);
ovsf=sumvolsf(1,1)/totvol(1,1);          % calculate the overall facto of safety
```

B.2 probabilty.m

```
%-------------------------------------------------------------------------%
% Taha Mohamed
%
% Thesis - APPLYING OF MECHANICAL FAILURE CRITERIA OF BRITTLE MATERIAL TO THE DESIGN %
OF HIGH TEMPERATURE HEAT EXCHANGER
%
% Department of Mechanical Engineering
% University of Nevada, Las Vegas
%
% Revision 0 - August 15, 2007
%
%-------------------------------------------------------------------------%
%
% %this program for calculation of the probability of failure according to
Webull distribution
%based on the values of principal element stresses
%we take the following value
%wiebull modulus(shape parameter)    m=8.89
%the characteristic strength (scale prameter) Su =0 Mpa
%the minimum strength (location parameter) S0 =(k*averagtemp01(n,1))+200e6
%MPa
% the input files for this program is
% 1- temperature for each node                ('temp01')
% 2-node in each element                      ('elecon01')
% 3-volume of each  element                   ('ev01')
% 4-elemental solution for principal stress   ('eps01'

clear all;
%%%%%%%%%%%%%%%
load ('temp01');                              % temperature for each node
te= size (temp01);
e=te(1,1);
ee= (1:e)';
temp001=[ee temp01];
%%%%%%%%%%%%%%%%
load ('elecon01');                            % node in each element
x= size (elecon01);
elem_no=x(1,1);
aa= (1:elem_no)';
elecon001=[aa elecon01];
nod_perelem=8;
%%%%%%%%%%%%%%%%%%
for t = 1:elem_no;
    sumtemp(t)=0;
    for q = 1:nod_perelem;
        sumtemp(t)=sumtemp(t)+temp001(elecon001(t,q+1),2);
    end
    averagtemp01(t)=sumtemp(t)/8;
end
averagtemp01= (averagtemp01');
save averagtemp01.mat
```

```
%%%%%%%%%%%
% averagtemp01=sum(elecon01')'/8; % calculate the average temperature for each
element

%%%%%%%%%
format long e;
%%%%%
load('ev01');                    % volume of each  element
e_n = size (ev01);
n_element= e_n(1,1);
en= (1:n_element)';
ev001=[en ev01];
%%%%%%%%%
load('eps01');                   % elemental solution for principal stress
eps001= [en eps01];
%%%%%%%%%%%
load('averagtemp01');
k=0.0142857*10^6;                 %slope of the liner relation between "sut" or
"suc" with temprature
sumv=sum(ev001(:,2));
for n = 1:n_element;
%%%%%%%%%%%%%
%Input Weibul curve parameters
su= 0.0;
s0(n,1)=(k*averagtemp01(n,1))+200e6;        %s0 as a function in temperature
m=8.89;
end
% prepare weibul integral power
for n=1:n_element;
    for k=1:3
        if eps001(n,k+1)>0;
            weibul_p(n,k)=((((eps001(n,k+1)-su)/s0(n,1))^m)*
(ev001(n,2)/sumv));
        end;
    end;
end;

% create weibul integral power by summing s*dv
for i=1:3
    weibul_p_s(i)=sum(weibul_p(:,i));
end;

% Calculate probability of failure for the three principal stresses
for i=1:3
    p(i)=1- exp(-weibul_p_s(i));
end;
```

BIBLIOGRAPHY

[1] Forsberg, C.W., P.S. Pickard, and P. Peterson, "The Advanced High-Temperature Reactorfor production of hydrogen or electricity," Nuclear News, February, 2003

[2] Brown, L., Besenbruch, G., Lentsch, R., Schultz, K., Funk, J., Pickard, P., Marshall, A., Showalter, S. 2003. "High Efficiency Generation of Hydrogen Fuels using Nuclear Power". Final Technical Report for the Period August 1, 1999 through September 30, 2002. Prepared under the Nuclear Energy Research Initiative (NERI) Program grant no. DE-FG03-99SF21888 for the US Department of Energy. General Atomics, USA

[3] Norman E. Dowling "Mechanical behavior of material ,engineering method for deformation fracture ,and fatigue" Prentice-Hall, Inc, 1993

[4] Jacques Lamon, "Statistical Approaches to Failure for Ceramic Reliability Assessment" Journal of the American Ceramic Society-Lumon Vol. 71, No. 2 pp. 106-112, 1988

[5] Freudenthal, pp. 592-621 in Fracture, Vol. 11. Edited by Harold Liebowitz.Academic Press, New York. 1969.

[6] T. Kuppan, "Heat exchanger Design Handbook". Marcel Dekker, Inc. 2000.

[7] IEEE Standards Board, "Guide for the Application of High-Temperature Insulation Materials in Liquid- Immersed Power Transformers" IEEE ,1997.

[8] Anna Lee Y. Tonkovich, Charles J. Call, Daniel M. Jimenez Robert S. Wegeng and M. Kevin Drost "Microchannel Heat Exchangers for Chemical Reactors" National Heat transfer Conference, Huston, Vol. 92, No.310, pp. 119-125,1996.

[9] HeeSung Park, JongIn Jo, JaeYoung Chang, and SunSoo Kim,"Methodology of Optimization for Microchannel". 22nd IEEE SEMI-THERM Symposium, 2006.

[10] N. Kayansayan, "Thermal design method of bayonet-tube evaporators and condensers" Elsevier Science Ltd and IIR, Vol. 19, No.3 pp. 197-207, 1996.

[11] T. O'Doherty et al, "Optimization of Heat Transfer Enhancement Devices in a Bayonet Tube Heat Exchanger" Applied Thermal Engineering, Vol. 21, pp. 19-36, 2001.

[12] David J. Green, "An Introduction to the Mechanical Properties of Ceramics" the Press Syndicate of the University f Cambridge,1998.

[13] Waloddi Weibull, 1939, "A Statistical Distribution Function of Wide Applicability" Journal of Applied Mechanics, pp. 293-297, 1951.

[14] John B. Wachtman, "Mechanical Properties of Ceramics" John Wiley& Sons, Inc. 1996.

[15] ANSYS, Inc, ANSYS 10. User's Guide, 2004, Canonsburg, PA.

[16] FLUENT Inc, FLUENT 6.2 User's Guide, 2005, Lebanon, NH

[17] R. G. Munro," Material properties of a Sintered a-SiC" American Institute of Physics and American Chemical Society, Vol. 26, No.5 pp. 1195-1203, 1997.

[18] Jacques Lamon, "Statistical Approaches to Failure for Ceramic Reliability Assessment". Journal of the American Ceramic Society. Vol. 71, Issue 2, pp.106–112, 1988.

[19] Valery Ponyavin, Taha Ibrahim, Merrill Wilson, Mohamed Trabia, Yitung Chen, Anthony E. Hechanova et al, "Comparison of Possible Designs for Ceramic High Temperature Heat Exchanger" Proceedings of the International Mechanical Engineering Congress & Exposition (IMECE) 2006.

[20] Valery Ponyavin, Taha Mohamed, Merrill Wilson, Mohamed Trabia, Yitung Chen, Anthony E. Hechanova et al, "Modeling and Parametric Study of A Ceramic High Temperature Heat Exchanger and Chemical Decomposer" Proceedings of the International Mechanical Engineering Congress & Exposition (IMECE) 2006.

[21] University of Nevada, Las Vegas January 1, 2006 to March 31, 2006 "High Temperature Heat Exchanger Project Quarterly Report"

[22] Valery Ponyavin, Taha Mohamed, Merrill Wilson, Mohamed Trabia, Yitung Chen, Anthony E. Hechanova et al, "Parametric Study of Sulfuric Acid Decomposer for Hydrogen Production" Proceedings of the 2nd COE-INES International Symposium on Innovative Nuclear Energy Systems, 2007.

[23] Valery Ponyavin, Taha Mohamed, Mohamed Trabia, Yitung Chen, Anthony E. Hechanova et al, "Transient Analysis of A Ceramic High Temperature Heat Exchanger and Chemical Decomposer" Proceedings of International Mechanical Engineering Congress & Exposition (IMECE), 2007.

[24] Vijaisri Nagarajan, Valery Ponyavin, Yitung Chen "Numerical Study of Sulfur Trioxide Decomposition in Bayonet Type Heat Exchanger and Chemical Decomposer with Porous Media Zone" Proceedings of the 2nd International

Conference on Porous Media and its Applications in Science and Engineering ICPM2, 2007.

[25] Gelbard F. et al, "Operational Characteristics and Performance of a Pressurized and Integrated H2SO4 Decomposition Section" Report. Sandia National Laboratories. Nuclear Hydrogen Initiative Study, 2006.

[26] Moore R. et al, "Preliminary Design of the Sulfuric Acid Section of the Integrated Lab Scale Experiment" Report. Sandia National Laboratories. Nuclear Hydrogen Initiative Study, 2006.

[27] http://www.escoproducts.com/html/a1_and_g1_fused_quartz.html

[28] James C. Govern, Cila Herman, Dennis C. Nagle, "High Temperature Heat Exchangers for Nuclear Applications" Proceedings of IMECE2006 2006 ASME International Mechanical Engineering Congress and Exposition (IMECE2006) 2006.

[29] Rampall, K. P. Singh, A. I. Soler, B. H. SCOTT (1995) "Application of Transient Analysis Methodology to Quantify Thermal Performance of Heat Exchangers" Journal of Heat Transfer Engineering, Vol. 18, No.4 pp. 22-32, 1997.

[30] Valery Ponyavin, Taha Mohamed, Mohamed Trabia, Yitung Chen, Anthony E. Hechanova, Merrill Wilson, "Design of Compact Ceramic High Temperature Heat Exchanger and Chemical Decomposer for Hydrogen Production – Part II: Parametric Study" International Journal of Heat Exchanger, 2007.(Submitted)

[31] Gelbard F, Vernon M, Moore R, Parma E, Stone H, Andazola J, Naranjo G, Reay A, Salas F (2006) "Operational Characteristics and Performance of a Pressurized and Integrated H2SO4 Decomposition Section". Report. Sandia National Laboratories. Nuclear Hydrogen Initiative Study. August 18.

VITA

Graduate College
University of Nevada, Las Vegas

Taha Mohamed

Local Address:
5383 S Maryland Parkway
Las Vegas, Nevada 89119

Home Country Address:
Alharam St. Aldobat Housing Al Shaab St.
Building No.15 Flat: 84 ,
Post Code 12111,Giza, Egypt

Degree:

Bachelor of Science, Mechanical Engineering, 2000
Al-Azhar University, Cairo

Publications:

1. Ponyavin, V., Chen, Y., Mohamed, T., Trabia, M., Wilson, M. and Hechanova, A.E. (2006), "Modeling and Parametric Study of a Ceramic High Temperature Heat Exchanger and Chemical Decomposer," Proceedings of International Mechanical Engineering Congress & Exposition (IMECE).

2. Ponyavin, V., Chen, Y., Mohamed, T., Trabia, M., Hechanova, A.E. and Wilson, M. (2006), "Comparison of Possible Designs for Ceramic High Temperature Heat Exchanger" Proceedings of International Mechanical Engineering Congress & Exposition (IMECE).

3. Ponyavin, V., Chen, Y., Mohamed, T., Trabia, M., Hechanova, A.E. and Wilson, M. (2007), "Transient Analysis of A Ceramic High Temperature Heat Exchanger And Chemical Decomposer" Proceedings of International Mechanical Engineering Congress & Exposition (IMECE).

4. Ponyavin, V., Chen, Y., Mohamed, T., Trabia, M., Hechanova, A.E. and Wilson, M. (2007), "Parametric Study of Sulfuric Acid Decomposer for Hydrogen Production," Proceedings of the 2nd COE-INES International Symposium on Innovative Nuclear Energy Systems.

5. Ponyavin, V., Chen, Y., Mohamed, T., Trabia, M., Hechanova, A.E. and Wilson, M. (2007), "Ceramic High Temperature Heat Exchanger And Chemical Decomposer For Hydrogen Production – Part I: Modling" International Journal of Heat Exchanger, 2007.(Submitted)

6. Ponyavin, V., Chen, Y., Mohamed, T., Trabia, M., Hechanova, A.E. and Wilson, M. (2007), "Ceramic High Temperature Heat Exchanger And Chemical Decomposer For Hydrogen Production – Part II: Parametric Study" International Journal of Heat Exchanger, 2007.(Submitted)

Thesis Title:

Applying of Mechanical Failure Criteria of Brittle Material to the Design of High Temperature Heat Exchanger

Thesis Examination Committee:

Chairperson, Dr. Mohamed Trabia Ph. D.
Committee Member, Dr. Yitung Chen Ph. D.
Committee Member, Dr. Ajit Roy Ph. D.
Committee Member, Dr. Brenden O'Tool Ph. D.
Graduate Faculty Representative, Dr. Aly Said Ph. D.